ANALYTICAL AND EXPERIMENTAL STUDIES OF VEHICLE DYNAMIC BEHAVIOR

Thesis by

John Arthur Carlson

In Partial Fulfillment of the Requirements

for the Degree of

Doctor of Philosophy

California Institute of Technology

Pasadena, California

1955

To my wife,

CAROL

ACKNOWLEDGMENTS

The research program herein described was made possible by the cooperation of many individuals and groups. Special thanks are given to my adviser, Dr. Peter Kyropoulos for his great help in organizing and coordinating the program, to Dr. Donald E. Hudson for his many suggestions and constructive criticisms, to Dr. G. D. McCann for his advice on computers, to the Research Laboratories Division of the General Motors Corporation which furnished the test car, to Mr. Maurice Olley, Chevrolet Division of the General Motors Corporation, for his cooperation in furnishing data on the test car, and to the Mechanical Engineering Shop personnel for their work in outfitting the test car.

I also wish to thank Mr. John E. Plapp for his help in preparing the thesis.

ABSTRACT

This thesis represents one step in the development of analysis in the field of vehicle dynamics made possible by modern computational techniques. A research program was set up, the main object of which was to conduct an appraisal of analysis by comparing the results of analysis with actual vehicle tests. Both experiment and theory are included in this one investigation.

The following general conclusions were drawn from the results of the research program:

1. Relatively simple systems giving good quantitative results can be used to represent a vehicle in motion over a variety of courses.
2. The effects of varying vehicle properties (spring rates, damping characteristics, masses) can be studied by using these simple systems. The results obtained are of sufficient accuracy to be used for design purposes.

An example of a design study demonstrating the application of analysis to a specific problem is presented. The problem was to investigate the possible use of the engine as a dynamic vibration absorber. The conclusion reached is that the engine mount stiffness may be chosen such that the shake of the frame caused by wheel bounce may be reduced.

Conclusions reached on the effects of some automobile properties (suspension bump stops, suspension damping, and tire damping) are summarized.

TABLE OF CONTENTS

TABLE OF CONTENTS (Cont'd)

PART 1. A COMPARISON OF ANALYSIS OF A VEHICLE AND VEHICLE TESTING

I. INTRODUCTION

The increasing ability of ground vehicles to attain and sustain higher speeds has made the dynamic behavior of such vehicles more critical, and the problems of vehicle comfort, safety, stability, and control, more complex and difficult. Basically, the problem is to design a vehicle such that it satisfies the requirements of the personnel or material transported. The goal is to obtain the optimum solution to this problem in the most economical way. Analysis of the vehicle and a determination of the validity of analysis are required.

In the present work the problem of obtaining the dynamic response of a vehicle was studied with the above goal in mind. A review of published material on the subject revealed that many analyses had been made from which general conclusions regarding the dynamic behavior of vehicles were drawn.[1, 2, 3] Practically all of the analyses found were limited to linear systems, and only in a very few cases was the response of a system computed. Most of the papers involved only a discussion of the qualitative effects of various terms which appear in the equations of motion, the discussion sometimes being based on knowledge of the one degree-of-freedom system. In practice, an attempt is made to apply the meager analytical conclusions available; however, most designs are evolved by testing. With the advent of modern computational techniques a need is seen for a reappraisal of the problem of analyzing a vehicle and thus predicting its behavior.[4, 5]

II. DEVELOPMENTS IN COMPUTERS AND VEHICLE TESTING LEADING TO THE PRESENT WORK

It is possible to analyze the vehicle as a mechanical system of many degrees of freedom in order to describe all motions of the vehicle components, such as wheels, frame, body, engine, and passengers. As an example of the difficulties facing a theoretical approach to the problem, consider the system shown in Figure 1. This system can be taken to represent an automobile and its suspension for small vertical motions if one assumes that the engine and the body and its contents are rigidly connected to the frame. The tire is assumed to contact the ground at a point directly below the wheel.

The equations of motion for this system may be obtained from Lagrange's equation for nonconservative systems,[6]

$$\frac{d}{dt}\left(\frac{\partial T}{\partial \dot{q}}\right) - \frac{\partial T}{\partial q} + \frac{\partial V}{\partial q} + \frac{\partial D}{\partial \dot{q}} = 0 , \tag{1}$$

in which the kinetic energy

$$T = \tfrac{1}{2} m_4 \dot{x}_5^2 + \tfrac{1}{2} I_1 \dot{\phi}^2 + \tfrac{1}{2} I_2 \dot{\theta}^2 + \tfrac{1}{2} m_1 \dot{x}_1^2 + \tfrac{1}{2} m_2 \dot{x}_2^2 + \tfrac{1}{2} \frac{I_3}{e^2} (\dot{x}_3 - \dot{x}_4)^2 + \frac{1}{8} m_3 (\dot{x}_3 + \dot{x}_4)^2 , \tag{2}$$

the potential energy

$$V = \tfrac{1}{2} K_1 (x_5 + \tfrac{d}{2}\theta + a\phi - x_1)^2 + \tfrac{1}{2} K_2 (x_5 - \tfrac{d}{2}\theta + a\phi - x_2)^2 + \tfrac{1}{2} K_3 (x_5 + \tfrac{e}{2}\theta - b\phi - x_3)^2 + \tfrac{1}{2} K_4 (x_5 - \tfrac{e}{2}\theta - b\phi - x_4)^2 + \tfrac{1}{2} K_5 (x_1 - y_1)^2 + \tfrac{1}{2} K_6 (x_2 - y_2)^2 + \tfrac{1}{2} K_3 (x_3 - y_3)^2 + \tfrac{1}{2} K_8 (x_4 - y_4)^2 + \tfrac{1}{2} K_9 \left(\theta - \frac{x_1 - x_2}{d}\right)^2 + \tfrac{1}{2} K_{10} \left(\theta - \frac{x_3 - x_4}{e}\right)^2 , \tag{3}$$

and the dissipation

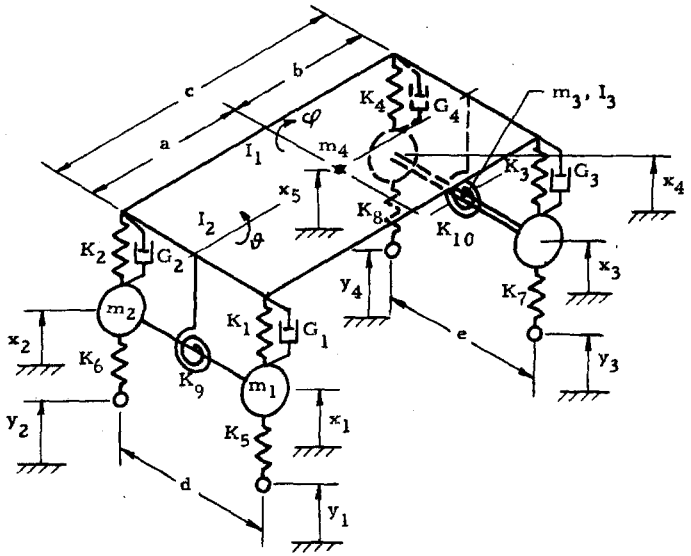

m_1 = unsprung mass at left front wheel.

m_2 = unsprung mass at right front wheel.

m_3 = total unsprung mass at rear.

m_4 = sprung mass

I_1 = moment of inertia of sprung mass about horizontal transverse axis through the C.G. of the sprung mass.

I_2 = moment of inertia of sprung mass about horizontal longitudinal axis through the C.G. of the sprung mass.

I_3 = moment of inertia of rear unsprung mass about a horizontal longitudinal axis through its C.G.

K_1, K_2 = front suspension spring constants.

K_3, K_4 = rear suspension spring constants.

K_5, K_6, K_7, K_8 = tire spring constants.

K_9 = front roll stabilizer spring constant.

K_{10} = rear roll stabilizer spring constant.

G_1, G_2 = front damping constants.

G_3, G_4 = rear damping constants.

a = horizontal distance from front wheel centers to the C.G. of the sprung mass.

b = horizontal distance from rear wheel centers to the C.G. of the sprung mass.

c = wheelbase.

d = front tread width.

e = rear tread width.

x_1, x_2, x_3, x_4 = vertical displacements of wheels.

x_5 = vertical displacement of the C.G. of the sprung mass.

y_1, y_2, y_3, y_4 = vertical displacements of the ground under the wheels.

φ = angular displacement of the sprung mass about the horizontal transverse axis through the C.G.

ϑ = angular displacement of the sprung mass about the horizontal longitudinal axis through the C.G.

All displacements are measured from the static equilibrium position.

Figure 1. Seven degree-of-freedom system for representing small vertical motions of an automobile.

$$D = \tfrac{1}{2}G_1(\dot{x}_5 + \tfrac{d}{2}\dot{\theta} + a\dot{\phi} - \dot{x}_1)^2 + \tfrac{1}{2}G_2(\dot{x}_5 - \tfrac{d}{2}\dot{\theta} + a\dot{\phi} - \dot{x}_2)^2$$

$$+ \tfrac{1}{2}G_3(\dot{x}_5 + \tfrac{e}{2}\dot{\theta} - b\dot{\phi} - \dot{x}_3)^2 + \tfrac{1}{2}G_4(\dot{x}_5 - \tfrac{e}{2}\dot{\theta} - b\dot{\phi} - \dot{x}_3)^2 \quad . \tag{4}$$

Substituting (2), (3), and (4) in (1), taking $q = x_1, x_2, x_3, x_4, x_5, \phi,$ or θ, yields the following equations of motion:

$$m_1\ddot{x}_1 - G_1(\dot{x}_5 + \tfrac{d}{2}\dot{\theta} + a\dot{\phi} - \dot{x}_1) - K_1(x_5 + \tfrac{d}{2}\theta + a\phi - x_1) - \frac{K_9}{d}\left(\theta - \frac{x_1 - x_2}{d}\right)$$

$$+ K_5(x_1 - y_1) = 0 \; ; \tag{5}$$

$$m_2\ddot{x}_2 - G_2(\dot{x}_5 - \tfrac{d}{2}\dot{\theta} + a\dot{\phi} - \dot{x}_2) - K_2(x_5 - \tfrac{d}{2}\theta + a\phi - x_2)$$

$$+ \frac{K_9}{d}\left(\theta - \frac{x_1 - x_2}{d}\right) + K_6(x_2 - y_2) = 0 \; ; \tag{6}$$

$$\left(\frac{m_3}{4} + \frac{I_3}{e^2}\right)\ddot{x}_3 + \left(\frac{m_3}{4} - \frac{I_3}{e^2}\right)\ddot{x}_4 - G_3(\dot{x}_5 + \tfrac{e}{2}\dot{\theta} - b\dot{\phi} - \dot{x}_3) - K_3(x_5 + \tfrac{e}{2}\theta - b\phi - x_3)$$

$$- \frac{K_{10}}{e}\left(\theta - \frac{x_3 - x_4}{e}\right) + K_7(x_3 - y_3) = 0 \; ; \tag{7}$$

$$\left(\frac{m_3}{4} - \frac{I_3}{e^2}\right)\ddot{x}_3 + \left(\frac{m_3}{4} + \frac{I_3}{e^2}\right)\ddot{x}_4 - G_4(\dot{x}_5 - \tfrac{e}{2}\dot{\theta} - b\dot{\phi} - \dot{x}_4) - K_4(x_5 - \tfrac{e}{2}\theta - b\phi - x_4)$$

$$+ \frac{K_{10}}{e}\left(\theta - \frac{x_3 - x_4}{e}\right) + K_8(x_4 - y_4) = 0 \; ; \tag{8}$$

$$m_4\ddot{x}_5 + G_1(\dot{x}_5 + \tfrac{d}{2}\dot{\theta} + a\dot{\phi} - \dot{x}_1) + G_2(\dot{x}_5 - \tfrac{d}{2}\dot{\theta} + a\dot{\phi} - \dot{x}_2) + G_3(\dot{x}_5 + \tfrac{e}{2}\dot{\theta} - b\dot{\phi} - \dot{x}_3)$$

$$+ G_4(\dot{x}_5 - \tfrac{e}{2}\dot{\theta} - b\dot{\phi} - \dot{x}_4) + K_1(x_5 + \tfrac{d}{2}\theta + a\phi - x_1) + K_2(x_5 - \tfrac{d}{2}\theta + a\phi - x_2)$$

$$+ K_3(x_5 + \tfrac{e}{2}\theta - b\phi - x_3) + K_4(x_5 - \tfrac{e}{2}\theta - b\phi - x_4) = 0 \; ; \tag{9}$$

$$I_1\ddot{\phi} + aG_1(\dot{x}_5 + \frac{d}{2}\dot{\theta}+a\dot{\phi}-\dot{x}_1)+aG_2(\dot{x}_5-\frac{d}{2}\dot{\theta}+a\dot{\phi}-\dot{x}_2)-bG_3(\dot{x}_5+\frac{e}{2}\dot{\theta}-b\dot{\phi}-\dot{x}_3)$$

$$-bG_4(\dot{x}_5-\frac{e}{2}\dot{\theta}-b\dot{\phi}-\dot{x}_4)+aK_1(x_5+\frac{d}{2}\theta+a\phi-x_1)+aK_2(x_5-\frac{d}{2}\theta+a\phi-x_2) \qquad (10)$$

$$-bK_3(x_5+\frac{e}{2}\theta-b\phi-x_3)-bK_4(x_5-\frac{e}{2}\theta-b\phi-x_4) = 0 \ ;$$

$$I_2\ddot{\theta} + \frac{d}{2}G_1(\dot{x}_5+\frac{d}{2}\dot{\theta}+a\dot{\phi}-\dot{x}_1)-\frac{d}{2}G_2(\dot{x}_5-\frac{d}{2}\dot{\theta}+a\dot{\phi}-\dot{x}_2)+\frac{e}{2}G_3(\dot{x}_5+\frac{e}{2}\dot{\theta}-b\dot{\phi}-\dot{x}_3)$$

$$-\frac{e}{2}G_4(\dot{x}_5-\frac{e}{2}\dot{\theta}-b\dot{\phi}-\dot{x}_4)+\frac{d}{2}K_1(x_5+\frac{d}{2}\theta+a\phi-x_1)-\frac{d}{2}K_2(x_5-\frac{d}{2}\theta+a\phi-x_2) \qquad (11)$$

$$+\frac{e}{2}K_3(x_5+\frac{e}{2}\theta-b\phi-x_3)-\frac{e}{2}K_4(x_5-\frac{e}{2}\theta-b\phi-x_4)+K_9(\theta-\frac{x_1-x_2}{d})$$

$$+K_{10}(\theta-\frac{x_3-x_4}{e}) = 0 \ .$$

It is not feasible to obtain solutions to these equations by conventional analytical methods unless many more simplifying assumptions are made.[7] As one makes simplifying assumptions the solutions become increasingly unrealistic and the information obtained loses value. The next step is to turn to the use of an electrical computer, but this is not as simple as it sounds. Solving these equations, which by no means represent the vehicle completely, with the addition of complications such as bump stops* and non-linear shock absorbers, would tax the capacity of even the largest computers available. These computers are very costly and require specialized personnel to operate them. That both of these factors tend to hinder the ready use of these devices by designers is a point which may be overlooked by computer engineers. Besides this, the given data may not be known with sufficient accuracy, or extreme accuracy may not be necessary for design purposes, to justify an elaborate computer setup.

---

*A glossary of terms which may be unfamiliar to the reader is found in Appendix VI.

A parallel development to that of computers has taken place in vehicle instrumentation and testing.[8, 9, 10, 11] Here, the development of modern instrumentation has made possible accurate and extensive determination of vehicle motions. Experimental investigations, however, have tended to be separated from analytical studies with the result that both suffer a lack of completeness. For instance, while much information can be gained experimentally, purely experimental design studies in which vehicle properties are to be varied must be limited within economic bounds. These limited studies give an incomplete picture and sometimes lead to inconclusive results (see Reference 12, concerning engine mounts).

In an effort to resolve the above difficulties, a research program was set up, the main object of which was to conduct this appraisal of analysis by comparing the results of analysis and actual vehicle tests. A report of work along this line has been published;[13] however, it was very limited in scope. The analysis in that case was performed independently of the vehicle tests. The present work included performing the vehicle tests as well as the analysis. Including both experiment and theory in one investigation allowed a complete study of all methods and procedures used. This is a necessity if the evaluation of the analysis and vehicle tests is to be valid.

The results compared are in the form of measurements of the response of the vehicle in traveling over specified courses at constant speeds. The vehicle tests were made first and the records were studied to see what could be learned from them about the system. It was hoped that simple systems could be used in the analysis

to represent the vehicle suitably for design purposes. This would allow the use of smaller computers which could conceivably become tools of the designer in the same category as the slide rule and desk calculator. How the actual vehicle measurements were made is described in the next two sections.

In order to obtain the response of the systems derived by analysis, an electric analog computer was used. A section of the thesis is devoted to the application of this type of computer. One factor influencing the choice of computer here was the availability of the electric analog type. It was also felt that this type was very suitable for studying dynamic behavior of mechanical systems. Other types of computers which could have been used are the mechanical differential analyzer,[14] the electronic differential analyzer (sometimes called "electronic analog computer"),[15] and the digital computer.[16] However, it is felt that digital computers at present do not offer the possibility of being used directly by designers for problems this complex.

III. INSTRUMENTATION OF THE VEHICLE

The response of the actual vehicle to road excitation was measured with accelerometers and displacement pickups. Accelerometers were chosen because they measure a significant characteristic of the motions and are available commercially in a very reliable form. Velocities and displacements could be obtained from the acceleration records by integration. Higher derivatives could also be calculated by differentiation of the records, but their significance in vehicle rideability is not well established.[17] Thus, by using acceleration as a measure for comparison, an adequate description of the response is assured.

The displacements of the wheels relative to the frame were measured by a specially designed pickup. The pickup consisted of a pulley and cable to convert linear motion to rotary motion and a potentiometer which was connected to the pulley shaft to measure the displacement electrically. A spiral spring was used to keep the cable taut. The displacement pickups were capable of determining position within a tolerance of about 0.05 inch.

A fifth wheel was used to indicate speed. Electrical pulses were obtained to indicate distance traveled by means of a set of cam-operated contacts which opened and closed once for each revolution of the wheel. The rolling circumference of the wheel was determined by counting the revolutions as the wheel was rolled 100.0 feet over the same type of surface as was used in the vehicle runs.

Appendix I lists and describes the equipment which was used. Accelerometers were mounted on the frame, front suspension,

and rear axle, in order to measure vertical accelerations in vertical planes through the wheel axes. Figure 2 shows the installation of accelerometers at the right front wheel. Accelerometers on the right rear frame and right rear axle appear in Figures 4 and 5, respectively. Locations on the left side were symmetric about the vehicle centerline. Brackets were designed so that the axes of all the accelerometers were vertical with the vehicle in the static loaded condition on a level surface. Deviations from the vertical were negligible in all cases.

The vertical accelerations of the front wheels were measured by mounting accelerometers at convenient points on the lower support arms (Figure 2). Measurements thus obtained were corrected to obtain the wheel accelerations. Since the accelerometer was mounted as far out on the arm as possible and the accelerations of the frame were found to be very much smaller than the wheel accelerations, the effect of the frame accelerations on the readings of this accelerometer were negligible.

In addition to the fore and aft specification of location mentioned, accelerometers on each side in the rear were mounted as nearly as possible in longitudinal vertical planes through the suspension springs. No corrections for position were felt to be necessary for the accelerometers other than those on the front support arms. The accelerometers were calibrated by inverting them, to obtain an acceleration of two times gravity.

The installation of a displacement pickup to measure the displacement of the rear axle relative to the frame is also shown in Figures 4 and 5. It can be seen that the vertical deflection of

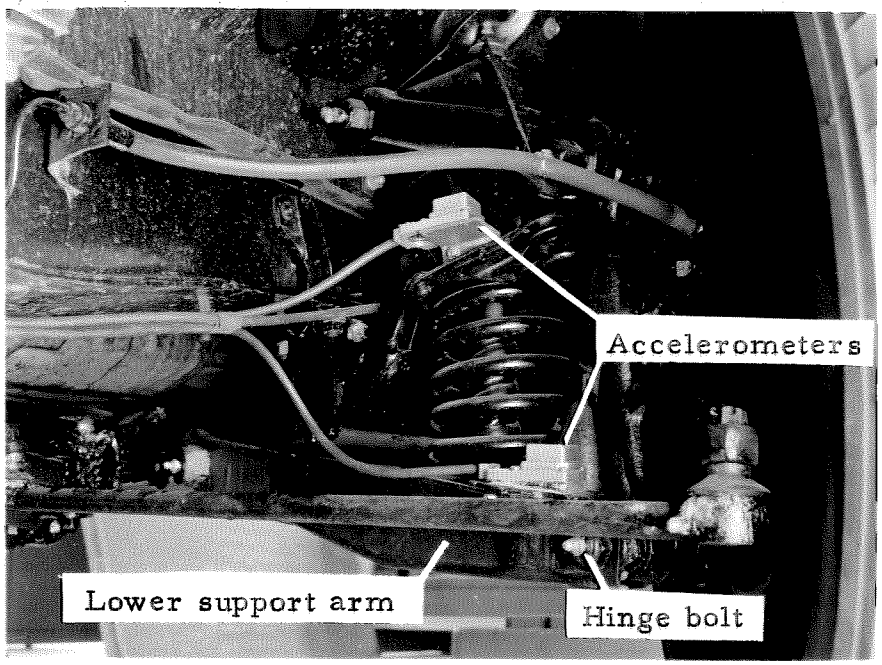

Figure 2. Installation of accelerometers at the right front wheel.

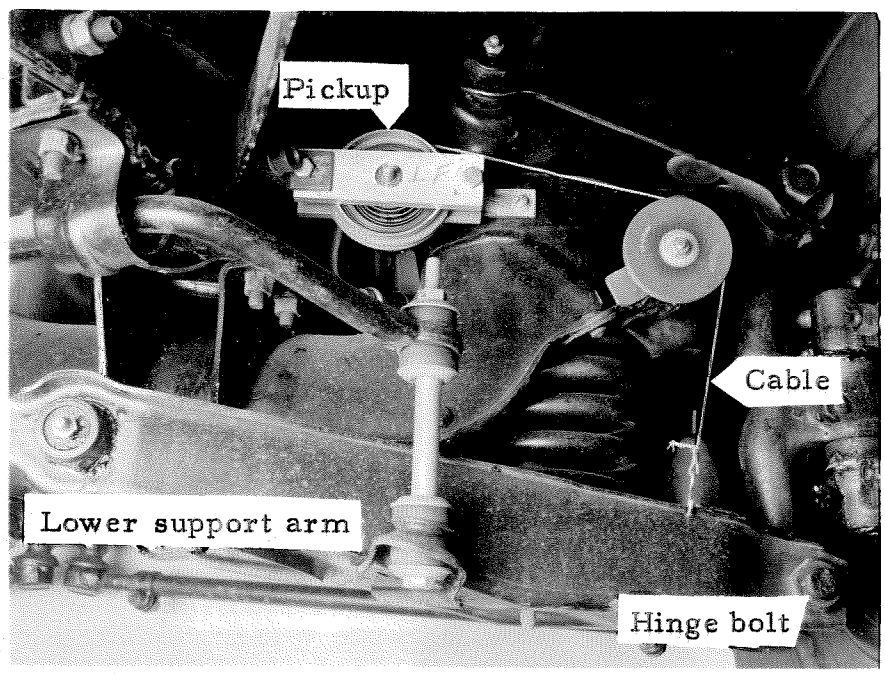

Figure 3. Installation of displacement pickup at the left front wheel.

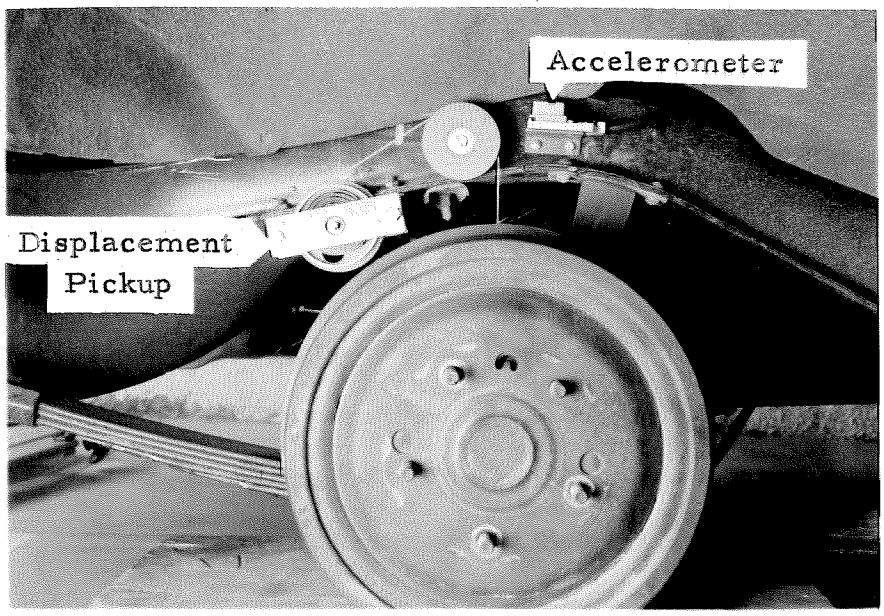

Figure 4. Displacement pickup and accelerometer mounted on the frame at the right rear wheel.

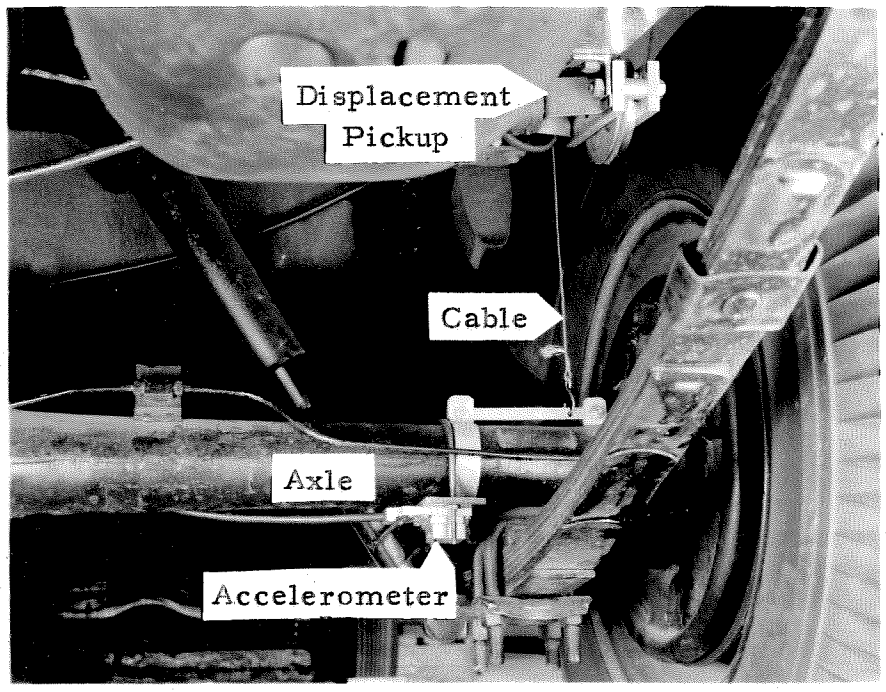

Figure 5. Displacement pickup and accelerometer mounted on the axle at the right rear wheel.

the rear suspension spring was thereby measured. Deviations of this measurement because of horizontal motions of the axle were negligible.

The displacements of the front wheels relative to the frame were measured as shown in Figure 3. The error resulting from the geometry of this setup was no greater than the minimum increment of motion which the pickup could detect (0.02 inch) for all motions except extreme compression of the left front suspension spring in which case the maximum error was 0.05 inch. Vertical motion of the wheel was considered to be represented by the vertical motion of the lower support arm outboard hinge bolt. Gains for the forward pickups were adjusted to compensate for the fact that the cable attachment point was not at this bolt.

Calibration of the displacement pickups was accomplished by inserting a three-inch link at the cable attachment point and observing the recorded deflection.

The recording equipment and associated power supplies were arranged in the automobile as shown in Figures 6 and 7. The amplifiers and oscillograph were practically unaffected by the motion of the vehicle. Only a slight high frequency disturbance of the trace was observed in runs made with zero amplifier input. Recorder elements used for the rear relative displacement traces received some excitation from the 60 cps timing motor drive circuit in the recorder.

A 1954 Chevrolet Model 2103 standard production automobile was used for the vehicle tests.

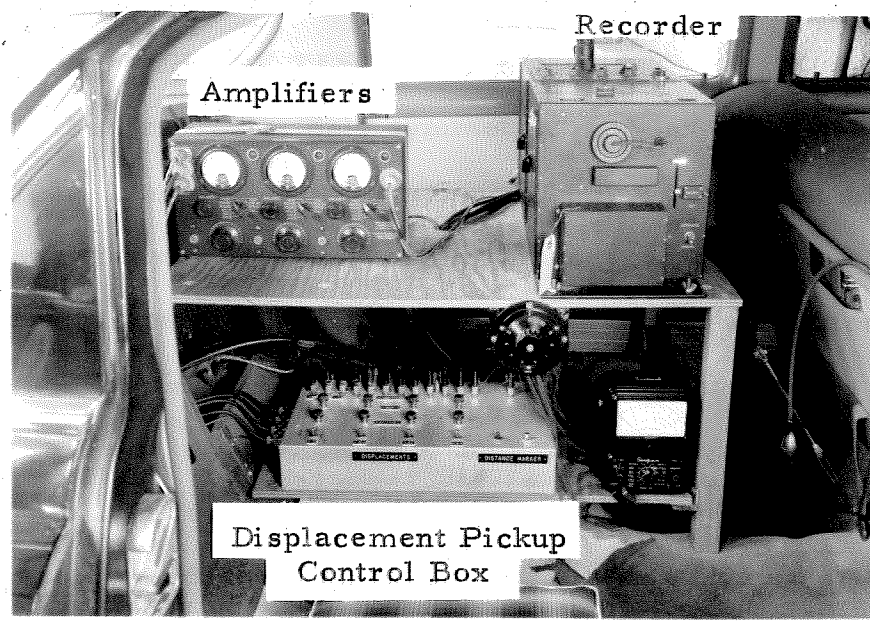

Figure 6. Arrangement of recording equipment in the test car.

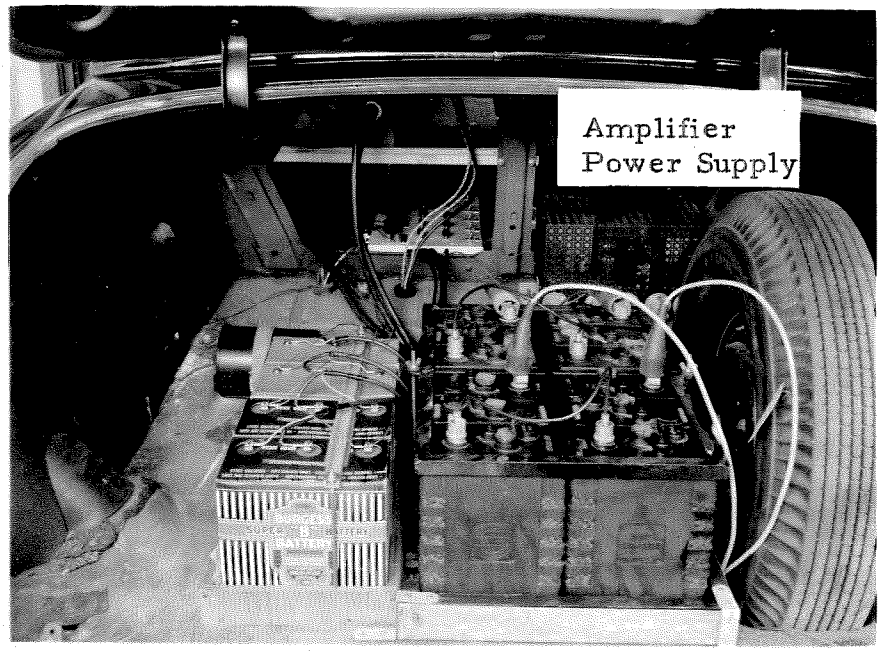

Figure 7. Power supplies in trunk of test car.

IV. VEHICLE TESTS AND RECORDS

For the first tests, only symmetric motions of the vehicle were excited. Long and short wavelength bumps were used so that low frequency body motions and high frequency wheel motions could be studied separately. The parking lot at the Santa Anita Race Track was chosen as the location for the tests. Here a long dip was found which gave rise to large symmetric body motions at moderate speeds (see Figure 8). A course was laid out over this dip (Figure 10) so that runs could be reproduced. This course was surveyed and profiles were obtained for the excitation received by each wheel. The average of the right and left profiles was taken as suitable for representing the dip in the analysis and computation which follow (Figure 9). A 1.4 per cent grade of the approach and leaving portions of the course was subtracted from these profiles to yield the level approach shown. This grade was so small that the effect of the deviation of the direction of gravity on the static deflections of the vehicle could be neglected.

Short-wave-length bumps were built out of hardwood, in the form of a one-half cycle of a sine-wave, two feet long and two inches high. These afforded maximum excitation of wheel bounce at speeds of about 15 to 20 miles per hour. A course was laid out and the bumps were placed on a smooth section of the parking lot as shown in Figure 11. The bumps were secured by nails driven into the asphalt pavement. This arrangement of the bumps produced a symmetric excitation of the car. Unsymmetric excitation was obtained by removing one of the bumps and running only one side of the car over the remaining one.

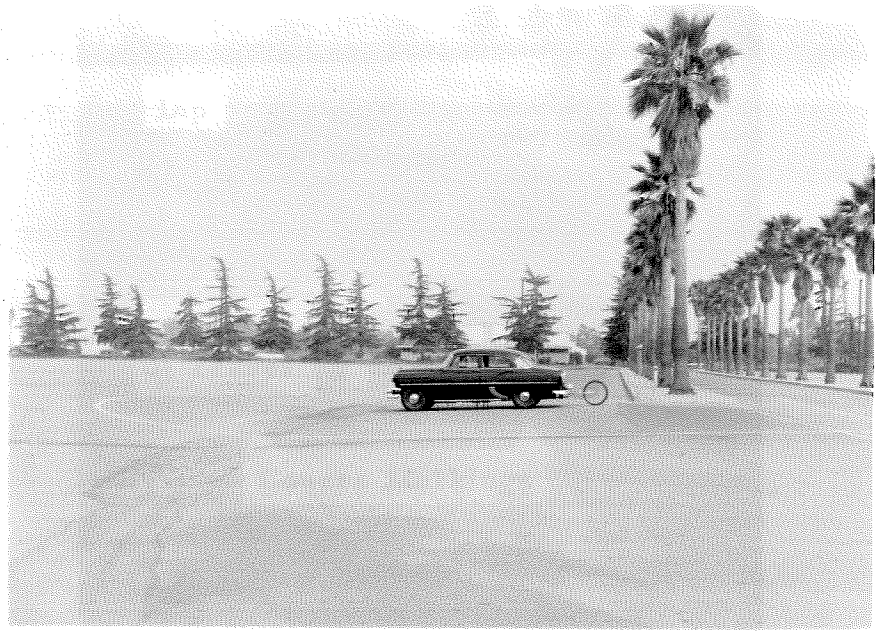

Figure 8. Side view of test dip with car shown headed east.

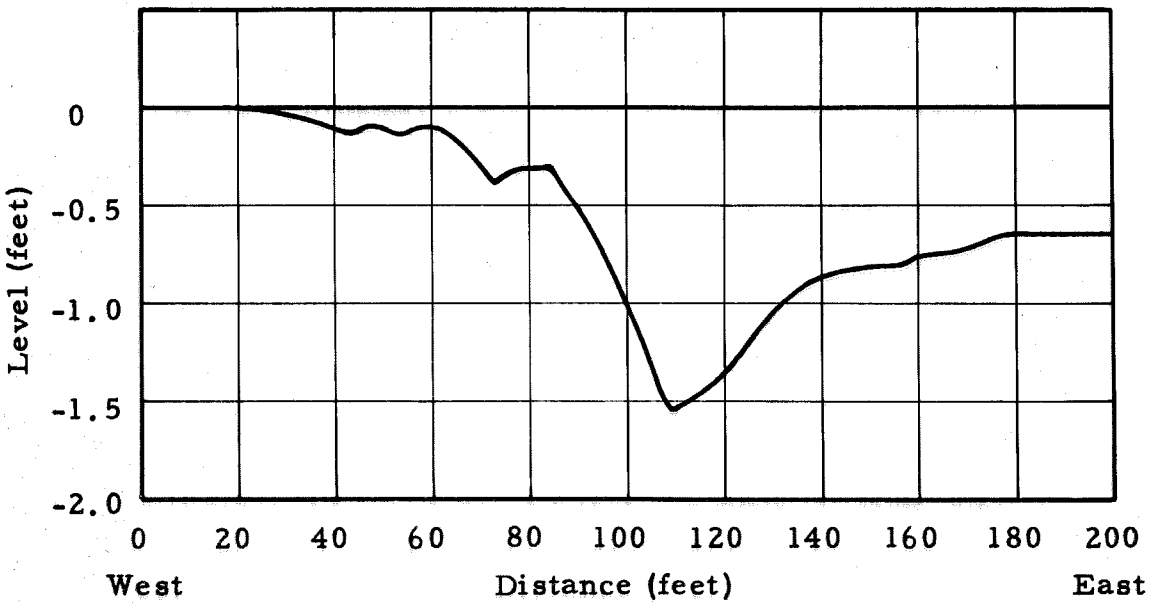

Figure 9. Profile of test dip.

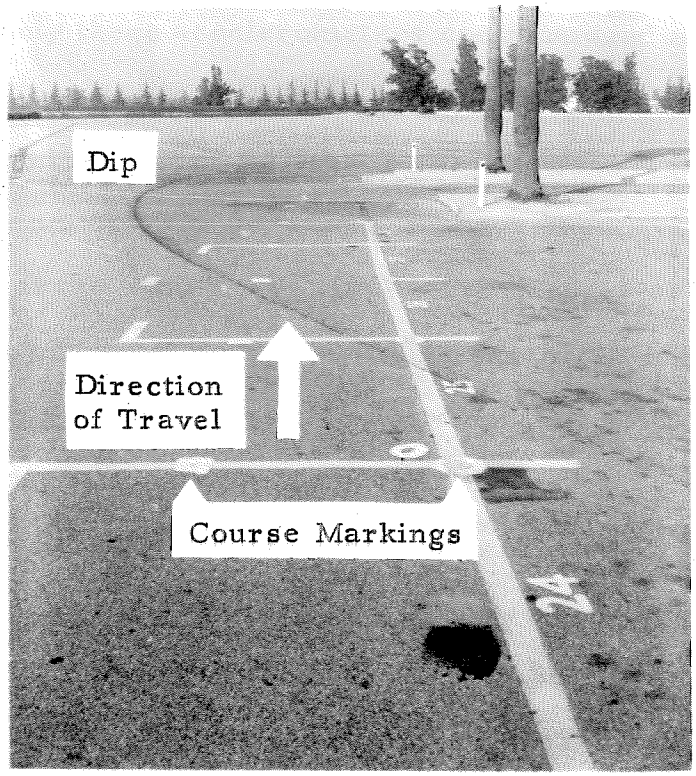

Figure 10. Course over test dip, looking east.

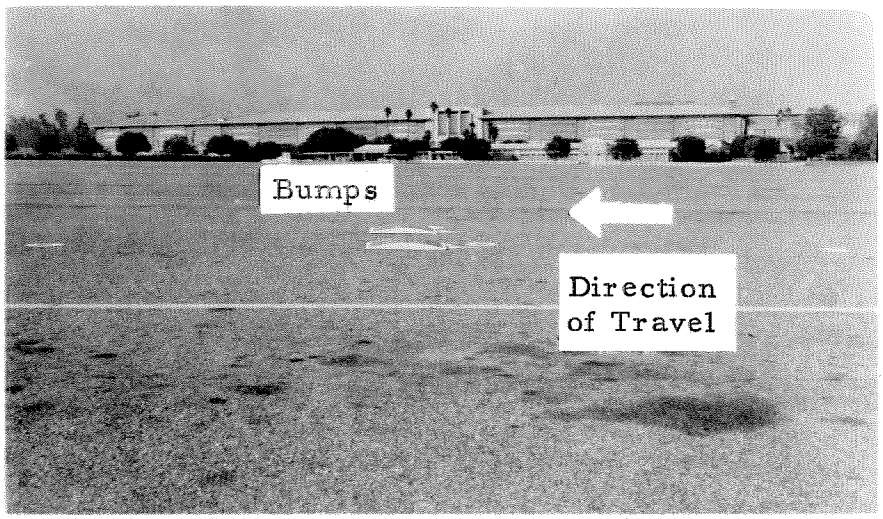

Figure 11. Side view of half-sine bumps placed symmetrically.

Since only three accelerometers could be used at one time, all of the positions described where acceleration was to be measured were not covered at the same time. However, runs were found to be quite reproducible. Consequently, measurements obtained on different runs at the same speed could be considered as resulting from the same motion of the vehicle. In Figures 12 and 13, vehicle records are shown illustrating reproducibility for the test dip and half-sine bumps, respectively.

The speeds used for runs over the test dip were 20, 25, and 28 miles per hour. For the half-sine bumps, speeds of 10, 15, and 20 miles per hour were used. The fifth wheel speedometer was mounted between the steering wheel and the instrument panel of the car so that the driver could see it at all times and maintain constant speed. The average speed on each run was calculated from the distance marks and timing lines on the oscillograph record.

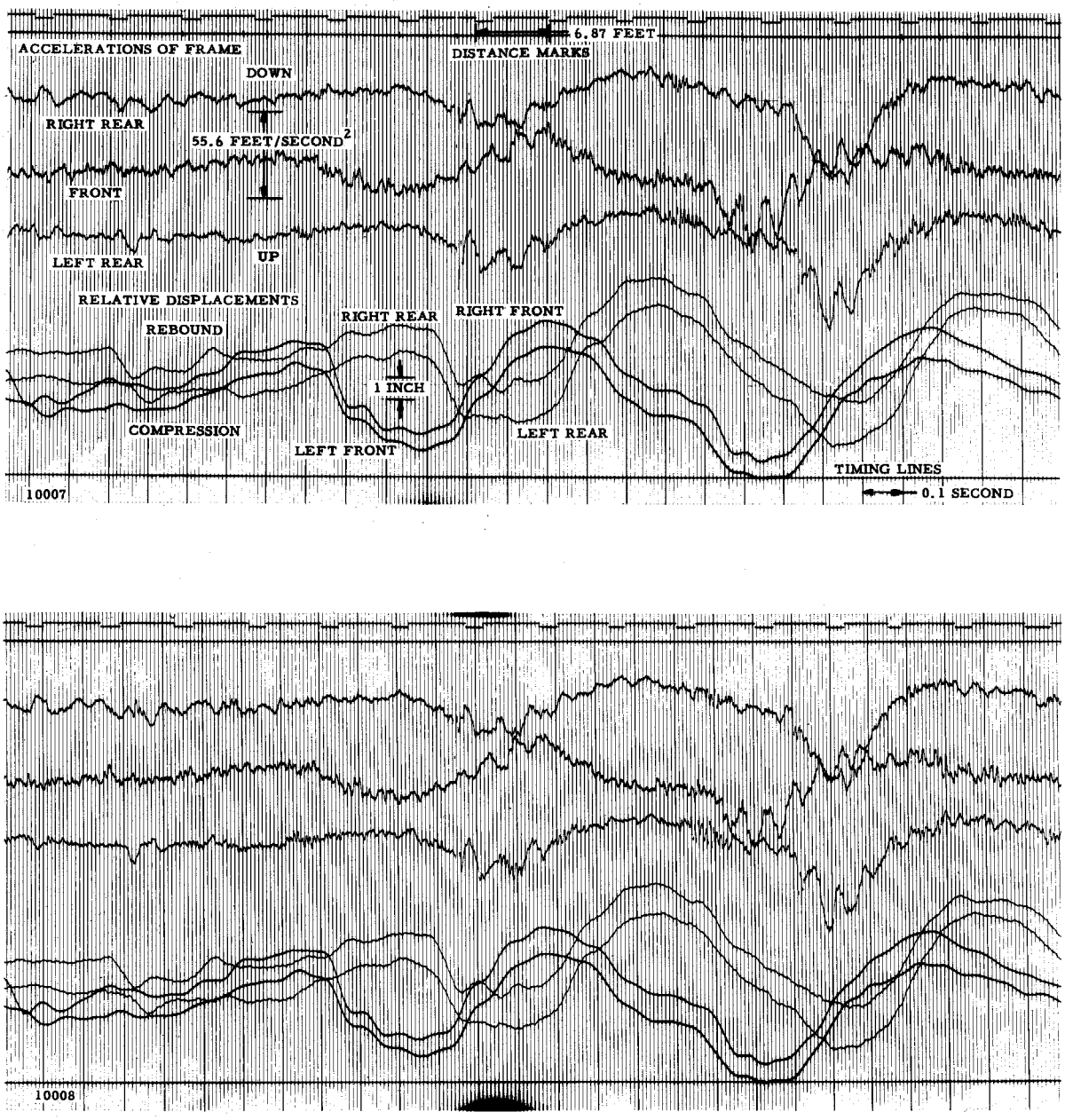

Figure 12. Vehicle records illustrating reproducibility, obtained in going over the test dip at 25 miles per hour.

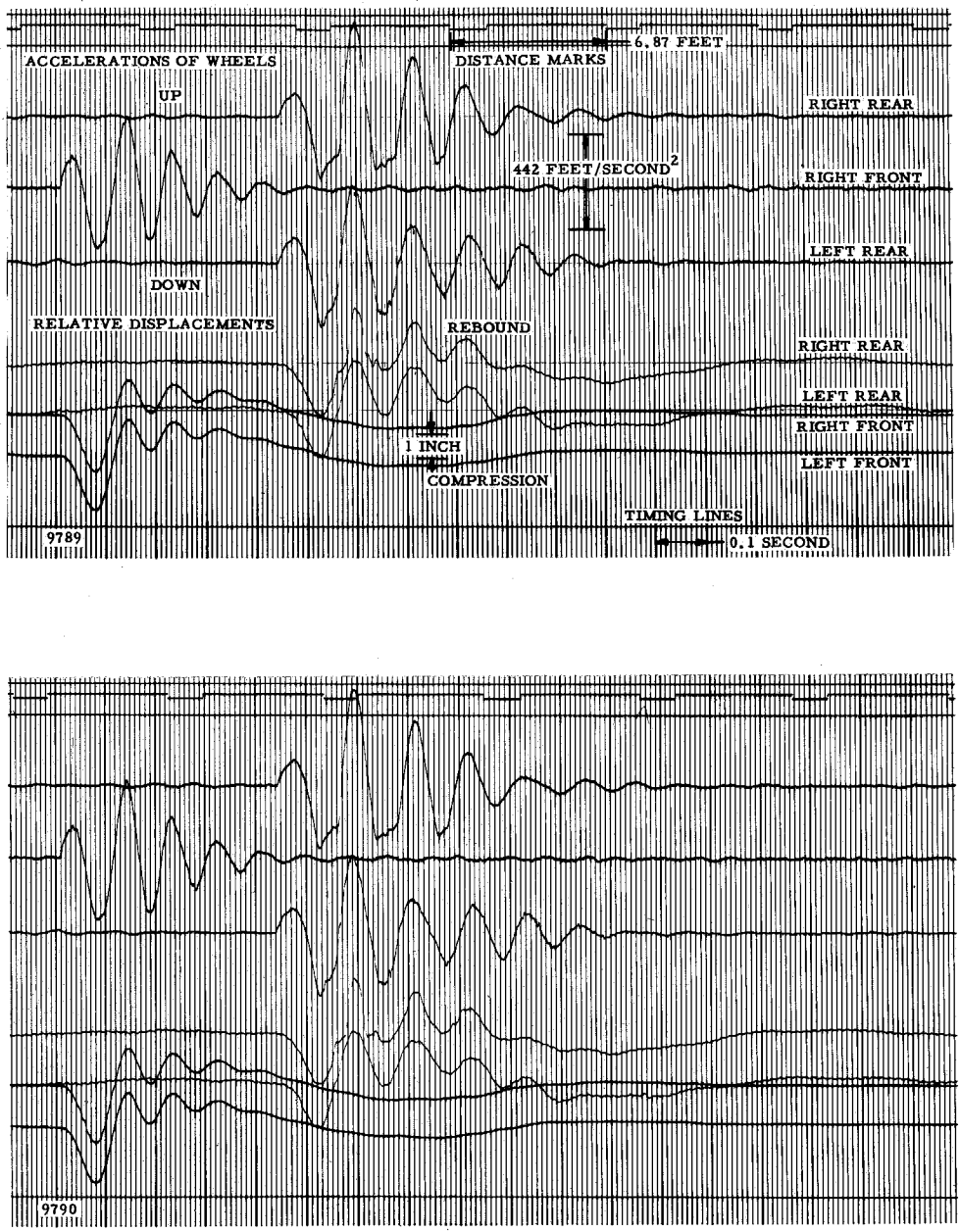

Figure 13. Vehicle records illustrating reproducibility, obtained in going over symmetrically placed half-sine bumps at 15 miles per hour.

V. ANALYSIS OF THE VEHICLE

To obtain quantitative results from analyzing the vehicle and computing its response to excitation, certain properties of the vehicle, such as masses, moments of inertia, spring constants, damping, etc., have to be known. Data for the vehicle used are presented in Appendix II. Some of this information was supplied by the manufacturer; other information had to be obtained by laboratory tests of the vehicle. It was also necessary to calculate some of the mass properties of the test car from measurements and weight data supplied, and to combine supplied and laboratory test data to obtain some characteristics. These tests and calculations are described in Appendix II.

From an examination of the vehicle records, some general conclusions were reached about the motion of the vehicle. In Figure 13 it can be seen that the motions at the front and rear in symmetric motion were practically independent. The reason for this independence may be ascertained by a study of the system in Figure 1. If the coordinates x_5 and ϕ for this system are expressed in terms of the vertical displacements of the center of the frame at front and rear, only one term remains which couples the two new equations which replace equations (9) and (10), page 4, for symmetric motion. The system of Figure 1 and its equations of motion reduce to the system and equations shown in Figure 14 as a result of the assumption of symmetric motion and the indicated coordinate transformation. A complete statement of all of the conditions leading to Figure 14 is given in Appendix III, together with definitions of the symbols in

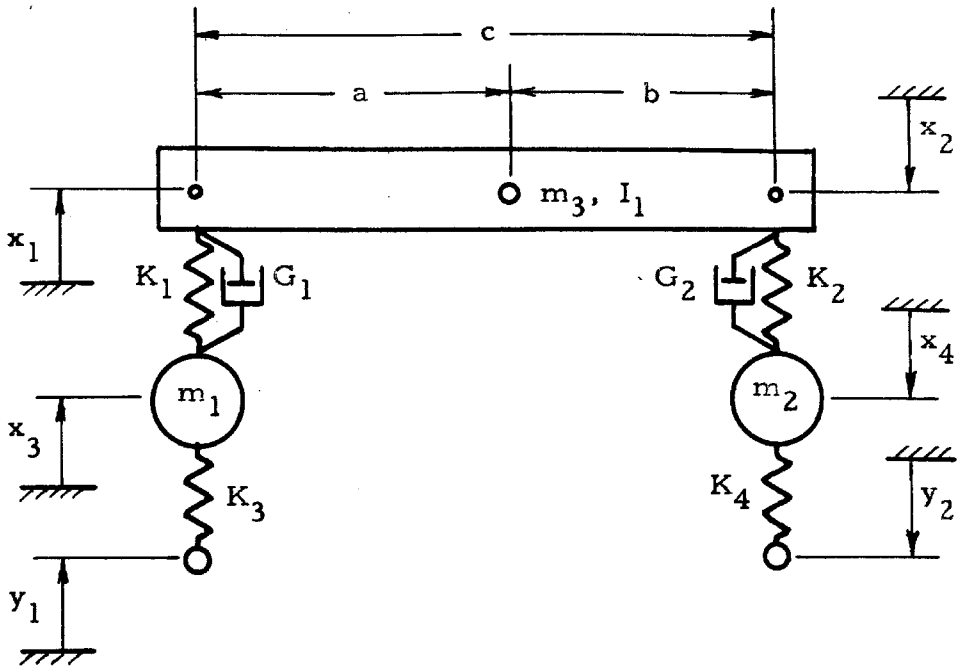

Equations of Motion

$$M_{11}\, p\dot{x}_1 - M_{12}\, p\dot{x}_2 + (G_1 + \frac{K_1}{p})(\dot{x}_1 - \dot{x}_3) = 0$$

$$- M_{12}\, p x_1 + M_{22}\, p\dot{x}_2 + (G_2 + \frac{K_2}{p})(\dot{x}_2 - \dot{x}_4) = 0$$

$$m_1\, p\dot{x}_3 - (G_1 + \frac{K_1}{p})(\dot{x}_1 - \dot{x}_3) + \frac{K_3}{p}(\dot{x}_3 - \dot{y}_1) = 0$$

$$m_2\, p\dot{x}_4 - (G_2 + \frac{K_2}{p})(\dot{x}_2 - \dot{x}_4) + \frac{K_4}{p}(\dot{x}_4 - \dot{y}_2) = 0$$

$$M_{11} = m_3 (\frac{b}{c})^2 + \frac{I_1}{c^2}; \quad M_{12} = m_3 \frac{ab}{c^2} - \frac{I_1}{c^2}; \quad M_{22} = m_3 (\frac{a}{c})^2 + \frac{I_1}{c^2}$$

Operator, $p = \frac{d}{dt}$.

Figure 14. Four degree-of-freedom system for representing an automobile in symmetric motion.

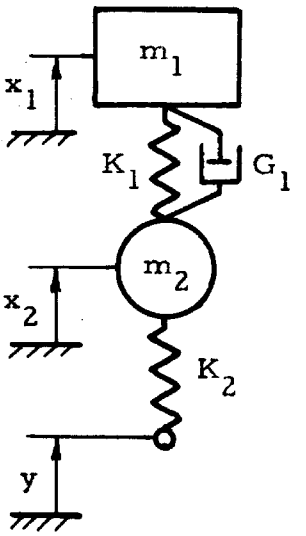

Equations of Motion

$$m_1 p\dot{x}_1 + (G_1 + \frac{K_1}{p})(\dot{x}_1 - \dot{x}_2) = 0$$

$$m_2 p\dot{x}_2 - (G_1 + \frac{K_1}{p})(\dot{x}_1 - \dot{x}_2) + \frac{K_2}{p}(\dot{x}_2 - \dot{y}) = 0$$

Operator, $p = \frac{d}{dt}$.

Figure 15. Two degree-of-freedom system for representing an automobile in symmetric motion.

terms of Figure 1. Calculation of the coupling term, M_{12}, and the self-coupling terms, M_{11} and M_{22}, revealed that the magnitude of M_{12} was only about 4 per cent of the magnitudes of the other two terms for the test car; this substantiates the experimental observation and indicates that M_{12} could be neglected. This property of the sprung mass is typical of most modern American cars. If M_{12} is neglected, Figure 14 reduces to two simpler systems like that shown together with its equations of motion in Figure 15.

The vehicle records shown in Figures 16 and 17 lead to the following conclusions: in going over the half-sine bumps unsymmetrically the right and left front wheel motions were independent of each other; this was not true for the rear. It may also be noted from the acceleration traces that the motion of the frame is practically negligible compared to that of the wheels for this high frequency excitation. This would lead one to think that more complicated motions of the unsprung masses, such as power hop and brake hop, could be studied assuming the frame to be fixed, thereby simplifying the analysis.

Unsymmetric motions of the rear axle were studied by considering the system shown in Figure 18. This system follows from Figure 1 by assuming that the motion of the rear axle is independent of the motion at the front of the vehicle. Account was also taken of the difference between the tread width and the distance between the springs. Definitions of the terms appearing in Figure 18 are given in Appendix III. The equations of motion may be derived by direct application of Newton's Second Law to the system.

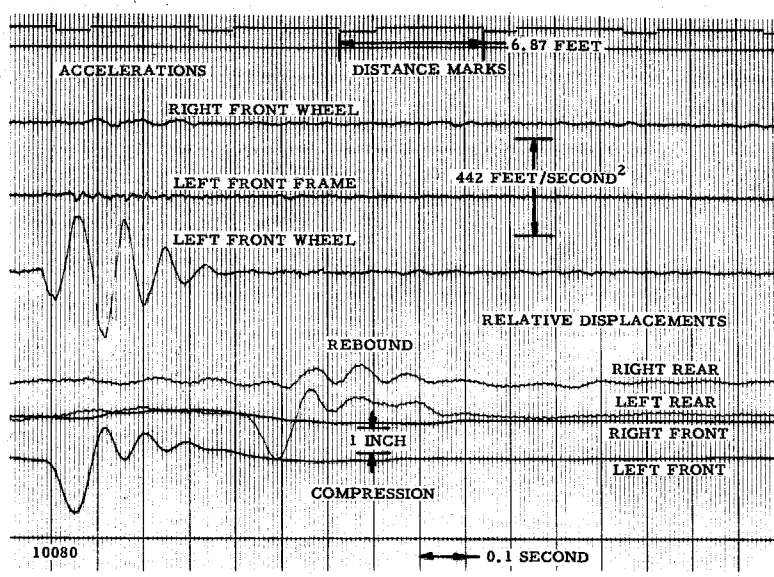

Figure 16. Vehicle record obtained in going over a half-sine bump with the left wheels only, at 15 miles per hour.

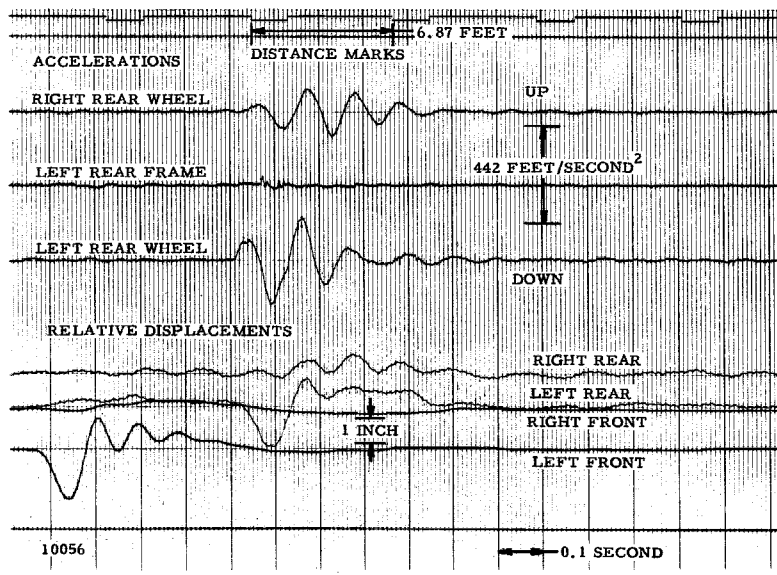

Figure 17. Vehicle record obtained in going over a half-sine bump with the left wheels only, at 15 miles per hour.

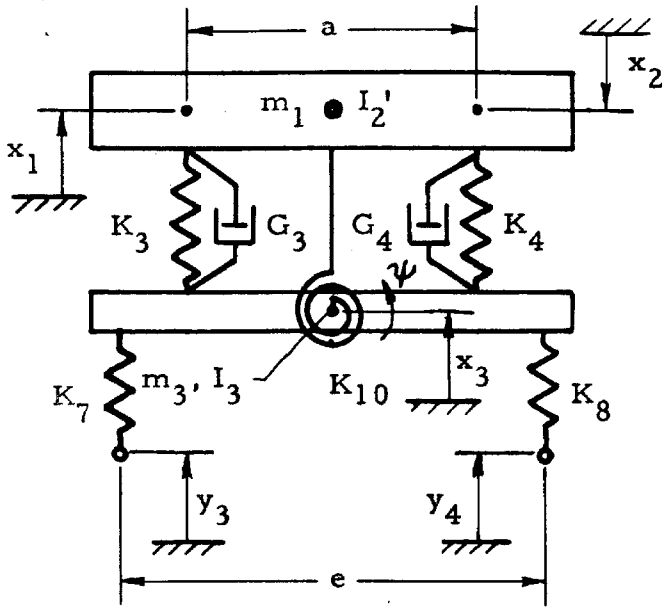

Equations of Motion

$$(\frac{m_1}{4}+\frac{I_2'}{a^2})p\,\dot{x}_1 - (\frac{m_1}{4}-\frac{I_2'}{a^2})p\,\dot{x}_2 + (G_3+\frac{K_3}{p})(\dot{x}_1 - \dot{x}_3 + \frac{a}{2}\dot{\psi}) + \frac{K_{10}}{a^2 p}(\dot{x}_1+\dot{x}_2+a\dot{\psi}) = 0.$$

$$-(\frac{m_1}{4}-\frac{I_2'}{a^2})p\,\dot{x}_1 + (\frac{m_1}{4}+\frac{I_2'}{a^2})p\,\dot{x}_2 + (G_4+\frac{K_4}{p})(\dot{x}_2+\dot{x}_3+\frac{a}{2}\dot{\psi}) + \frac{K_{10}}{a^2 p}(\dot{x}_1+\dot{x}_2+a\dot{\psi}) = 0.$$

$$m_3 p\,\dot{x}_3 - (G_3+\frac{K_3}{p})(\dot{x}_1 - \dot{x}_3 + \frac{a}{2}\dot{\psi}) + (G_4+\frac{K_4}{p})(\dot{x}_2+\dot{x}_3+\frac{a}{2}\dot{\psi}) + \frac{K_7}{p}(\dot{x}_3 - \frac{e}{2}\dot{\psi} - \dot{y}_3)$$
$$+ \frac{K_8}{p}(\dot{x}_3 + \frac{e}{2}\dot{\psi} - \dot{y}_4) = 0.$$

$$I_3 p + \frac{a}{2}(G_3+\frac{K_3}{p})(\dot{x}_1 - \dot{x}_3 + \frac{a}{2}\dot{\psi}) + \frac{a}{2}(G_4+\frac{K_4}{p})(\dot{x}_2+\dot{x}_3+\frac{a}{2}\dot{\psi}) + \frac{K_{10}}{a\,p}(\dot{x}_1+\dot{x}_2+a\dot{\psi})$$
$$- \frac{e\,K_7}{2p}(\dot{x}_3 - \frac{e}{2}\dot{\psi} - \dot{y}_3) + \frac{e\,K_8}{2p}(\dot{x}_3 + \frac{e}{2}\dot{\psi} - \dot{y}_4) = 0.$$

Operator, $p = \frac{d}{dt}$.

Figure 18. Four degree-of-freedom system for representing motion of the rear axle.

VI. APPLICATION OF THE ELECTRIC ANALOG COMPUTER TO THE ANALYSIS

To obtain solutions to the equations of motion for arbitrary input functions in a reasonable time, computers are a necessity, especially when some of the terms are non-linear. A small analog computer was available for this purpose. The use of this type of computer for obtaining solutions is based on the fact that the mathematical equations describing the reaction of electrical circuits containing inductors, resistors, and condensers, are the same as those for analogous mechanical systems. Reference 18 will serve to introduce the reader to the method used. It is possible to obtain non-linear electrical elements by using electronic amplifiers and other equipment; these methods are described in Reference 19.

Figure 19 is an overall view of the computer used. Rack "A" contains inductors, condensers, resistors, and transformers. Values for the various elements can be selected to three significant figures. At the top of Rack "B" are synchronous switches used to start the solution. Below these are located D-C amplifiers and the photoformers used here as input function generators. On the table are a dual-beam cathode ray oscillograph on which the solutions were displayed and photographed with the record camera, and a 1000 c/sec timing fork used to furnish a time base on the oscillograph records.

Electrical analogies for the mechanical systems in Figures 14, 15, and 18 are given in Figures 20, 21, and 22, together with the equations describing them. The mechanical-to-electrical conversion equations are presented in Table 1. Substitution of the conversion equations into the analog equations will yield the equations

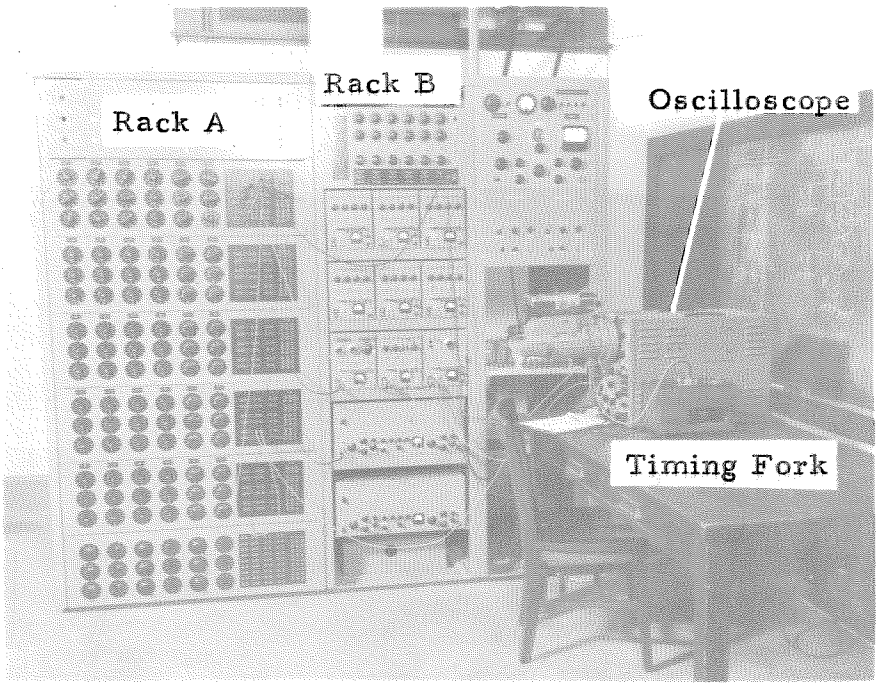

Figure 19. Overall view of analog computer.

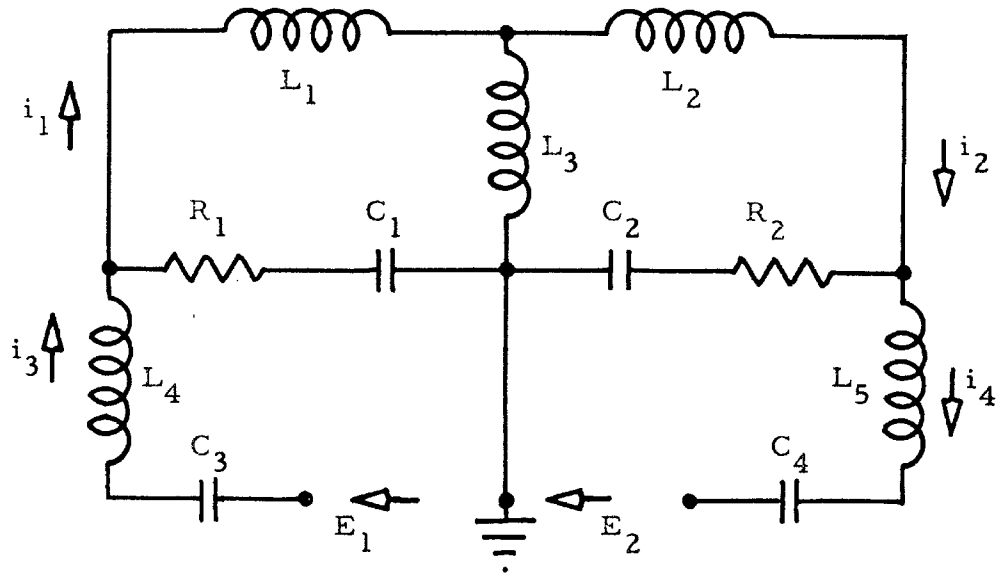

Circuit Equations

$$(L_1 + L_3)\bar{p}\,i_1 - L_3\bar{p}\,i_2 + (R_1 + \frac{1}{C_1\bar{p}})(i_1 - i_3) = 0$$

$$- L_3\,\bar{p}\,i_1 + (L_2 + L_3)\,\bar{p}\,i_2 + (R_2 + \frac{1}{C_2\bar{p}})(i_2 - i_4) = 0$$

$$L_4\,\bar{p}\,i_3 - (R_1 + \frac{1}{C_1\bar{p}})(i_1 - i_3) + \frac{1}{C_3\bar{p}}\,i_3 = E_1$$

$$L_5\,\bar{p}\,i_4 - (R_2 + \frac{1}{C_2\bar{p}})(i_2 - i_4) + \frac{1}{C_4\bar{p}}\,i_3 = E_2$$

Operator, $\bar{p} = \frac{d}{d\bar{t}}$.

Figure 20. Electrical analogy of the four-degree-of-freedom system used to represent an automobile in symmetric motion.

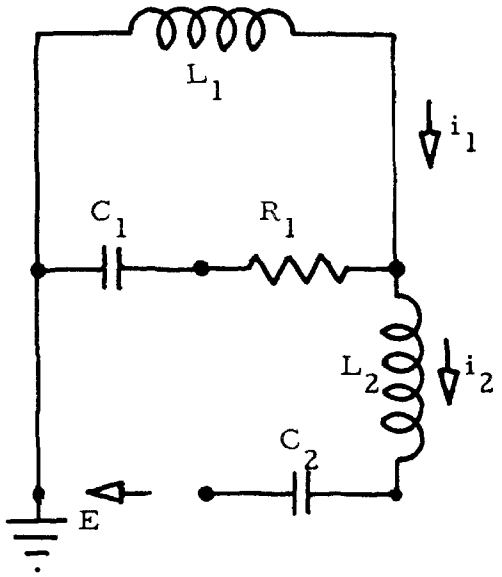

Circuit Equations

$$L_1 \bar{p}\, i_1 + (R_1 + \frac{1}{C_1 \bar{p}})(i_1 - i_2) = 0$$

$$L_2 \bar{p}\, i_2 - (R_1 + \frac{1}{C_1 \bar{p}})(i_1 - i_2) + \frac{1}{C_2 \bar{p}}\, i_2 = E$$

Operator, $\bar{p} = \frac{d}{d\bar{t}}$.

Figure 21. Electrical analogy of the two-degree-of-freedom system.

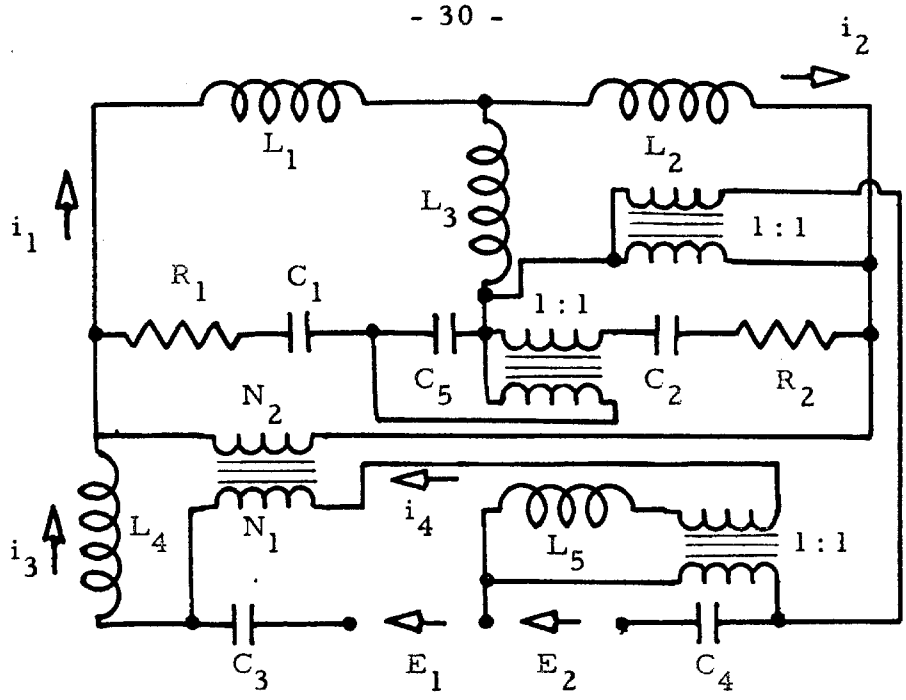

Circuit Equations

$$(L_1 + L_3)\bar{p}\,i_1 - L_3\bar{p}\,i_2 + (R_1 + \frac{1}{C_1\bar{p}})(i_1 - i_2 + \frac{N_1}{N_2}i_4) + \frac{1}{C_5\bar{p}}(i_1 + i_2 + \frac{2N_1}{N_2}i_4) = 0$$

$$-L_3\bar{p}\,i_1 + (L_2 + L_3)\bar{p}\,i_2 + (R_2 + \frac{1}{C_2\bar{p}})(i_2 + i_3 + \frac{N_1}{N_2}i_4) + \frac{1}{C_5\bar{p}}(i_1 + i_2 + \frac{2N_1}{N_2}i_4) = 0$$

$$L_4\bar{p}\,i_3 - (R_1 + \frac{1}{C_1\bar{p}})(i_1 - i_2 + \frac{N_1}{N_2}i_4) + (R_2 + \frac{1}{C_2\bar{p}})(i_2 + i_3 + \frac{N_1}{N_2}i_4) + \frac{1}{C_3\bar{p}}(i_2 - i_4)$$

$$+ \frac{1}{C_4\bar{p}}(i_2 + i_4) = E_1 + E_2$$

$$L_5\bar{p}\,i_4 + \frac{N_1}{N_2}(R_1 + \frac{1}{C_1\bar{p}})(i_1 - i_2 + \frac{N_1}{N_2}i_4) + \frac{N_1}{N_2}(R_2 + \frac{1}{C_2\bar{p}}(i_2 + i_3 + \frac{N_1}{N_2}i_4)$$

$$+ \frac{2N_1}{N_2C_5\bar{p}}(i_1 + i_2 + \frac{2N_1}{N_2}i_4) - \frac{1}{C_3\bar{p}}(i_3 - i_4) + \frac{1}{C_4\bar{p}}(i_3 + i_4)$$

$$= -E_1 + E_2$$

Operator, $\bar{p} = \frac{d}{dt}$.

Figure 22. Electrical analogy of the four-degree-of-freedom rear axle system.

Table 1

Mechanical to Electrical Conversion Formulas

Item Converted	Computer Quantity	Value in Terms of Mechanical Quantity
Mass to inductance-	L	$(f^2/N^2)M$
Viscous damping to resistance-	R	$(f^2/N)G$
Spring constant to capacitance-	C	$1/f^2K$
Velocity to current-	i	$N\dot{x}/kf$
Force to voltage-	e	$(f/k)F$
Operator-	$\bar{p}$	Np
Time-	$\bar{t}$	$(1/N)t$
Energy level-	$\bar{U}$	$(1/k^2)U$

for the respective mechanical systems. Values of the conversion constants used are given in Appendix III. In order to include the effects of the non-linear vehicle properties, certain circuits must be substituted for some of the elements shown in the electrical analogies. The circuits used to approximate the variation in the main suspension spring rates and shock absorber rates, and the effect of the tire leaving the ground, as well as the method of generating the input function, are presented in Appendix III.

In order to determine the overall accuracy of the computer, the solution obtained from the computer for the case of the two degree-of-freedom system going over the half-sine bump at 15 miles per hour was compared with the exact solution obtained analytically. Non-linearities were not included. The analytical solution is derived in Appendix IV. Comparison of these solutions as given in Figure 23 indicates that the agreement during the first two feet of travel is almost exact. The discrepancies in the amplitudes obtained for the free vibration are less than 10 per cent of the maximum amplitudes. Reading of the oscillograph records from the computer was limited to an accuracy of about 5 per cent for a deflection of one-half inch on the screen. The overall accuracy of the computer as used may be taken as five to ten per cent.

Reproducibility of the computer results is illustrated in Figures 24 and 25. Other than the shifting of the scales, the patterns are almost identical. Any difference in Figure 24 has approximately the same magnitude as the noise. The noise level is about 15 to 20 millivolts and can be seen on the right, at the start of the traces in Figure 24. This noise is inherent in the electronic equipment, i.e., photoformers and amplifiers, used.

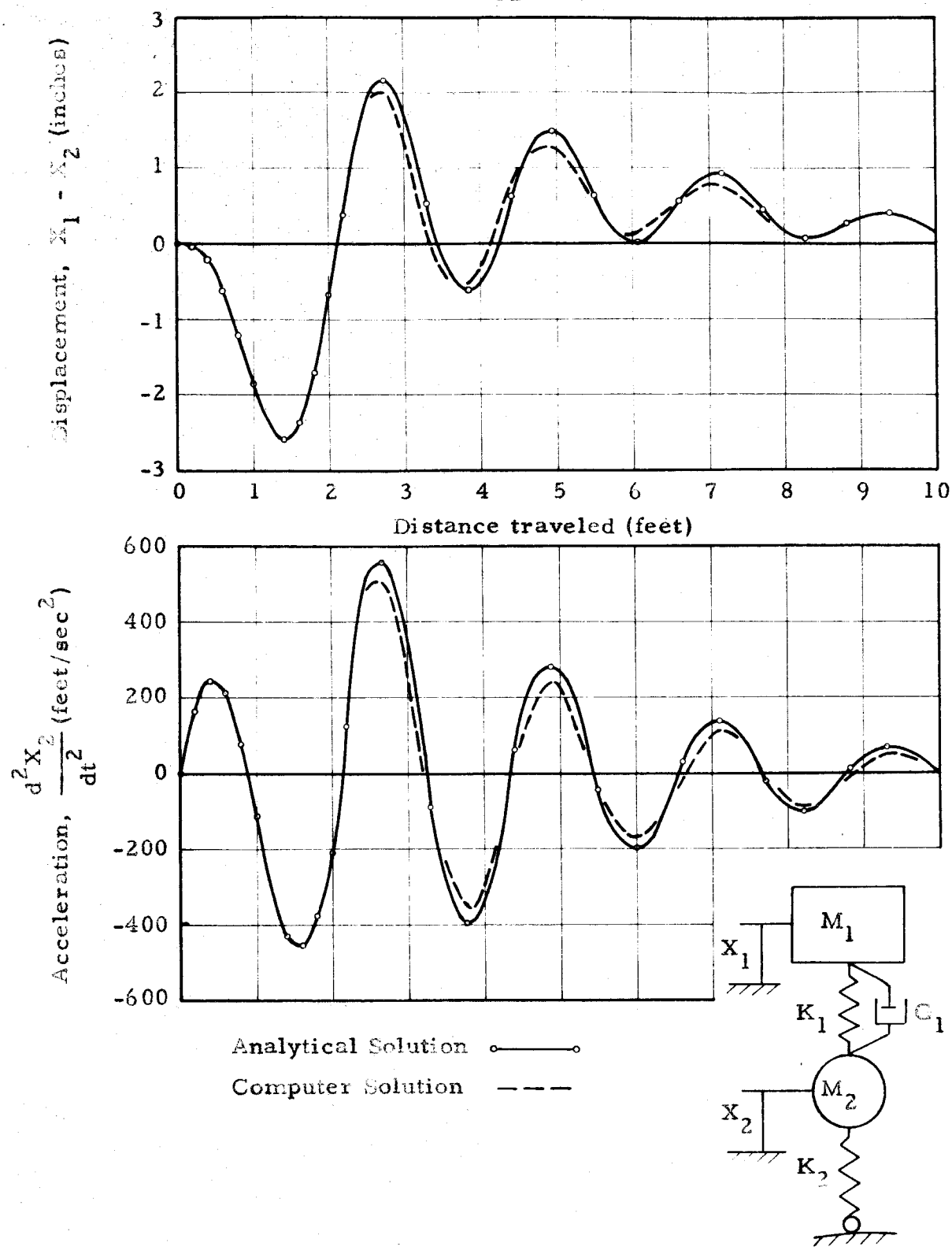

Figure 23. Comparison of computer and analytical solutions for a linear system going over a half-sine bump at 15 miles per hour.

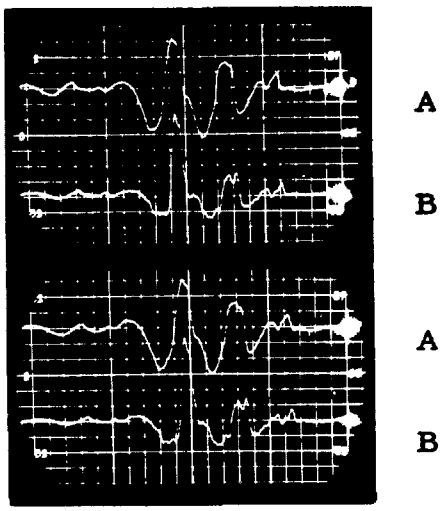

A = relative displacement.
B = acceleration of frame.

Figure 24. Computer reproducibility, rear motion over test dip at 25 miles per hour.

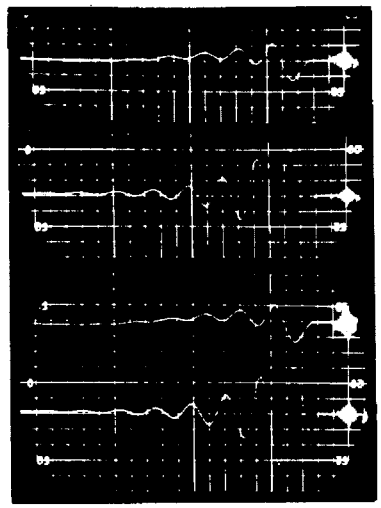

A = relative displacement.
B = acceleration of wheels.

Figure 25. Computer reproducibility, front motion over half-sine bumps at 15 miles per hour.

4 degree-of-freedom system

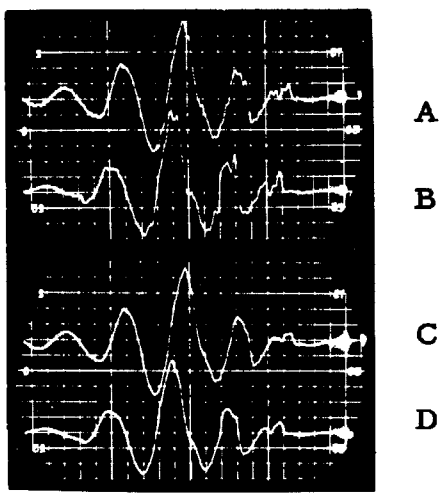

2 degree-of-freedom systems

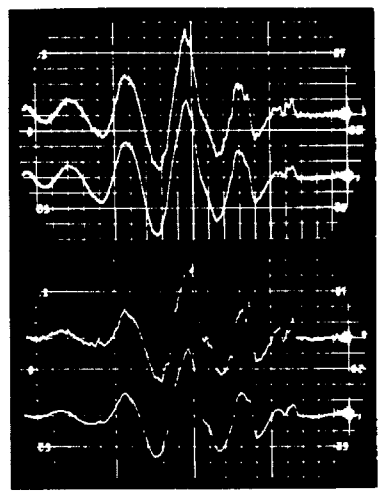

A = acceleration of frame at front.
B = acceleration of frame at rear.
C = relative displacement at front.
D = relative displacement at rear.

Figure 26. Comparison of two 2 degree-of-freedom systems with a 4 degree-of-freedom system.

VII. RESULTS

Comparisons of Vehicle Tests and Analysis

The results are presented in the form of graphical comparisons of the records obtained by testing the vehicle and by the computer.

Linear systems were used first in the computer studies in order to determine how much could be learned in spite of this simplifying assumption. The assumption that the front-to-rear mass coupling term could be neglected when considering symmetric motion was checked on the computer and found to be valid. Figure 26 shows the agreement between the records of two two-degree-of-freedom systems and the four-degree-of-freedom system which they replace. The two-degree-of-freedom systems were used in all succeeding studies of symmetric motion. This means that the motions at the front and rear were considered separately.

Records showing the response of the vehicle in going over the test dip are reproduced in Figures 27 to 30. The measurements used in these comparisons are the relative displacements between the frame and the wheels, and the accelerations of the sprung mass. Low frequency motion of the sprung mass on its suspension predominated, and higher frequency motion of the unsprung mass as well as noise present in the frame largely due to the engine were neglected. The vehicle measurements plotted are an average of those made on the left and right hand sides, since the motion was not exactly symmetric. In Figures 27 to 30 the system used to represent the vehicle is shown together with the curves. The system consists of the sprung mass, unsprung mass, springs, and damping device. The computer solutions

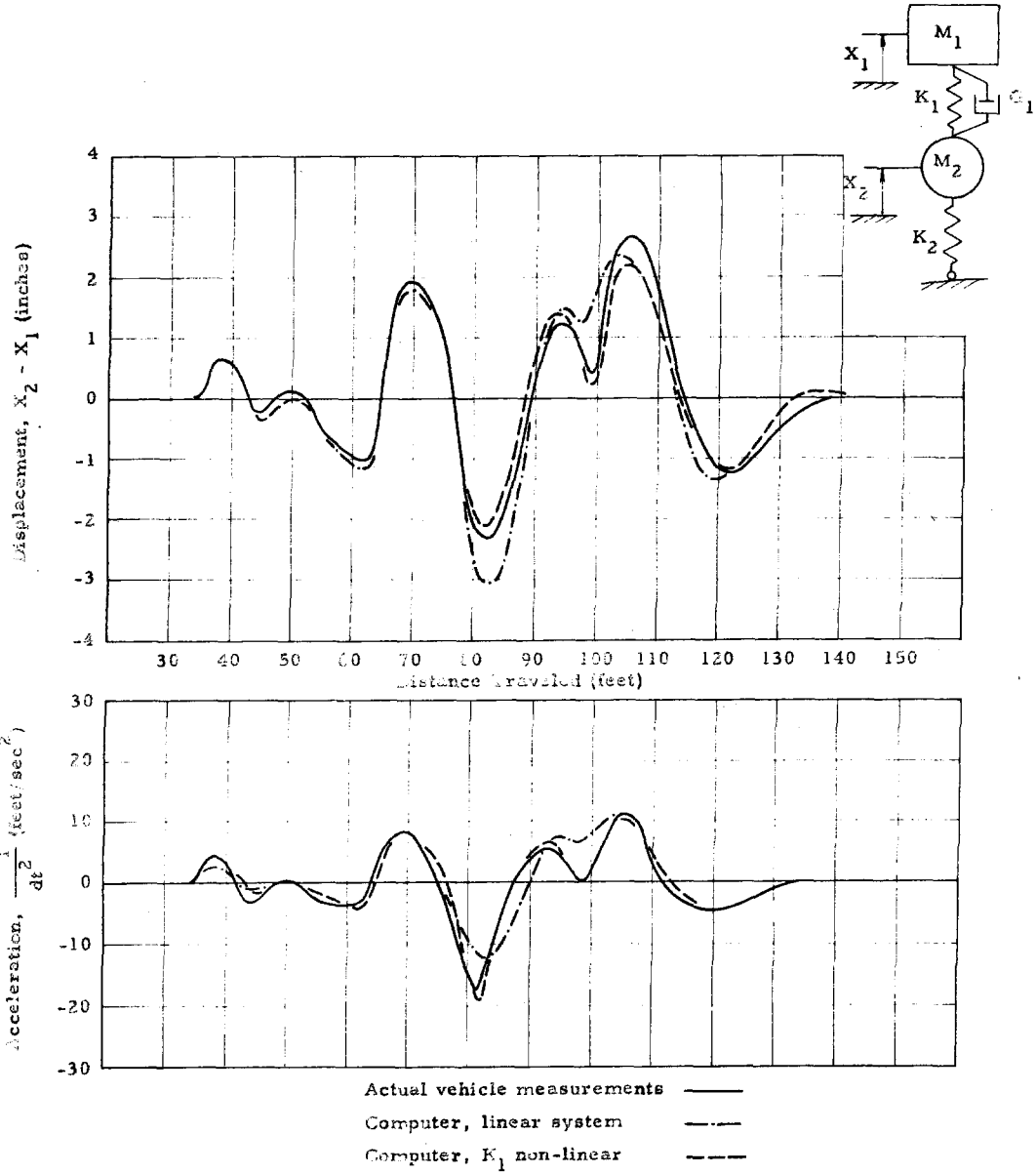

Figure 27. Motion at front wheels in going over test dip at 20 miles per hour.

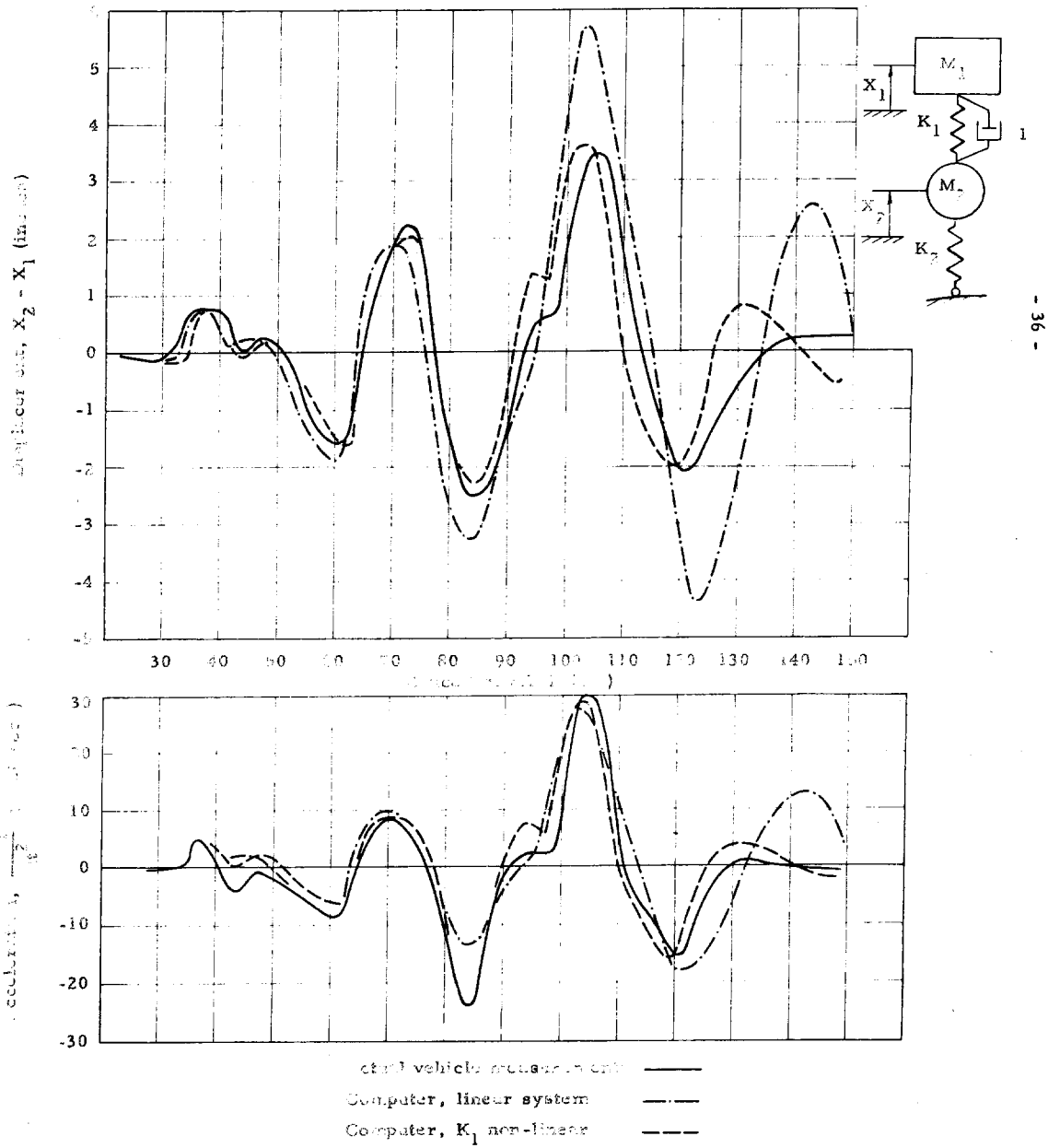

Figure 26. Motion at front wheels in going over test dip at 25 miles per hour.

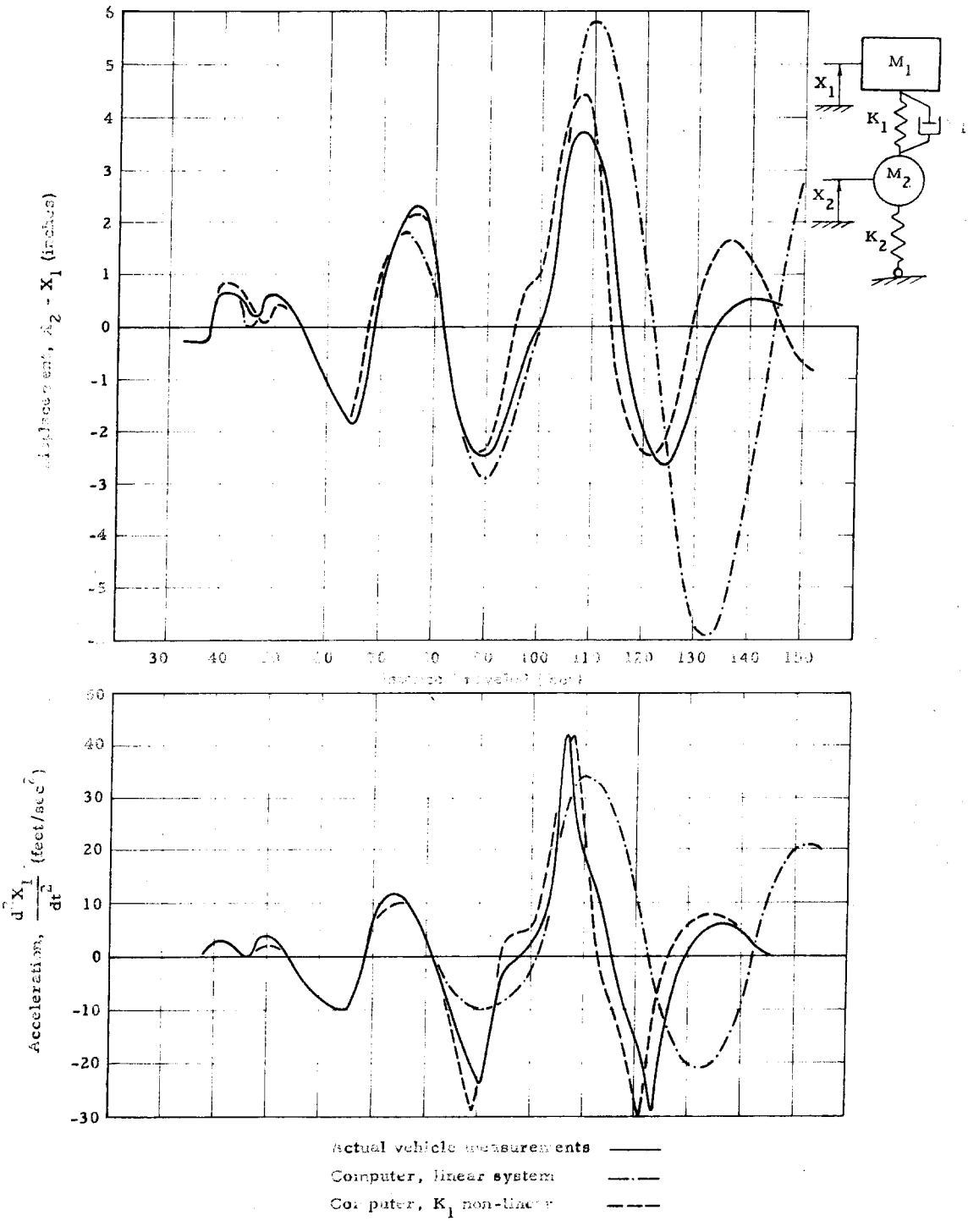

Figure 29. Motion at front wheels in going over test dip at 20 miles per hour.

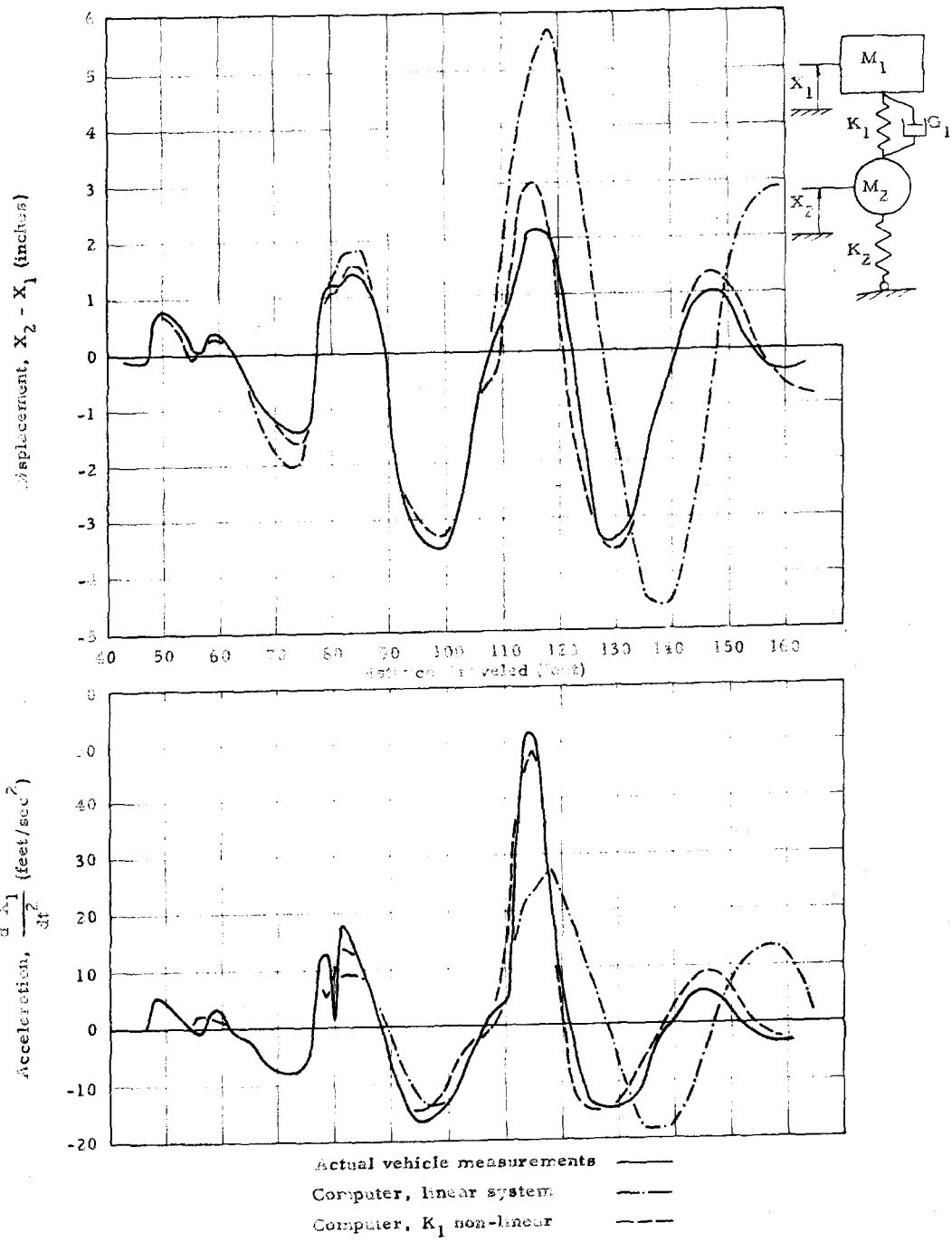

Figure 30. Motion at rear wheels in going over test dip at 75 miles per hour.

appear only where they depart from the vehicle measurements. Both linear and non-linear systems were used, and the results from both are shown. The only non-linearity taken into account was that of the main suspension spring on account of the rubber bump stops. Figures 27 to 29 give the response at the front for speeds of 20, 25, and 28 miles per hour, respectively. The response at the rear at 25 miles per hour is shown in Figure 30. For these results the tire pressure was 24 psi gage, and the values of viscous damping used for each wheel in the front and rear were 44.0 slug/sec and 47.8 slug/sec, respectively.

Motions at the front wheels in going over the half-sine bumps symmetrically at 10, 15, and 20 miles per hour are shown in Figures 31, 32, and 33. Measurements used for comparison in the cases of half-sine-bump excitation were the accelerations of the wheels and the relative displacements between the wheels and the frame. The vehicle results for symmetric motion are the averages of the measurements obtained on the right and left hand sides of the car. Tire pressures for these records, as well as those in Figures 34 and 35, were maintained at 24 psi gage. Here again, results are presented both considering the system completely linear and taking certain non-linearities into account. The value of viscous suspension damping, G_1, was taken as 44.0 slug/sec per wheel. In the non-linear cases, non-linear damping and the effect of the tire leaving the ground were considered.

It became evident, by comparing the first non-linear studies made using the system of Figure 17 with vehicle tests for motion over the half-sine bumps, that additional damping was present in

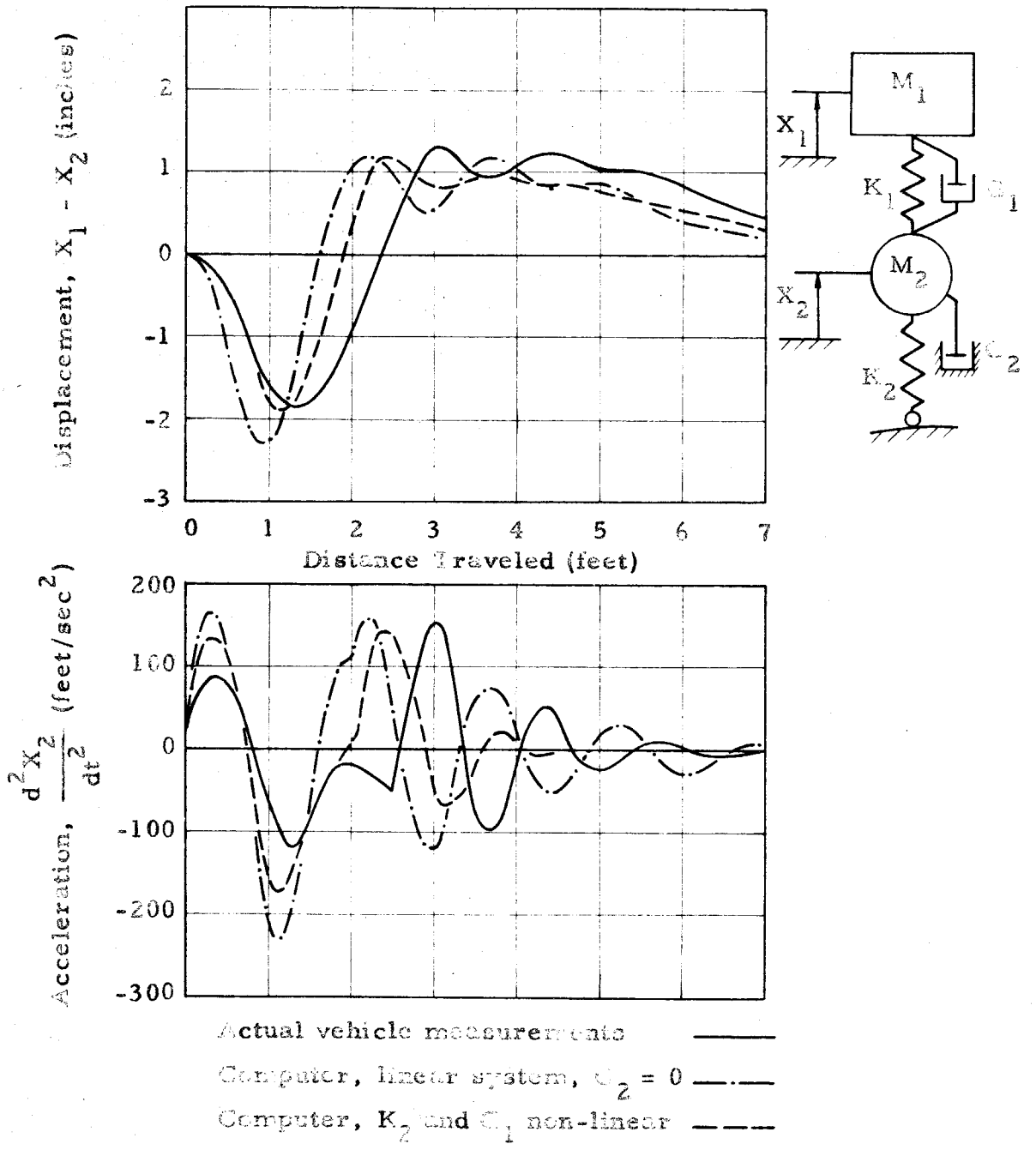

Figure 31. Motion at front wheels in going over symmetric half-sine bumps at 10 miles per hour.

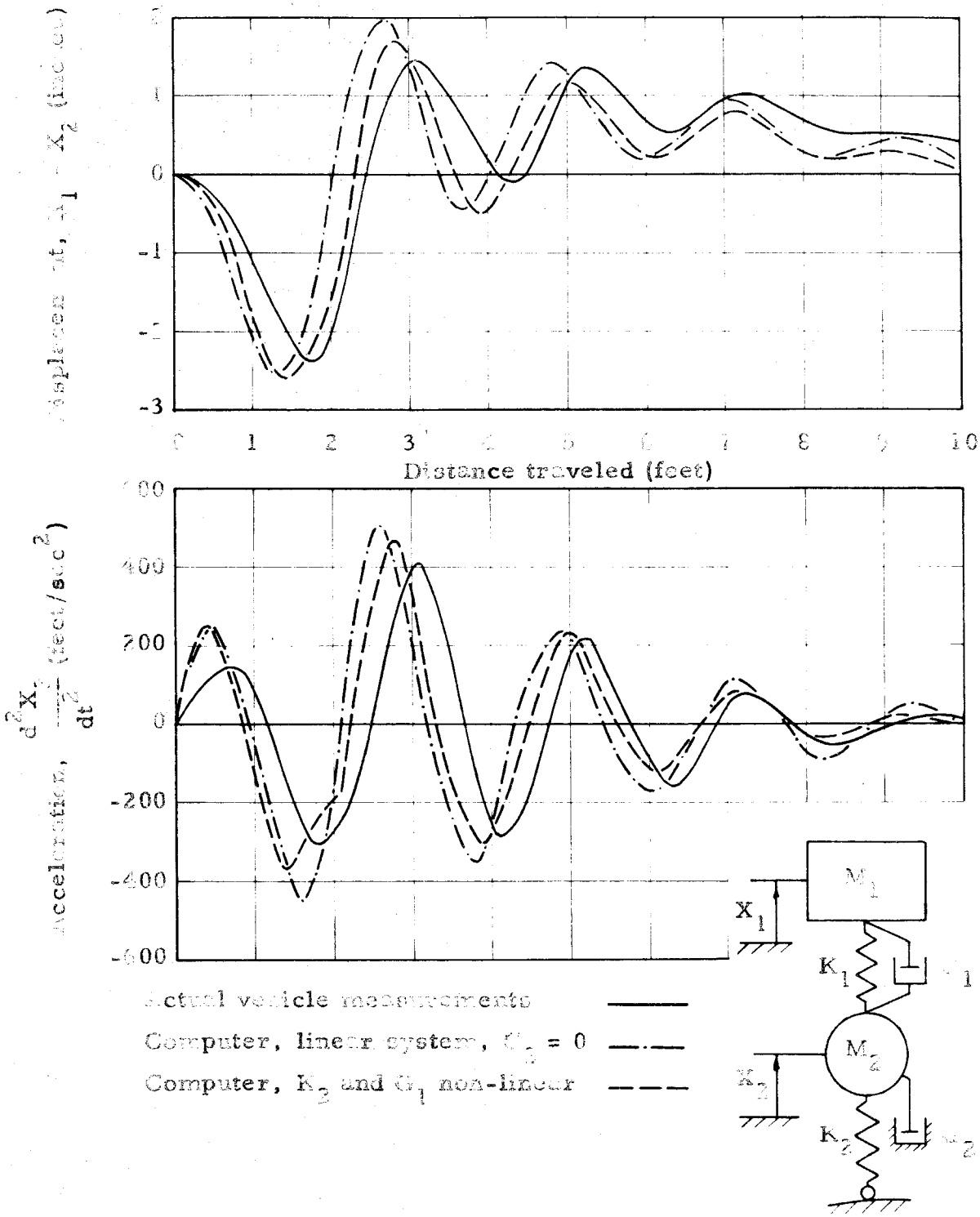

Figure 32. Motion of front wheels in going over symmetric half-sine bumps at 15 miles per hour.

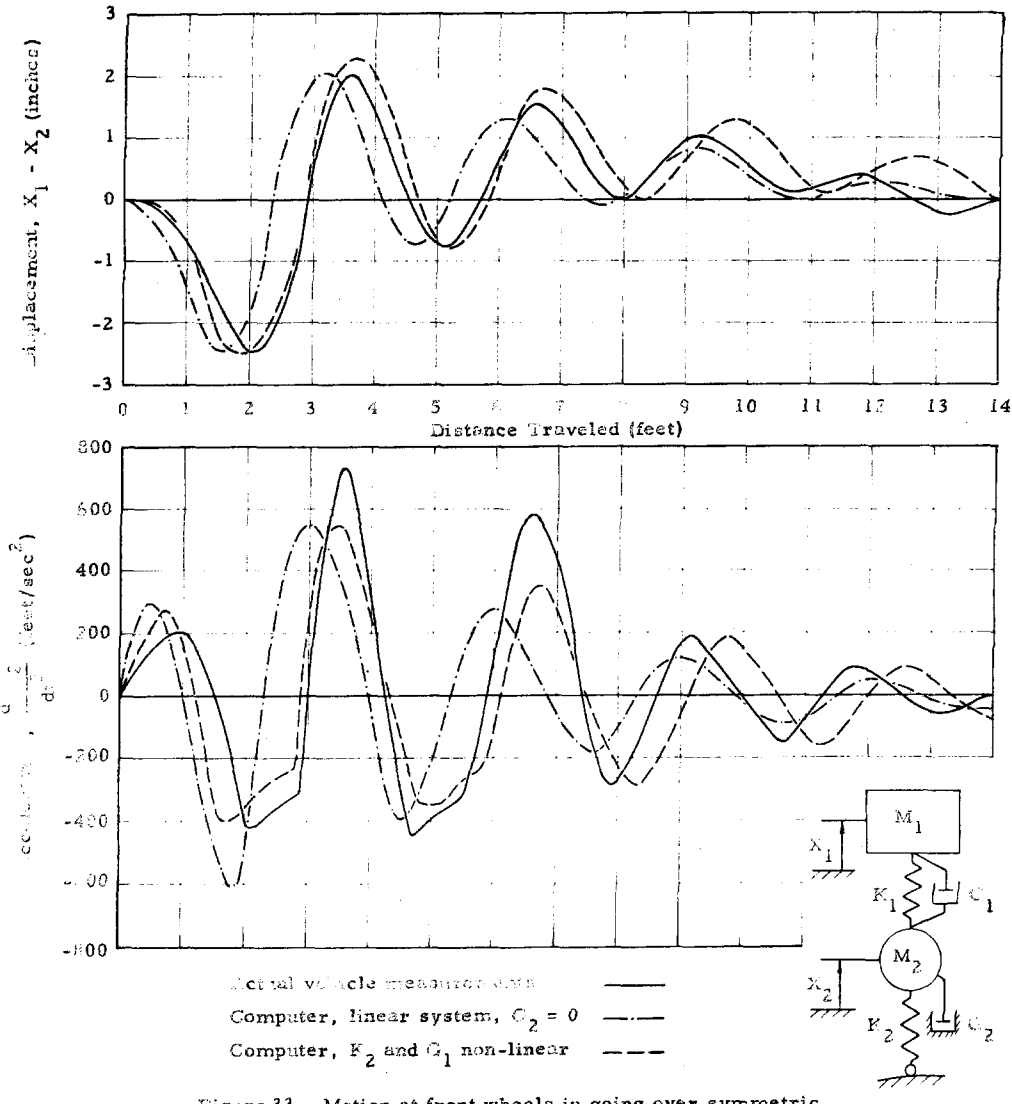

Figure 33. Motion at front wheels in going over symmetric half-sine bumps at 20 miles per hour.

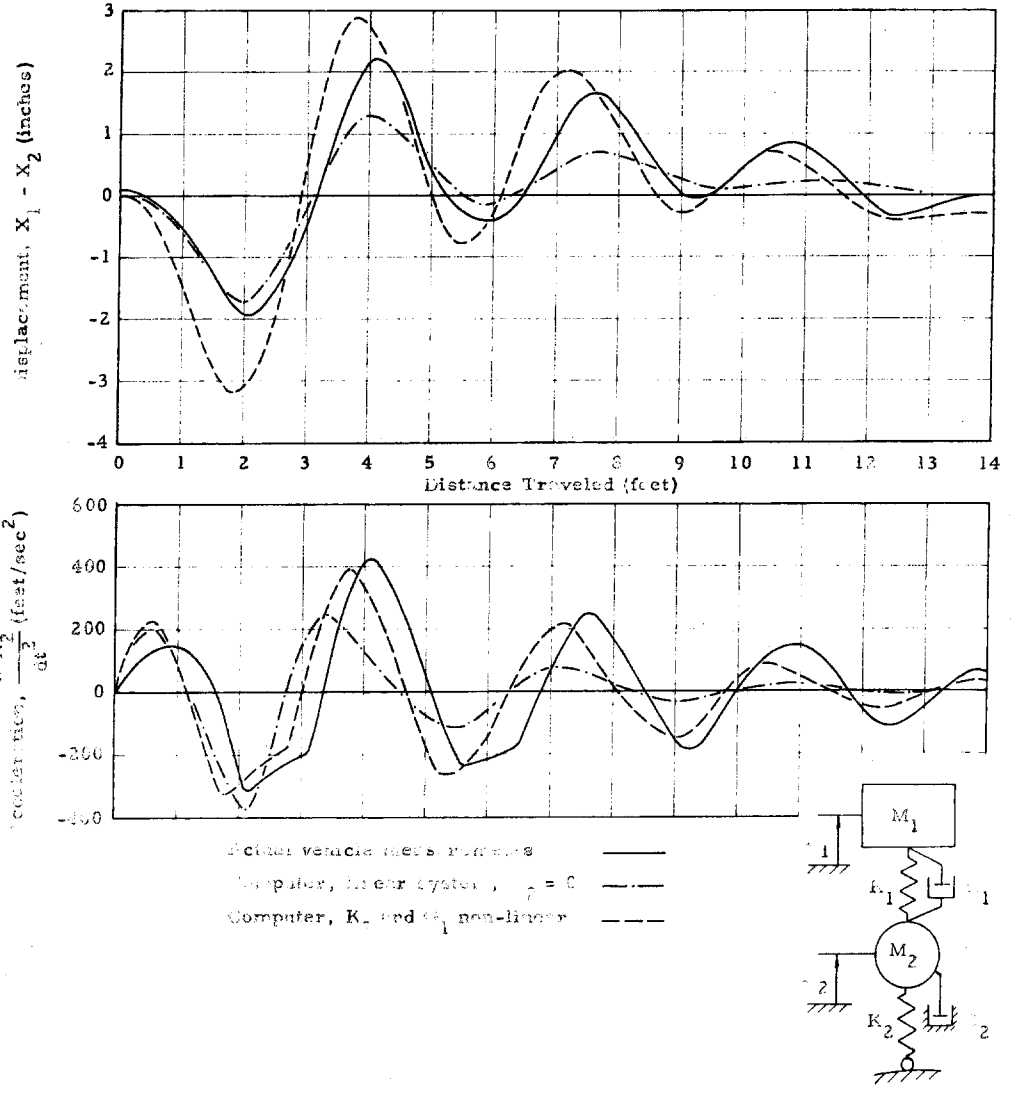

Figure 34. Motion at rear wheels in going over symmetric half-sine bumps at 20 miles per hour.

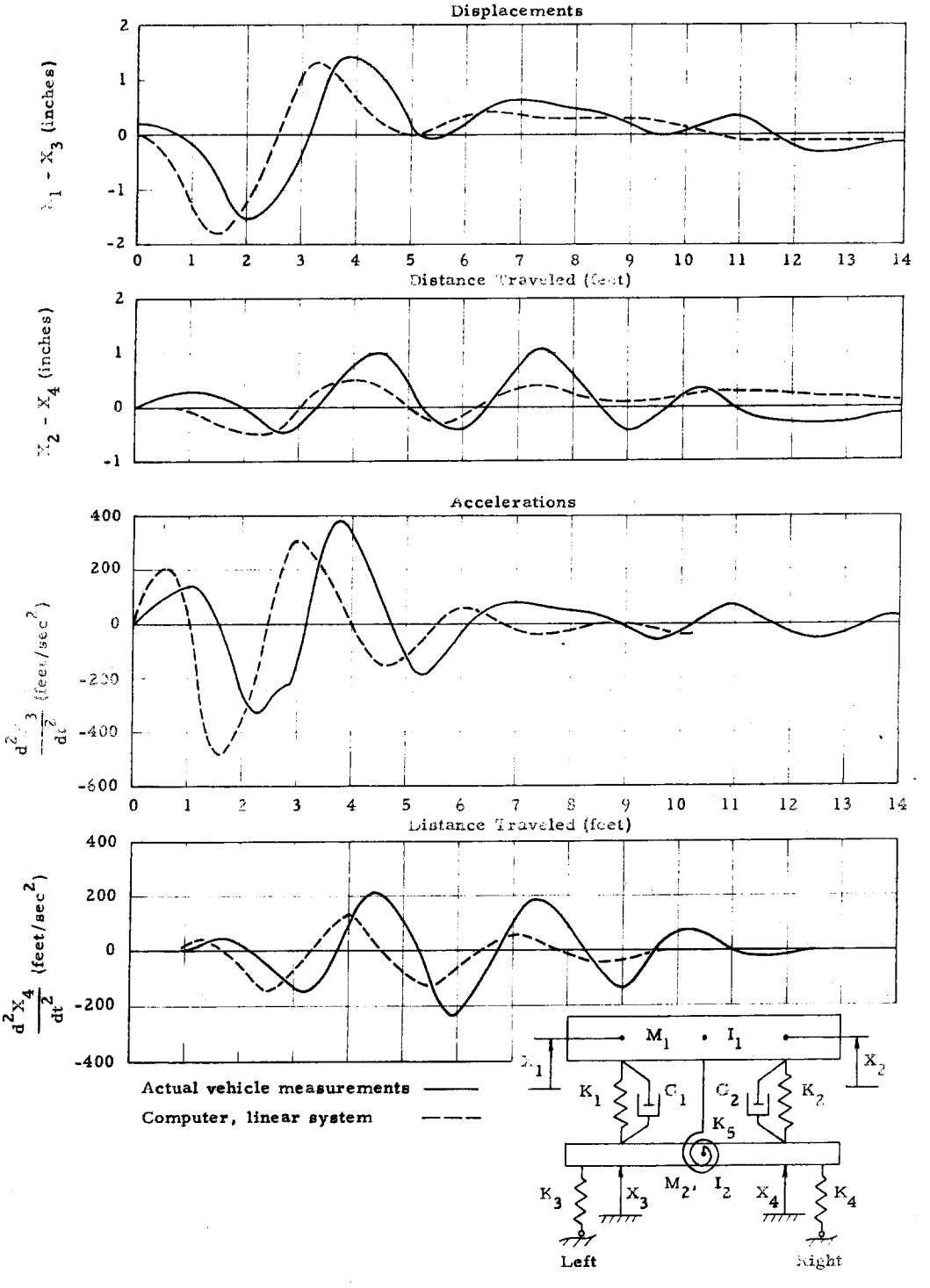

Figure 35. Motion of rear suspension in going over half-sine bump with left wheels only at 20 miles per hour.

the vehicle that was not taken into account in the analysis. The load-deflection curves obtained for the tires (Figure 52) exhibit a definite hysteresis loss in the tire. It was assumed then, that the additional damping not previously included was due to the tire and that it acted on the wheels, as indicated by G_2 (Figure 31). Different values of this damping were used at different speeds, 32 slug/sec at 10 miles per hour, 20.4 slug/sec at 15 miles per hour, and 2.6 slug/sec at 20 miles per hour, at each wheel, in order to obtain the agreement shown. At 10 miles per hour viscous damping of 25.5 slug/sec was added to the non-linear damping between the wheel and frame. This gave only slightly better results than adding this amount of damping to G_2.

Figure 34 depects the motion at the rear wheels in going over the half-sine bumps symmetrically at 20 miles per hour. Here, the value of viscous damping used in the linear case was 90.5 slug/sec at each wheel. Non-linear damping and the effect of the tire leaving the ground were included in the non-linear case, together with an additional damping, G_2, of 2.6 slug/sec at each wheel. The main suspension spring constants were used here as well as for the front, the effect of the suspension bump stops not being included.

The motion of the rear axle when the wheels on only one side of the test car were driven over a half-sine bump is shown in Figure 35. Computer records obtained by using the system indicated on the figure, assuming it to be linear, are compared with the actual vehicle measurements. A value of 90.5 slug/sec was used for the suspension damping on each side. No non-linear studies were made with this system.

Effects of Varying Parameters on the Computer

The effects of varying some of the parameters were studied on the computer for symmetric motions over both the test dip and half-sine bumps. Figure 36 shows the changes in the motion at the front wheels in going over the test dip at 25 miles per hour when the main suspension spring stiffness was varied. The profile of the test dip appears at the top of the figure.

Peak rebound relative displacement and downward acceleration of the frame at the front wheels in going over the test dip at 20 miles per hour varied as shown in Figure 37 when the rebound bump stop clearance was changed. When the stiffnesses of both the compression and rebound stops at the front were varied in going over the test dip at 25 miles per hour, the effects on the maximum compression and rebound relative displacements and on the peak frame accelerations were as plotted in Figure 38. The equivalent viscous damping at the rear was varied, and the resultant changes in peak relative displacements and frame accelerations are given in Figure 39 for motion over the test dip at 25 miles per hour.

The effect of changing the front main suspension spring stiffness is shown in Figure 40, for a linear system going over the half-sine bumps at 15 miles per hour. Varying the tire spring rate for a linear system affected the maximum accelerations of the front wheels in going over the half-sine bumps at 15 miles per hour as plotted in Figure 43.

A computer record showing the acceleration of the wheels, tire force, suspension spring force, main suspension damping force, and the acceleration of the frame for the car going over symmetric

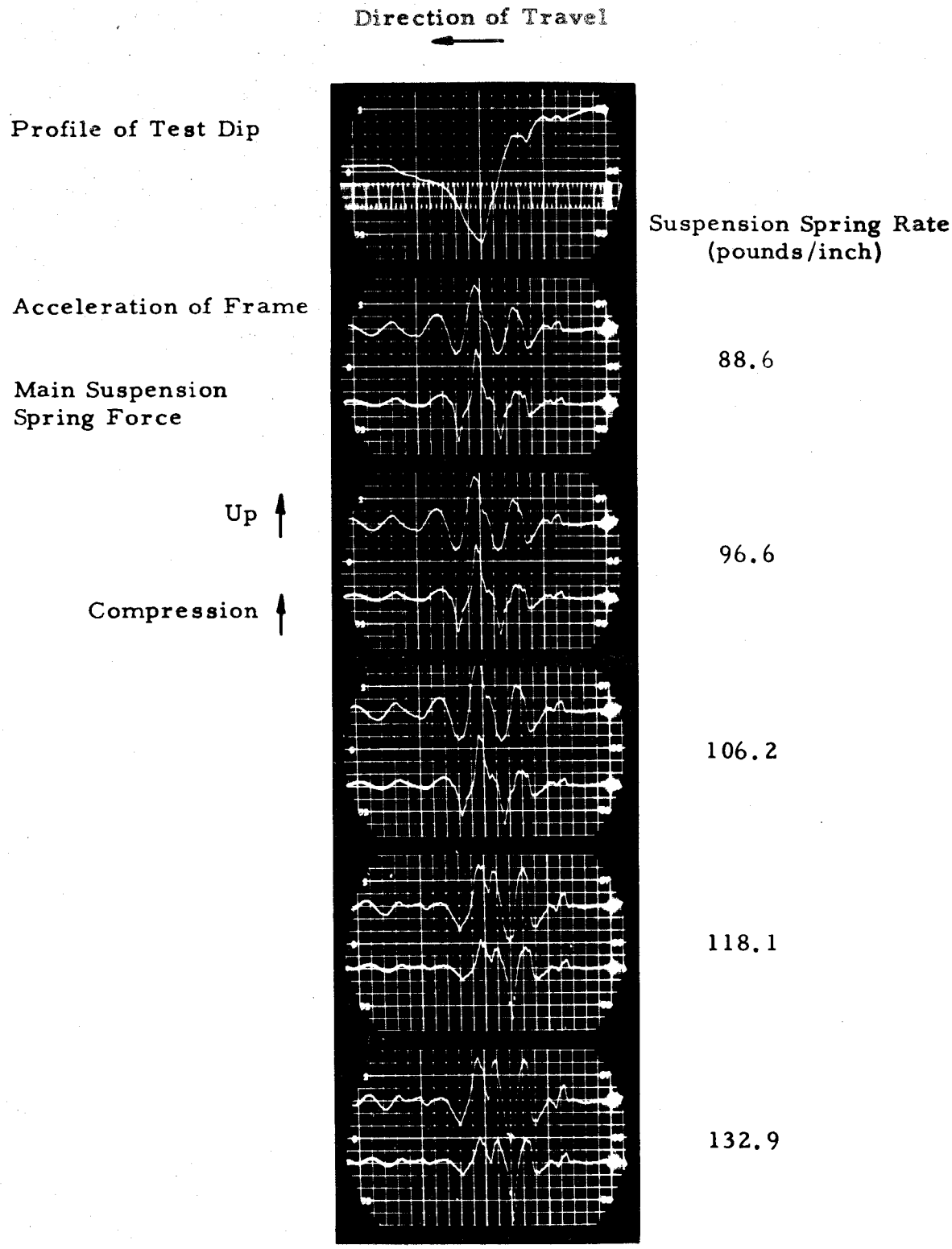

Figure 36. Effect of varying the main suspension spring rate on the motion at front wheels in going over test dip at 25 miles per hour.

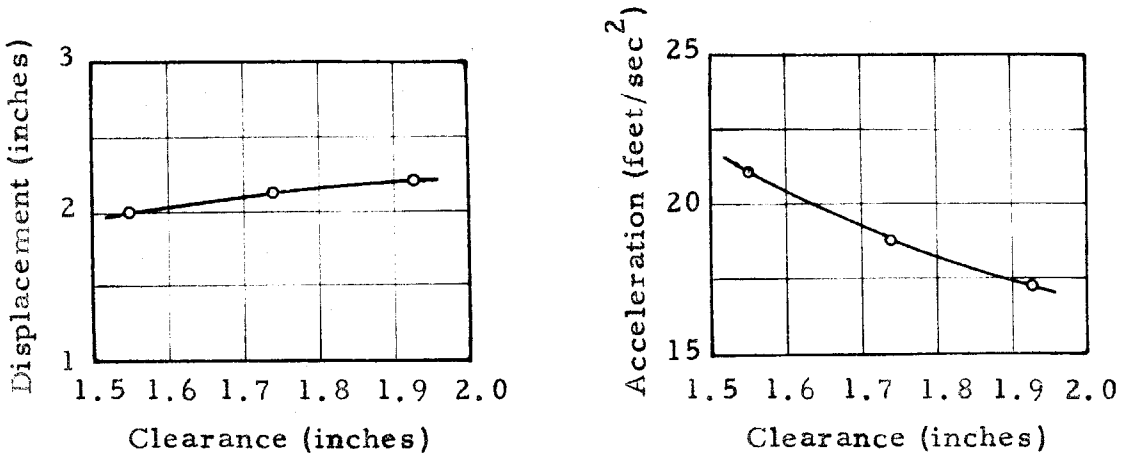

Figure 37. Effect of varying the rebound stop clearance at the front wheels in going over the test dip at 20 miles per hour.

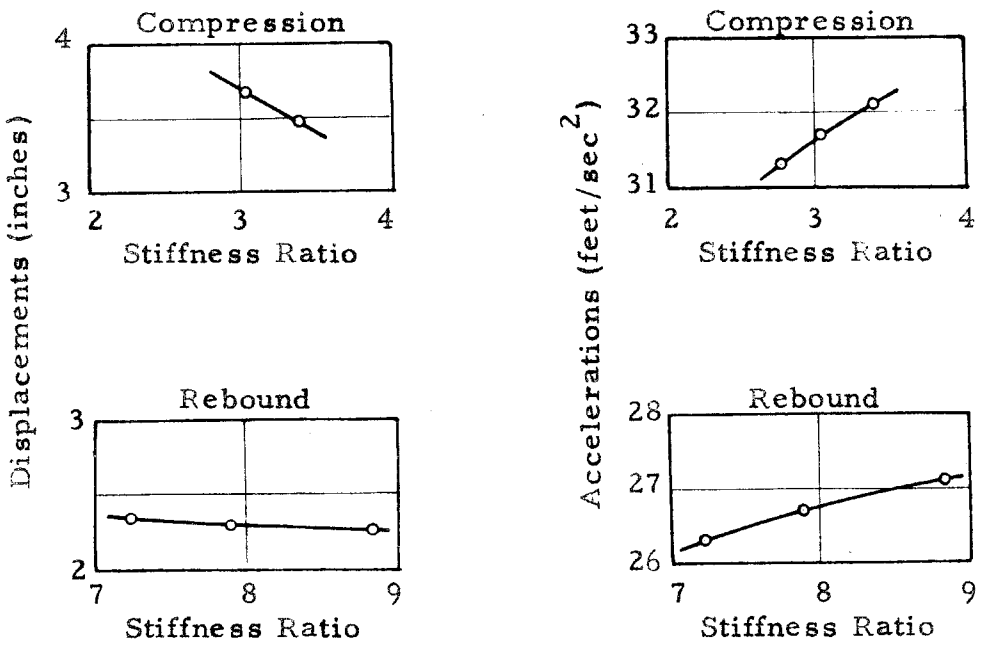

Figure 38. Effect of varying bump stop stiffnesses at the front wheels in going over the test dip at 25 miles per hour.

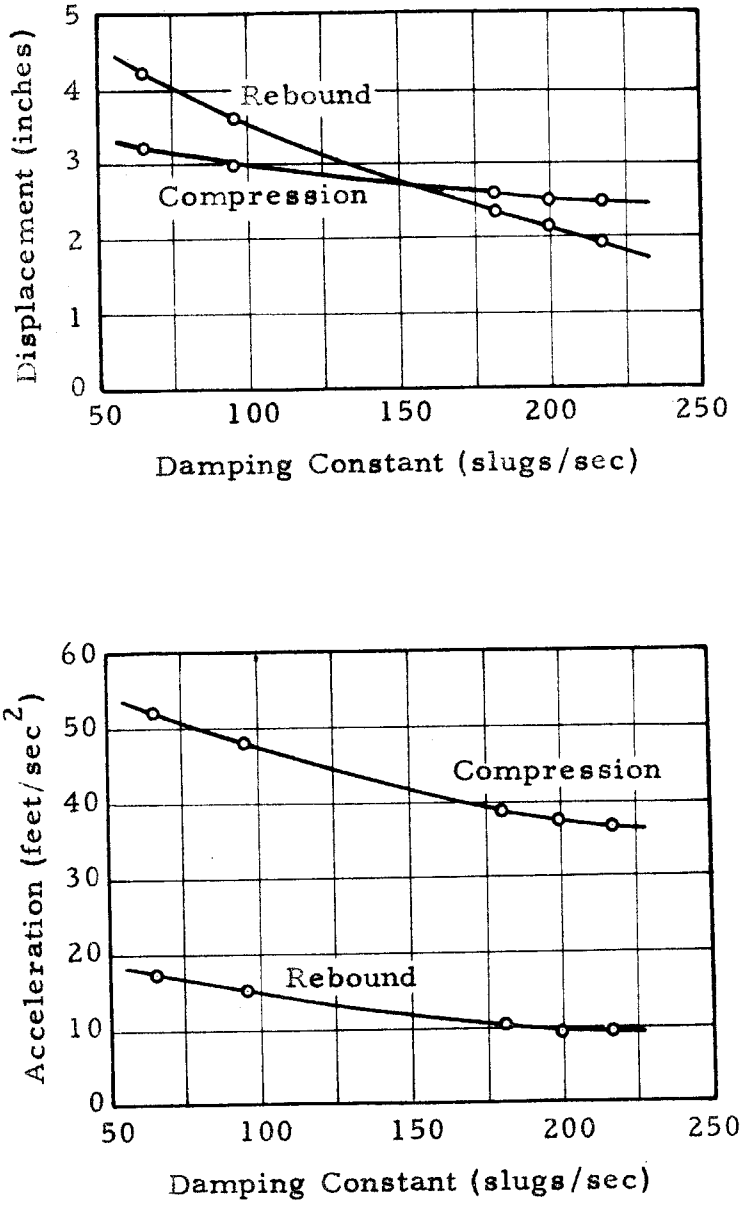

Figure 39. Effect of varying viscous suspension damping at the rear wheels in going over the test dip at 25 miles per hour.

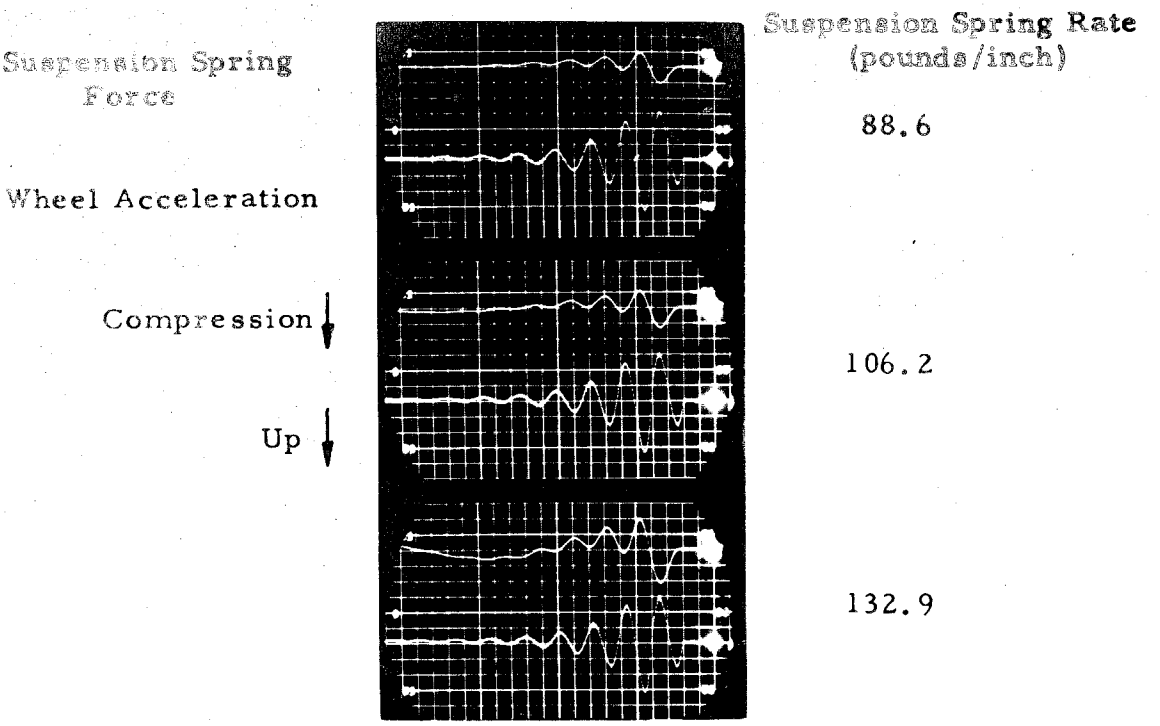

Figure 40. Effect of varying main suspension spring rate at front, over half-sine bumps at 15 miles per hour.

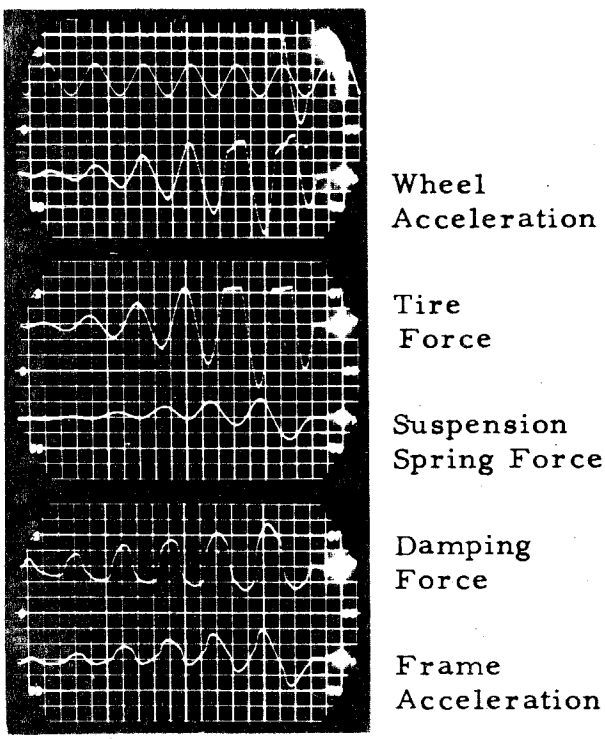

Figure 41. Computer record showing motion at front wheels, over half-sine bumps at 20 miles per hour.

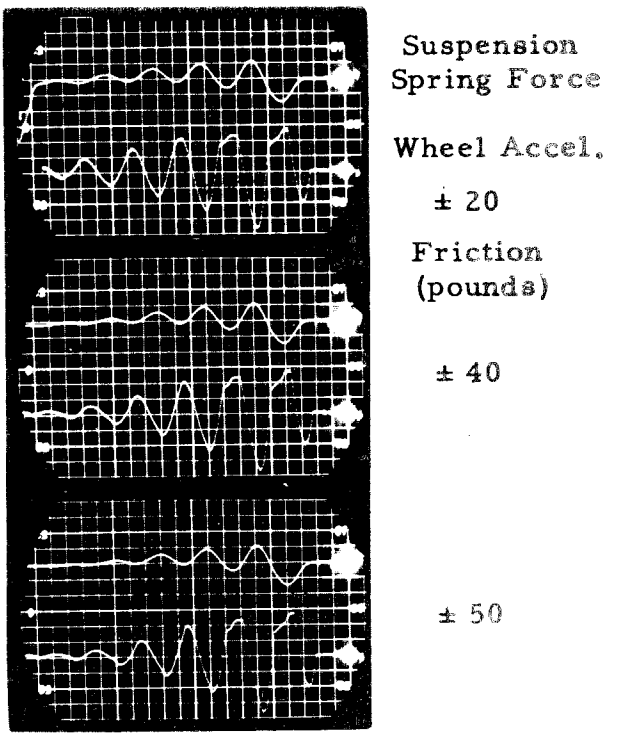

Figure 42. Effect of varying suspension static friction at front wheels, over half-sine bumps at 20 miles per hour.

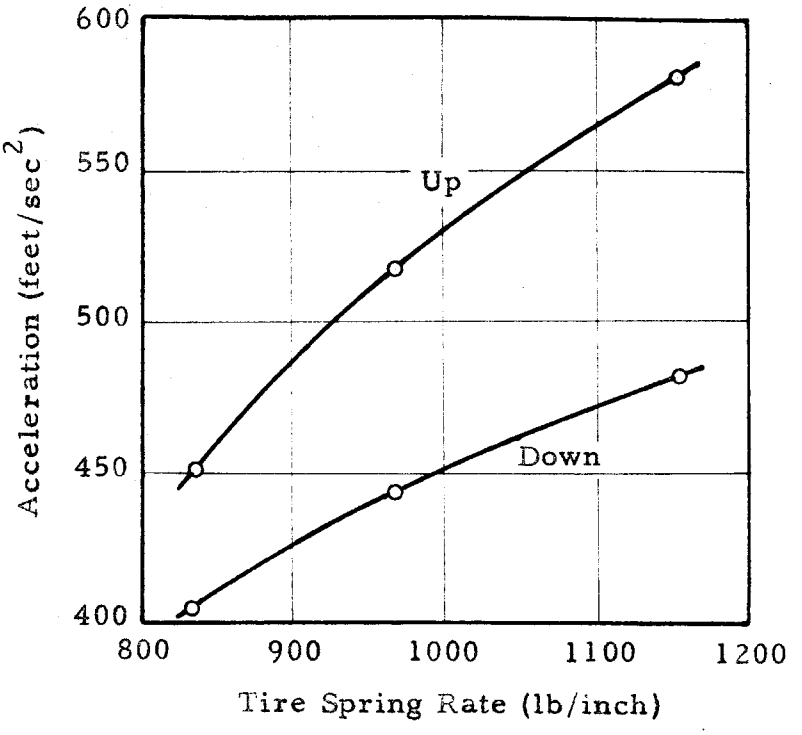

Figure 43. Effect of varying the tire spring rate at the front wheels, half-sine bumps, 15 miles per hour.

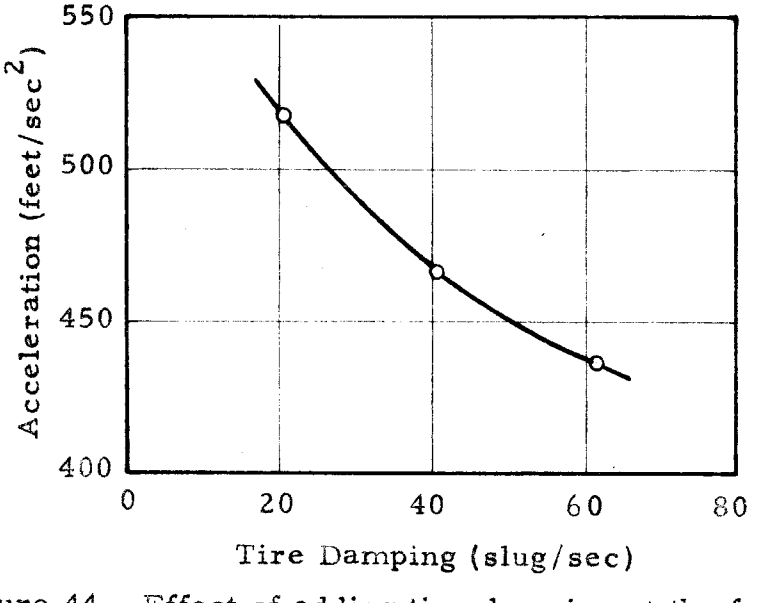

Figure 44. Effect of adding tire damping at the front wheels, half-sine bumps, 15 miles per hour.

half-sine bumps at 20 miles per hour appears in Figure 41. Non-linear damping and the effect of the tire leaving the ground were included. The damping force because of static friction was varied from the measured value, and records of the relative displacement and wheel acceleration were made (Figure 42).

The peak upward acceleration of the front wheels in going over the half-sine bumps at 15 miles per hour varied with the amount of damping added to the wheels as shown in Figure 44. This damping is labelled as tire damping in the figure.

VIII. DISCUSSION OF RESULTS AND CONCLUSIONS

Many measurements, as well as the assumptions and approximations of the analysis, enter into the records of the vehicle motions presented. Standard test equipment, except for the displacement pickups, was used in the vehicle tests, and the results obtained are subject to the errors of these instruments. The operation of this equipment was considered satisfactory because no significant errors in the vehicle test data were indicated. The accuracy of the computer used was considered adequate, or as good as or better than the data fed into it. Of course, measurements of the properties of the vehicle involve errors.

Certain assumptions were made in the conversion of measured properties of the vehicle into properties of the electrical analogies. For instance, it was assumed that the friction in the suspensions indicated by the hysteresis loops of the spring force-deflection curves could be treated separately from the spring rates. This friction was included in the damping. Another assumption was that the friction force remained constant; this is reasonable since the velocities of sliding of the rubbing surfaces in the suspension system were low, less than six inches per second.

The agreement between the computer results and the vehicle tests for motion over the test dip is surprisingly good if one considers all the sources of error mentioned above. There is no apparent change in agreement with increasing speed (Figures 27 to 29). From the results for both front and rear it may be concluded that the most important non-linearity in the system, as far as primary motion is concerned, is that of the suspension springs, on account of the

presence of the bump stops. The bump stops have a large effect on the motion and accelerations experienced by the sprung mass.

Apparently, the form of the suspension damping has no effect on the primary motion, since the viscous damping used gave satisfactory results. The actual damping characteristics (Figures 53 and 54) were strongly non-linear. The values of viscous damping used were chosen by estimating the maximum relative velocity between the wheels and frame from the slope of the relative displacement trace on the vehicle test record, and then approximating the damping characteristic up to this velocity by a straight line. If necessary, the actual damping characteristics could be used as was done in the case of the half-sine-bump excitation. Figure 39 shows that increasing the amount of viscous damping lowered the amplitudes of the motion obtained. This is what one would expect for steady state motion of a one-degree-of-freedom system if the excitation frequency were close to the natural frequency of the system. Analysis of the motion of the wheels, which closely followed the profile of the dip, reveals that, for the speeds used, this motion contained a large component with a frequency close to the natural frequency of the sprung mass on the suspension springs. Since this component dominated the motion of the sprung mass, the observed effect of damping was as would be expected. The conclusion reached is that for low frequency excitation the damping of the sprung mass should be close to critical.

Neglecting tire damping in the analysis appears to be justified by the results in the case of motion over the test dip.

Part of the differences in the peak amplitudes obtained from the vehicle and from the computer was due to probable

errors in the measurement of the bump stop clearances and the somewhat crude straight line approximations to the non-linearities. Figure 37 indicates that the bump stop clearance has a pronounced effect on the accelerations experienced by the sprung mass, while Figure 38 shows that varying the bump stop stiffness also has an effect. Both of these variations are in the direction which would be expected; more important, however, is the fact that significant variations were observed. From Figure 30 the small difference in the maximum relative displacements and accelerations indicates that the bump stop clearance assumed might have been slightly different from that on the vehicle. It would be desirable to have the bump stop characteristics measured separately from the main suspension springs. This would have required that they be removed or that the main suspension springs be removed; this could not be done readily and was not felt to be necessary here. In the analysis these factors were considered as independent of the suspension springs, which were essentially linear.

In one case significant secondary motion effects were observed in the computer results for the test dip, motion at the rear at about 80 feet distance traveled (Figure 30). The higher frequency acceleration variation was not as strong for the computer results, as would be expected, since the reproduction of the dip in the computer could not take minor disturbances into account.

Results for the half-sine bump show a little less agreement between vehicle tests and computer results. Also, the agreement changes with speed (Figures 31 to 33), the largest discrepancies

being found at low speeds in the wheel accelerations (Figure 31). The assumption of point contact of the tire with the ground becomes worse as the ground becomes more uneven. Actually the length of tire ground contact was at least 8 inches; this means that the edge of the half-sine bump was enveloped by the tire and the input function was effectively smoothed. As a result the initial impulse received by the wheel was spread out and its magnitude decreased. This may account for part of the differences in locations of the peak relative displacements and accelerations.

Another factor which enters is the hysteresis of the tire. This hysteresis is exhibited by the static load-deflection curves for the tire in Figure 52. The effect of this hysteresis was approximated by adding viscous damping, G_2, to the wheel. This damping was not added in the linear studies which were conducted first, since its importance could not be established until the known nonlinearities were taken into account. It was felt that nothing would be gained by making additional linear studies including this term. The values finally used for this damping were determined by trial and error. Computer results using different values were compared with the vehicle test records until the best agreement was obtained. It was found that the values thus determined varied considerably with the speed of travel and, consequently, with the amplitudes of the motion.

The reason for the small effect of adding some damping to the suspension damping, G_1, at 10 miles per hour is very uncertain. Adding this damping to G_1 instead of including it in G_2 probably compensated slightly for some unknown action of the tire in going

over the bump. As stated previously, the motion was such that it made little difference at which location the damping was added. However, it is felt that this damping is most rightly attributed to the tire, since the suspension damping was known with a fair amount of accuracy. In the following discussion, all of the added damping will be considered as caused by the tire. The value at 10 miles per hour will be taken as 57.5 slug/sec, the sum of the values mentioned for this speed.

If one looks at the tire load-deflection curve for a tire pressure of 24 psi gage and assumes that the hysteresis loop is due to coulomb type friction (i.e., the width of the hysteresis loop remains constant regardless of amplitude), the magnitude of this friction force may be estimated as one half of the difference in load across the loop at a given deflection. The static deflection of the tire was approximately one inch; the coulomb friction force estimated from this portion of the curve is about $\pm$ 40 pounds. The equivalent viscous friction[20] g which will effect the same dissipation of energy as coulomb friction $\pm$ F for sinusoidal motion with an amplitude A and a frequency w is given by

$$g = 4F/\pi Aw . \qquad (12)$$

This equation may be derived by calculating the amount of energy dissipated by each form of damping in one cycle and equating these energies. For motions of the unsprung mass, the natural frequency may be calculated from the vehicle test records. From the acceleration records in Figure 13, the period of this motion

is about 0.11 second so that $w = 2\pi/0.11 = 57$ radians/second. The amplitude of the relative motion between the wheels and the frame for the first cycle of vibration after going over the half sine bumps may be used for A. This amplitude may be read from the graphs of the vehicle records. Using values of A obtained from Figures 31 to 33, and the values of F and w given above, the values of g given in Table 2 were calculated from equation (12). Also listed are the values of tire damping used on the computer.

Table 2

Speed	Amplitude	Equivalent Viscous Damping	
	A	g, Equation (12)	Computer
(miles/hour)	(inches)	(slug/sec)	(slug/sec)
10	0.2	54	57.5
15	0.75	14	20.4
20	1.4	7.7	2.6

Considering the rather crude assumptions involved, the agreement between the values calculated and those determined by trial and error is good enough to conclude that the tire damping can be approximated from measurements of the static friction. Also, the agreement substantiates the statement that the damping added to obtain agreement between the computer results and the vehicle tests should be attributed to the tire.

It can be seen from Figures 32 to 34 that the approximation to the tire spring characteristic was quite adequate and that the effect of the tire leaving the ground was faithfully reproduced.

The inclusion of non-linear damping was indicated by comparing the linear system computer results with the vehicle test records for different speeds (Figures 32 and 33). While good agreement is obtained in Figure 32, too large a damping is indicated in Figure 33. The form of the suspension damping has no effect on the character of the displacement or wheel acceleration records. Figure 41 shows the effect of suspension friction on the accelerations experienced by the frame. It can be seen that coulomb friction gives rise to high rates of change of acceleration; the quality of the resultant ride experienced by a passenger in the vehicle is commonly referred to as "jerky". The magnitude of this effect may be measured quantitatively on the computer from records such as in Figure 41. Changing the amount of friction (Figure 42) did not seem to affect the peak wheel accelerations or peak relative displacements; however, the motion was damped out faster as friction was increased. The unsymmetrical shock absorber characteristic is reflected by the damping force curve (Figure 41), which has greater peaks in rebound.

In Figure 33 the relatively large differences between the peaks at 3.5 and 6.5 feet distance traveled are attributed to neglecting the effect of the rebound stops. Similarly, for motion at the rear (Figure 34) the compression bottoming stop limited the displacement of the axle relative to the frame on the vehicle.

The value of linear damping used at the rear (Figures 34 and 35) was apparently too large in the case of the half-sine bumps. It may be concluded from the results obtained for symmetric motion that the inclusion of the non-linear damping and the effect

of the tire leaving the ground in the system used for studying the rear axle motion (Figure 35) would yield results showing agreement similar to that of Figure 34. There may have been some error in the results at the rear because of the effect of power hop; however, since runs were made at constant speeds involving low power, it was felt that this effect was very small.

Figure 36 shows that the amplitude of the motion as the vehicle traveled over the first part of the dip increased as the main suspension spring stiffness was increased. The frequency of the primary motion also increased, indicated by the change in the motion where the bottom of the dip was encountered. This indicates how the movement of the vehicle in going over several bumps may be influenced by changing parameters. An increase in response amplitude and frequency of the primary motion also took place in going over the half-sine bumps as the suspension spring was stiffened (Figure 40).

No significant change in the primary motion over the test dip took place with variation in the tire spring rate (tire pressure). However, varying the tire spring rate did have a strong effect on the accelerations experienced by the wheels in motion over the half-sine bumps (Figure 43). Higher frequencies of secondary motions were observed with increasing tire spring rate, as would be expected.

Conclusions reached on the effects of some automobile properties are summarized below:

1. The maximum accelerations experienced by the frame are strongly influenced by the presence of the suspension bump stops. Decreasing bump stop clearance and increasing the stiffness of these stops both have adverse effects.

2. Neither the non-linearity of the suspension damping characteristics nor the unsymmetrical action of the shock absorbers have significant effects on low frequency (about 1 cycle/sec) motion of the sprung mass.

3. Coulomb friction in the suspension system has a considerable effect on the accelerations of the frame caused by motion of the wheels at higher frequencies.

4. The incorporation of damping between the wheels and the frame is wrong in principle. Ideally, the absolute motions of the sprung and unsprung masses should be damped independently. The practice of damping the relative motions between these masses is a compromise, at best. As a result, there is a wide variation of opinions about what the characteristics of shock absorbers should be.

5. Damping in the tire may be assumed to be the result of a coulomb type friction. Therefore, the effect of this damping is greatest for small amplitudes of wheel motion, and the effect decreases as the amplitudes increase. Whether or not this damping may be neglected depends on the road excitation.

The following general conclusions were drawn from the results of the research program:

1. Relatively simple systems giving good quantitative results can be used to represent the vehicle in motion over a variety of courses.

2. The effects of varying vehicle properties can be studied by using these simple systems. The results obtained are of sufficient accuracy to be used for design purposes. It is possible to study the effects of different properties (spring rates, damping characteristics, masses) separately. The practically unlimited number of variations make studies possible which yield a clearer picture of phenomena taking place.

IX. RECOMMENDATIONS FOR FURTHER STUDY

The field of vehicle dynamics is so broad that it would be impossible to cover it completely in a single work. This thesis represents one step in the development of analysis in this field. It seems appropriate, therefore, to offer some specific recommendations for future study.

1. Quantitative objective criteria must be established for judging the response of a vehicle to a given excitation.

2. Studies similar to the present work should be made of other motions of vehicles caused by different forms of excitation, and the significant factors affecting those motions should be determined.

PART 2. AN EXAMPLE OF THE APPLICATION OF ANALYSIS TO A VEHICLE DESIGN PROBLEM; THE ENGINE AS A DYNAMIC VIBRATION ABSORBER

I. INTRODUCTION, A STATEMENT OF THE PROBLEM

In Part 1 it was found that motions of the vehicle could be obtained with satisfactory accuracy for design by representing the vehicle with relatively simple mechanical systems and applying forcing functions to these systems. Low frequency motions of the frame and body were reproduced and forces on the frame caused by motions of the unsprung masses at higher frequencies were recorded through analysis using a computer. The vibrations of the unsprung masses were also found to be accurately represented. Changing certain parameters in these simple mechanical systems was found to have significant effects on the resultant motions. The conclusion was reached that the results of analyzing the vehicle were of sufficient accuracy that design studies could be performed on computers and the findings applied directly to the vehicle. An example of such a design study is presented here, demonstrating the application of analysis to a specific problem.

In Part 1 the assumption that the frame, body, and other components mounted on the frame and in the car constituted a rigid mass held for low frequency body motions and motions of the unsprung masses. Of course, this is not the case, actually, and it may be expected that other vibrations exist in these components and that some of these vibrations may influence the motions of the frame.

The engine on its mountings is a mass-spring system of sizable proportions and its motion might be expected to have a

noticeable effect on the motion of the frame. Some experimental work has been reported[12] indicating that this mass-spring system might be used as a dynamic vibration absorber. In the present study, small vertical motions of the engine on its mounts, arising from the vertical movement of the chassis caused by road excitation, was considered. The vibrations caused by the running of the engine were neglected. Symmetric motion of the vehicle was studied.

II. ANALYSIS

The automobile was represented by the five-degree-of-freedom mechanical system shown in Figure 45. Here, the engine mounts were replaced by a single spring and a damper, K_3 representing the combined vertical spring rate and G_3 the combined vertical damping of the mounts acting in parallel; M_2 is the mass of the engine and transmission. This mass was located on the frame at the center of gravity of the engine. The motor mounts were assumed to be made of rubber and the equivalent viscous damping for them was taken to be .05 times the critical damping for the engine mass-spring system, $G_3 = 0.05\, G_{3\ crit} = 0.1\, \sqrt{K_3 M_2}$. This value of damping corresponds to a decrease in amplitude of free vibrations of 30 per cent per cycle.[21] The system was assumed to be linear and the tire damping was neglected. Values of physical parameters of the vehicle were approximately those of a 1953 Chevrolet.

It was expected that any effect of the engine would be strongest near the natural frequency of the engine on its mounts. The effect on the double amplitude of the motion at the midpoint of the chassis of varying the engine mount stiffness was studied as the vehicle was assumed to be traveling over a continuous wavy surface, as shown, at constant speeds. The dimensions of this sinusoidal road surface are given in Figure 46. The midpoint of the chassis is the approximate location of the front seat of an automobile.

The electrical analogy which was used in the study of this mechanical system is shown in Figure 45. The same computer was used which is described in Part 1. An oscillator was used to

SCHEMATIC DIAGRAM OF VEHICLE

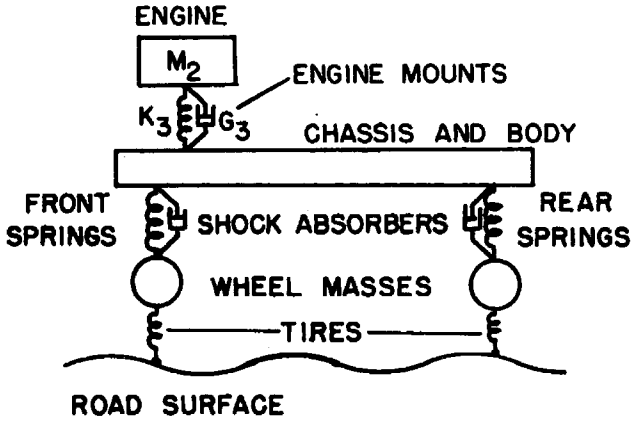

ELECTRICAL ANALOGY

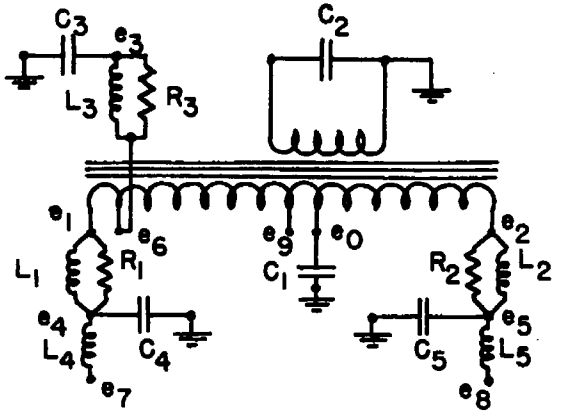

K_3 = STIFFNESS OF ENGINE MOUNTS

$\frac{1}{K_3}$ = COMPLIANCE OF ENGINE MOUNTS

G_3 = EQUIVALENT VISCOUS DAMPING OF ENGINE MOUNTS

$C_3 \propto M_2$

$L_3 \propto \frac{1}{K_3}$

$R_3 \propto \frac{1}{G_3}$

Figure 45. Mechanical system and electrical analogy used in studying the effect of varying engine mount stiffness.

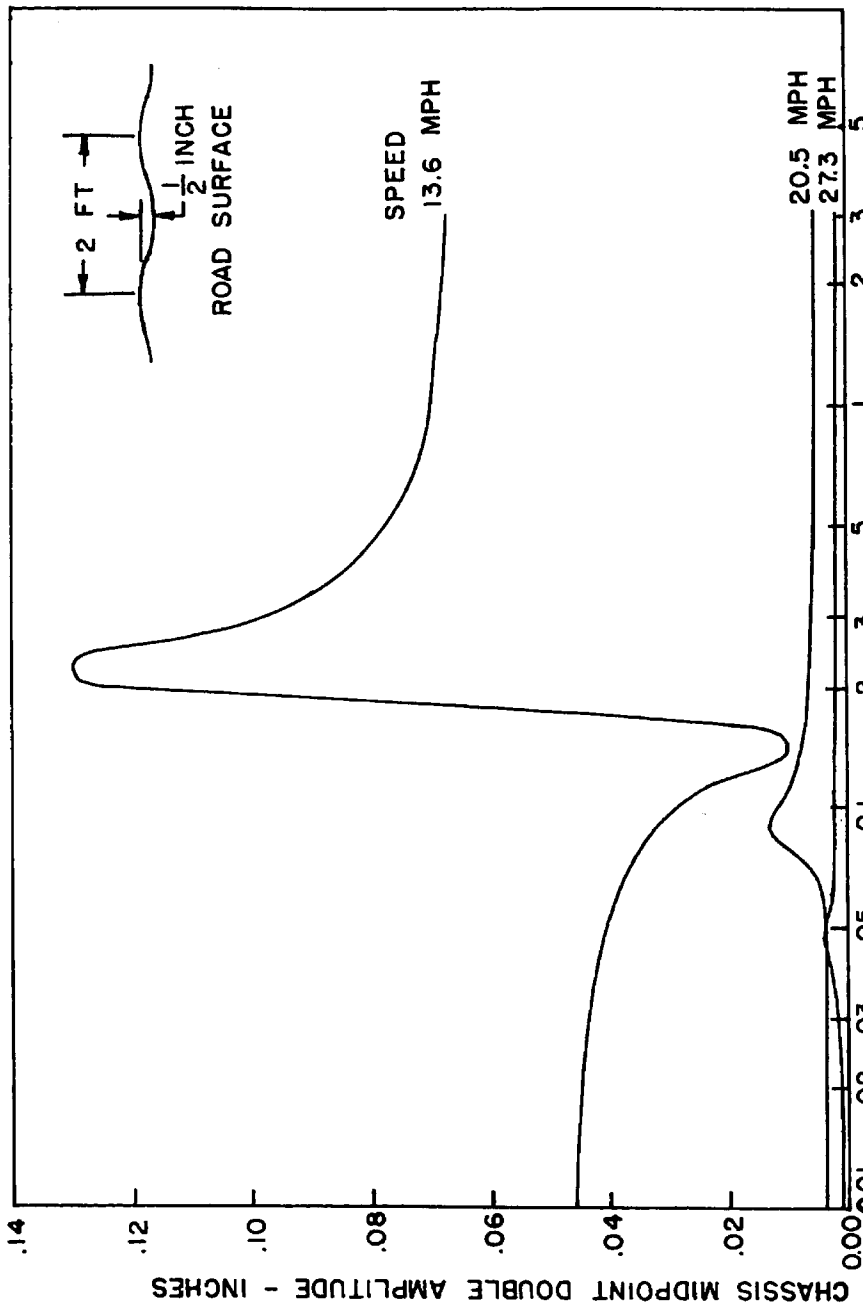

Figure 46. Effect of varying engine mount stiffness on the motion of the chassis.

generate the input functions. These were sinusoidal voltages which were proportional to the vertical velocities of the tire-road contact points and were applied to the circuit at e_7 and e_8. Equations for the mechanical system, analogy, and conversion from one to the other, are given in Appendix V.

III. RESULTS OF THE ANALYTICAL STUDY

The curves presented in Figure 46 show the variation of the frame midpoint double amplitude with engine mount compliance at three speeds. Additional measurements were made of the amplitudes of the front wheel motion and the relative motion between the engine and the frame. The wheel amplitudes remained practically constant at each speed, as given in Table 3. Significant values of the double amplitude of the relative motion between the engine and the frame for a speed of 13.6 miles per hour are .23 inch for an engine mount compliance, $1/K_3 = .14 \times 10^{-4}$ ft/lb, and 2.3 inches for $1/K_3 = .20 \times 10^{-4}$ ft/lb.

Table 3

Speed (miles/hour)	Double Amplitude of Front Wheels (inches)
13.6	5
20.5	0.46
27.3	0.18

IV. CONCLUSIONS

As would be expected, the action of the engine mass-spring system as a dynamic vibration absorber on the vehicle system was greatest at a particular excitation frequency, that arising from going over the wavy surface at 13.6 miles per hour, as seen from Figure 46. This frequency, 10 cycles per second, was approximately the natural frequency of wheel bounce. It is apparent from Table 3 that the front wheels were in resonance with the excitation received from the road. The conclusion reached here is that the engine mount may be chosen such that the shake of the frame caused by wheel bounce may be reduced. Static deflection of the engine on its mounts for minimum motion of the frame under this condition was 0.117 inch, $1/K_3 = .14 \times 10^{-4}$ ft/lb. Greater values than this lead to larger motions of the frame and excessive vibration of the engine, because of a resonance condition.

For higher speeds, higher frequencies, the peaks caused by engine resonance are much lower and occur at greater engine mount stiffnesses. The large change in amplitude with speed indicates the sharpness of the wheel bounce resonance peak which makes the use of a dynamic absorber more feasible. At some speed between 13.6 and 20.5 miles per hour the peak of the corresponding curve will occur at $1/K^3 = .14 \times 10^{-4}$ ft/lb. If this peak is too large a slightly lower engine static deflection may be chosen as a compromise. Lower frequencies of excitation below the wheel resonant frequency would result in lower amplitudes until the natural frequency of the sprung mass on its suspension was approached. At this frequency the engine is effectively rigidly attached to the frame if its static

deflection is as indicated above. The fact that this motion is highly damped makes the use of a dynamic vibration absorber for this low frequency impractical. Besides, the required static deflection of the engine would be excessive.

This study sets an upper bound on the vertical static deflection of the engine to avoid excessive vibrations of the engine and of the frame from road excitation. This limit may have to be compromised by considering the effectiveness of the engine mount in isolating other engine vibrations from the frame.

REFERENCES

1. Guest, James J., "The Free Vibrations of an Autocar". Engineering (1925), Vol. 120, p. 367.

2. Slaby, Rudolf, "Einfluss der Achsmasse auf die Federungseigenschaften eines Fahrzeuges". Automobiltechnische Zeitschrift (1936), Vol. 39, pp. 593-598.

3. Schilling, R., and Fuchs, H. O., "Modern Passenger-Car Ride Characteristics." Journal of Applied Mechanics (1941), Vol. 8, pp. A59-A66.

4. Lange, A., and Dute, J., "Electronic Simulation as an Aid to the Design of Vehicle Suspension Systems". Society of Automotive Engineers Preprint No. 753 (1952).

5. Grover, Horace, "Analog Helps Solve Suspension Problems". Society of Automotive Engineers Journal (April, 1955), Vol. 63, pp. 44-46.

6. v. Karman, Th., and Biot, M. A., Mathematical Methods in Engineering. McGraw-Hill (1940), pp. 217-220.

7. Mercier, P. E., "Theory of Vehicle Suspension". Journal of Applied Physics (1942), Vol. 13, pp. 484-495.

8. Colwell, A. W., "Mobile Instrumentation for Automotive Equipment". Proceedings of the Society for Experimental Stress Analysis (1952), Vol. X, pp. 65-76.

9. Bassette, A. S., "Instrumentation of Vibration in Automobile Body". SAE Journal (November 1951), Vol. 59, pp. 37-39.

10. Saxon, Robert J., "Measuring for Car Shake", SAE Preprint No. 274 (1954).

11. Ruegg, M., "Laboratory Simulation of Car Shake". SAE Preprint No. 275 (1954).

12. Kamins, M. and Love, W. B., "Shake Control on Convertibles". SAE Preprint No. 273 (1954), p. 3.

13. Jeska, R. D., "A Comparison of Real and Simulated Automobile Suspension Systems". University of Michigan Report UMM-117 (February 1953).

14. Bush, V., and Caldwell, S. H., "A New Type of Differential Analyzer". Journal Franklin Institute (1945), Vol. 240, pp. 255-326.

15. Korn, G., and Korn, T., Electronic Analog Computers. McGraw-Hill (1952).

16. Gruenberger, Fred, Computing Manual. University of Wisconsin Press (1953).

17. Jacklin, H. M., and Liddell, G. J., "Riding Comfort Analysis". Engineering Bulletin, Purdue University (1933), Vol. XVII, p. 51.

18. McCann, G. D., and Criner, H. E., "Mechanical Problems Solved Electrically". Westinghouse Engineer (1946), Vol. 6, pp. 49-56.

19. McCann, G. D., Wilts, C. H., and Locanthi, B. N., "Application of the California Institute of Technology Electric Analog Computer to Non-linear Mechanics and Servomechanisms". Transactions of the American Institute of Electrical Engineers (1949), Vol. 68, pp. 652-660.

20. Housner, G. W., and Hudson, D. E., Applied Mechanics-Dynamics. D. Van Nostrand (1950), p. 96.

21. Keys, W. C., "Rubber Springs". Mechanical Engineering (1937), Vol. 59, p. 345.

APPENDIX I

EXPERIMENTAL EQUIPMENT

A. Vehicle testing equipment

1. Accelerometers, William Miller Company, model 402-C, serial numbers: 5, 139, 140.
2. Three channel carrier amplifier, Miller, type CD-2, model CDA3, serial number 24.
3. Amplifier power supply, Miller, model DP-6, serial number 31.
4. 12 channel oscillograph, Miller, model H, serial number 125.
5. Displacement pickup potentiometers, Helipot Corporation, model G.
6. Fifth wheel, Design: General Motors Corporation. Built by the California Institute of Technology.
7. Fifth wheel meter, Weston, model 901, serial number 3600.
8. Lead-acid batteries, Willard, type SMR-2-135.
9. Dry cell batteries, Burgess 21308, RCA VS 157.

The circuit used in conjunction with the displacement pickups is shown in Figure 47. It may be seen that the relation between the galvanometer element deflection and the pulley rotation is non-linear. However, for the values of resistors and battery voltages used, the departure from linearity was so small that it could be neglected.

B. Computer and associated equipment

1. Electric analog computer, Servomechanisms Laboratory, California Institute of Technology.

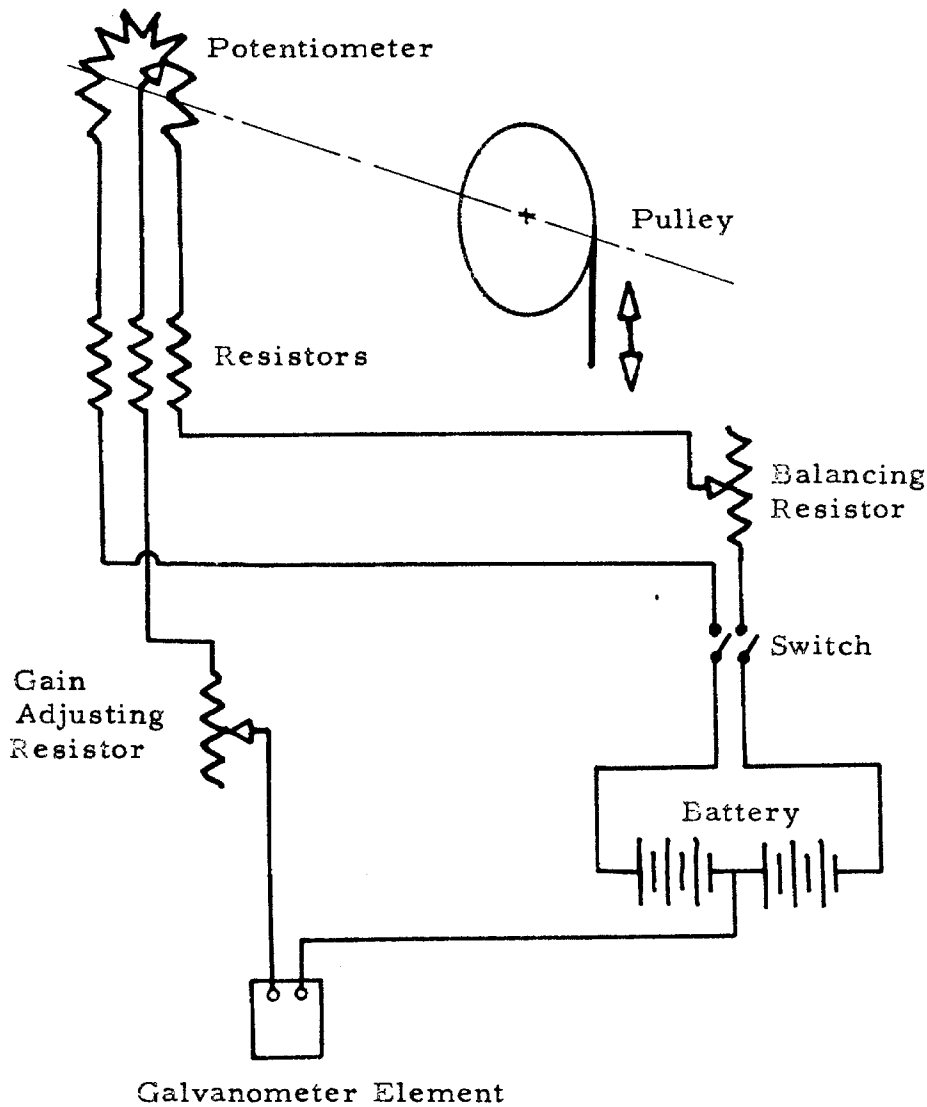

Figure 47. Circuit Diagram for Displacement Pickups.

2. Photoformers, C.I.T., model 2, serial numbers 1 and 2.
3. Dual-beam cathode-ray oscillograph, Allen B. DuMont Laboratories, Inc., type 322-A, serial number 8A07.
4. Oscillograph record camera, DuMont, type 297, serial number 2A75.
5. Vacuum-tube fork, 1000 c/sec., General Radio Company, type 723-6, serial number 651.

APPENDIX II

PHYSICAL PROPERTIES OF THE VEHICLE

Vehicle

Chevrolet, 1954, model 2103.

Accessories: radio, clock, back-up lights, outside rear-view mirror, glove compartment light, license plate frames.

A. Mass properties

Sprung Mass

Curb weight with accessories, assumed to be symmetrically distributed about the vehicle centerline:*

Weight on front wheels - 1585 lb.

Weight on rear wheels - 1264 lb.

Total sprung weight - 2848 lb.

Weight data for vehicle as used:

Passengers -	Driver and Observer	Driver
Weight on left front wheel -	838 lb.	831 lb.
Weight on right front wheel -	807	780
Weight on left rear wheel -	921	896
Weight on right rear wheel -	941	840
Total test sprung weight -	3507 lb.	3347 lb.
Test sprung mass -	109 slugs	104 slugs
Distance, front wheels to C.G. -	61.0 in.	59.6 in.

Unsprung Masses

	Front	Rear
Total unsprung weight -	211 lb.	297 lb.
Unsprung mass, both wheels -	6.55 slugs	9.22 slugs

*Production Weights, 1954 Chevrolet Passenger Cars. Chevrolet Engineering Department Technical Data Group, Chevrolet Division, General Motors Corporation, March 15, 1954.

Moment of inertia of sprung mass in pitch

The following information was obtained by letter from Mr. Maurice Olley, Chevrolet, Division of General Motors, for a 1953 Chevrolet, model 1503. This model was practically the same as the test car regarding mass data.

Weight, includes sprung and unsprung weight - 4008 lb.

Moment of inertia of whole car in pitch about the C.G. - 76,250 lb-ft^2.

Location of C.G. - 57.2 in. behind front wheels,
24.1 in. above ground.

The moment of inertia of the sprung mass was found by considering the unsprung masses concentrated at their respective wheel centers and subtracting the second moments of these masses about the C.G.

Sprung weight (includes load): On front wheels - 1786 lb.
On rear wheels - 1714
Total - 3500 lb.

Moment of inertia of sprung weight - 64,205 lb-ft^2.

The difference in load distribution between the above and the test vehicle was assumed to be due to the battery load carried in the trunk of the test car. This load shift would increase the moment of inertia. Therefore, the weight of the batteries was considered to be concentrated at their composite C.G. and the second moment of this weight about the sprung mass C.G. was added to the above moment of inertia to yield the following:

Test moment of inertia of the sprung mass in pitch about the C.G. - 72,500 lb-ft^2 or 2250 slug-ft^2.

Moment of inertia of the sprung mass in roll

No experimental data on this parameter were available. The radius of gyration in roll was assumed to be equal to the ratio of the tread width to the wheelbase times the radius of gyration in pitch. Thus, the following figure was obtained:

Test moment of inertia of the sprung mass in roll about the C.G. = 354 slug-ft^2.

This approximation is valid for a uniform rectangle with a mass equal to that of the car, and with dimensions equal to the wheelbase and tread width. The assumption was therefore very crude; however, the value as used in the system for studying motion of the rear axle did not have much effect on the results. In fact, this motion was not noticeably effected even if the value was changed by 50 per cent. For more exact studies of the motion of the sprung mass this property would have to be calculated more accurately or measured experimentally.

Moment of inertia of the rear axle in roll

The moment of inertia of the rear axle in roll was calculated from the weight data furnished by the manufacturer. Figure 48 shows the configuration of the axle and wheels. The axle and torque tube assembly was considered as a uniform bar with concentrated masses at each end and at the center, and its moment of inertia was computed. The spring and shock absorber unsprung weights were taken as concentrated at their attachment points. Their second moments about the axle midpoint, as well as the moments of inertia of the tires and wheels, were added to that of the axle to yield:

Moment of inertia of the rear axle in roll = 32.5 slug-ft^2.

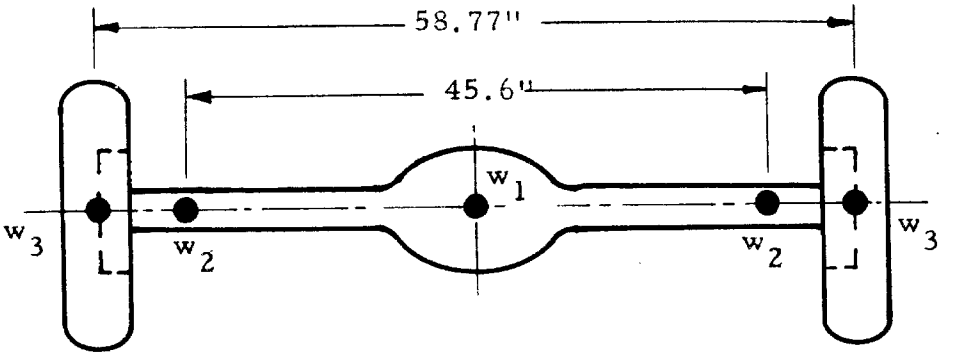

Unsprung weight of axle and torque tube assembly,

$$w_1 = 184.5 \text{ lb.}$$

Unsprung weight of spring and shock absorber, $w_2 = 13.2$ lb.

Weight of wheel and tire, $w_3 = 42.125$ lb.

Figure 48. Configuration of rear axle and wheels.

B. Spring and damping data

Suspension spring force-deflection curves

Figures 49 and 50 contain the main suspension spring force-deflection curves for the test car. These were obtained by gradually loading and unloading the front and rear, respectively, and measuring the deflections. The hysteresis loops are due to the effect of static friction in the suspensions. These curves were approximated by the dashed straight line segments for purposes of computation; the center section represents the main suspension springs, and the bump-stop non-linearities were approximated by the corresponding line segments of increased slope. The data taken from these line segment approximations are presented in Table 4.

Table 4

Summary of Suspension Spring Data

	Left Front	Right Front	Left Rear	Right Rear
Main suspension spring rate (lb/in)	106.2	106.2	112.8	116.6
Bump-stop to suspension spring stiffness ratio:				
Compression	3.04	3.04	4.40	4.22
Rebound	7.82	7.99	4.33	3.63
Force at bump-stop contact:				
Compression (lb)	1094	1084	1069	1075
Rebound (lb)	641	634	188	164

Tire load-deflection curves

The deflection of one of the tires was measured as it was loaded radially in an Olsen Universal Testing Machine, 15,000 lb. range, as shown in Figure 51. Load deflection curves obtained for

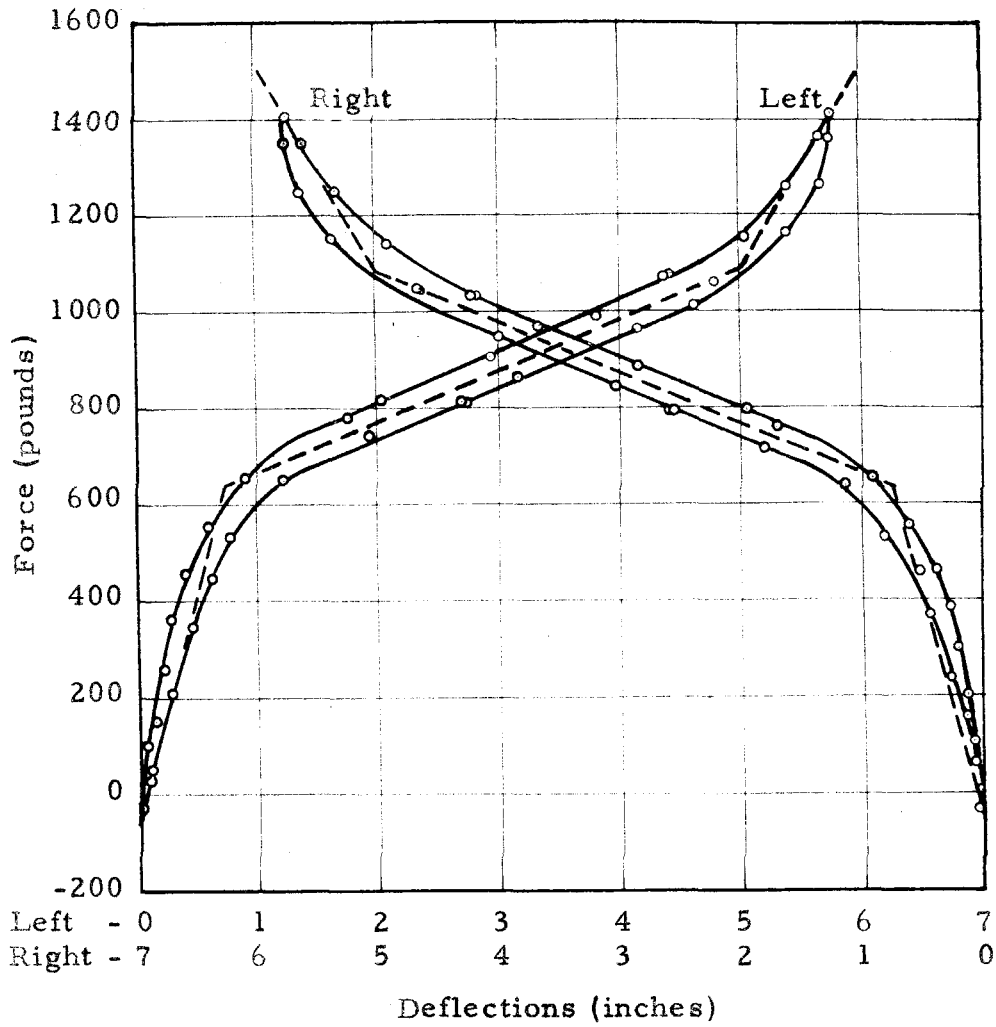

Figure 49. Front suspension spring force-deflection curves.

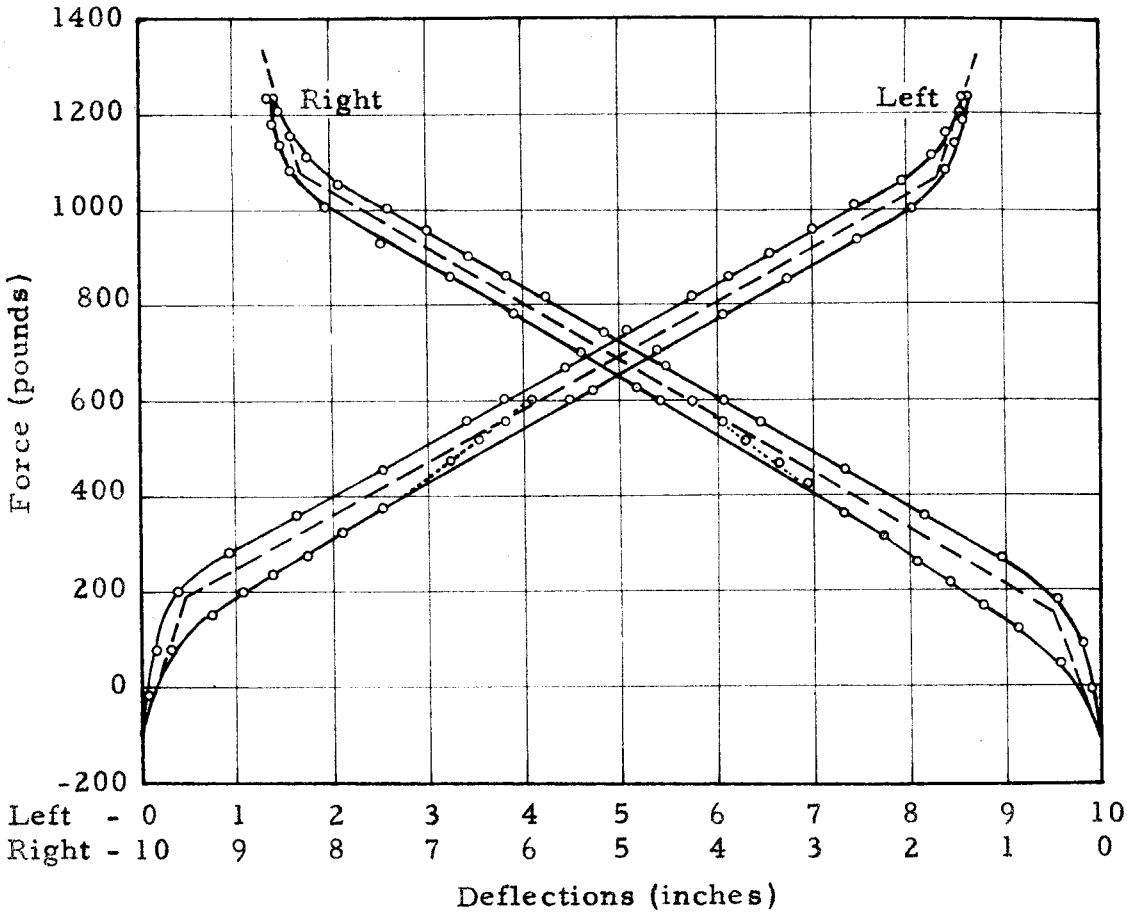

Figure 50. Rear suspension spring force-deflection curves.

tire pressures of 24 and 30 lb/in^2 gage are shown in Figure 52. These curves were obtained under static loading conditions and a "static" friction of the tire is indicated by the hysteresis loops. These curves were approximated by linear spring rates as follows:

Tire pressure (lb/in^2 gage)	Spring Rate (lb/in)
24	970
30	1150

Main suspension damping

Load velocity curves for the front and rear shock absorbers were obtained from Mr. Olley. These curves were approximated by straight lines, and load-velocity curves for equivalent vertical dampers located at the wheels were calculated. The static friction of the suspension was included as a jump in the force at "0" velocity. This jump is equal to the average width of the respective suspension spring hysteresis loop (Figures 49 and 50). Figures 53 and 54 show the resultant non-linear damping functions for the front and rear, respectively.

C. Dimensions

Wheelbase - 115 inches.

Front tread width - 56.7 inches.

Rear tread width - 58.77 inches.

Distance between rear springs - 45.6 inches.

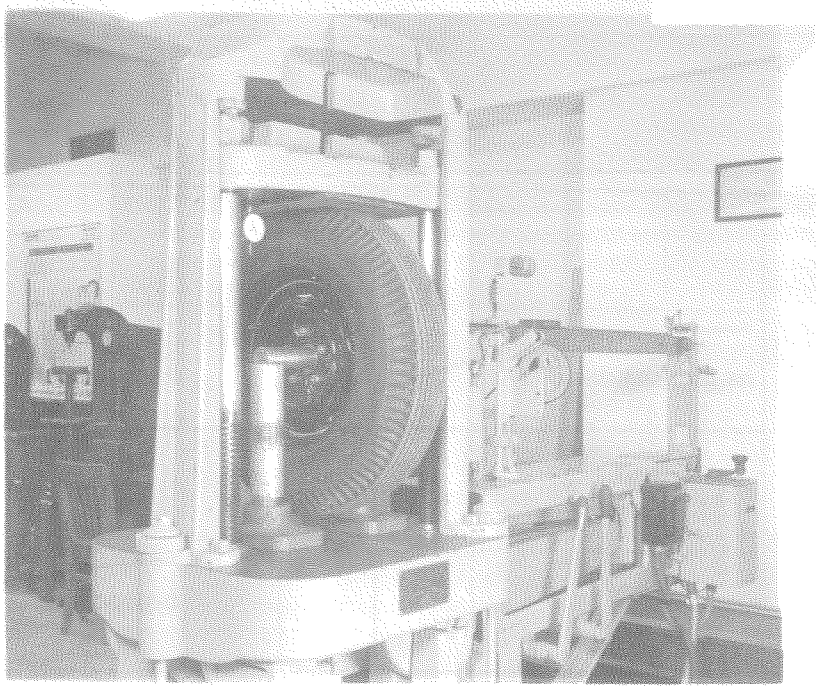

Figure 51. Setup for measuring static load-deflection characteristics of tires.

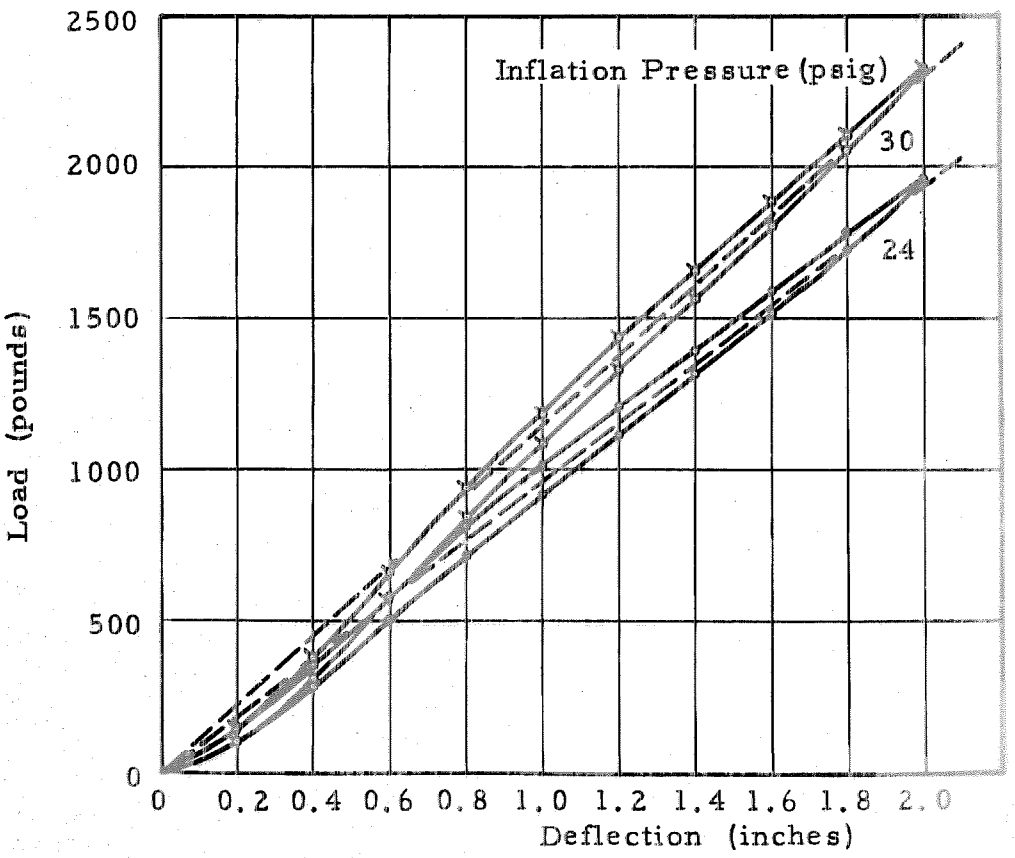

Figure 52. Tire load-deflection curves.

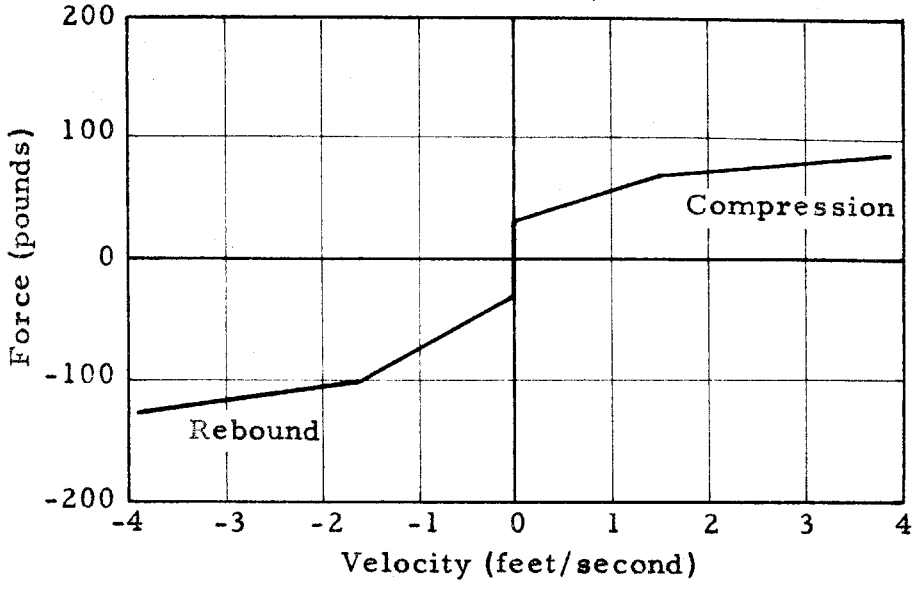

Figure 53. Front suspension damping force-velocity curve.

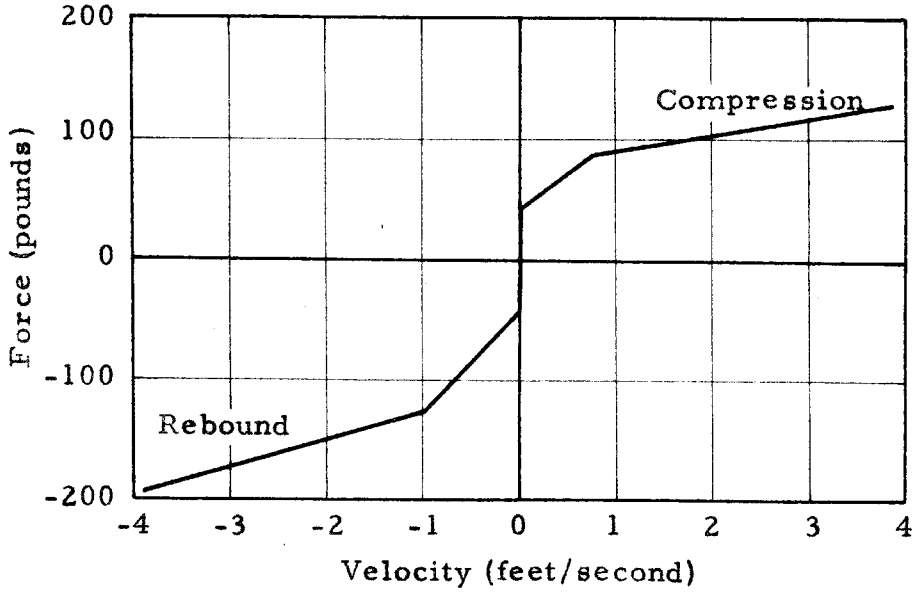

Figure 54. Rear suspension damping force-velocity curve.

APPENDIX III

MECHANICAL SYSTEMS AND ELECTRICAL ANALOGIES

A. Equations for mechanical systems

The mechanical systems used to represent the vehicle (Figures 14, 15, and 18) are simplifications of the system shown in Figure 1.

Symmetric motion

Since the equations of motion for Figure 1 were derived in the text, it will suffice to indicate the assumptions made in going from Figure 1 to Figure 14 and to define the terms of Figure 14 in terms of Figure 1.

The assumption of symmetric motion means the following, in terms of Figure 1: $\theta = 0$; $x_1 = x_2$; $x_3 = x_4$; $y_1 = y_2$; $y_3 = y_4$; $m_1 = m_2$; $K_1 = K_2$; $K_3 = K_4$; $K_5 = K_6$; $K_7 = K_8$; $G_1 = G_2$; $G_3 = G_4$.

The notation of Figure 14 is defined in terms of Figure 1 as follows, where the left and right hand sides refer to Figures 14 and 1, respectively: $m_1 = m_1+m_2$; $m_2 = m_3$; $m_3 = m_4$; $I_1 = I_1$; $K_1 = K_1+K_2$; $K_2 = K_3+K_4$; $K_3 = K_5+K_6$; $K_4 = K_7+K_8$; $G_1 = G_1+G_2$; $G_2 = G_3+G_4$; $x_1 = x_5+a\phi$; $x_2 = x_5-b\phi$; $x_3 = x_1$; $x_4 = x_3$; $y_1 = y_1$; $y_2 = y_3$.

With the above assumptions and definitions the equations of Figure 14 follow directly from equations (5) to (10), pp. 4-5; equations (5), (6), (7), and (8) reduce to two equations, and equation (11) drops out altogether.

Unsymmetric motion of the rear axle

In Figure 18 it was assumed that the motion of the rear axle

was independent of the motion at the front of the vehicle. Account was also taken of the difference between the tread width and the distance between the springs. The terms in Figure 18 are defined as follows:

m_1 = mass corresponding to the sprung weight on the rear wheels.

$I_2' = (m_1 \text{ (above)} / m_4) I_2$.

x_1 = vertical deflection of the frame above the axle and the left rear suspension spring.

x_2 = vertical deflection of the frame above the axle and the right rear suspension spring.

x_3 = vertical deflection of the C.G. of the rear unsprung mass.

ψ = angular displacement of the rear axle in roll.

All other symbols are defined in Figure 1.

B. Electrical Analogies

The electrical analogies used in Part 1 are of the mass-inductance type described in reference 18, and the equations for the circuits of Figures 20 to 22 follow directly by applying Kirchhoff's second law.

Conversion Constants

Factors which govern the choice of conversion constants are the sizes and electrical limits of the computer elements. Since the properties of the elements used in this type of computer depend on time rates of change of current and voltage, predominating frequencies of the circuits must be chosen within the operating range of the computer. Table 5 summarizes the values of the constants used.

Table 5

Conversion Constants

System figure number and course (Test dip or half-sine)	Constant N	Constant f	Constant K
Figure 20, test dip	100	14	14000
Figure 21, test dip	100	14	14000
Figure 21, half-sine	100	14	2800
Figure 22, half-sine	100	20	2000

Generation of input function

As stated in the text, photoformers were used here to generate the input functions. If it is assumed that the tire spring rate is constant and that the tire does not leave the ground, the input or forcing function in the mechanical equations of motion is equal to the tire spring rate times the ground di splacement, Ky. Thus, the input function is proportional to the ground displacement, and the function used in the photoformer is the profile of the course. The output of the photoformer is a voltage proportional to the ground displacement at a given point, which is determined by the photoformer input. Since the test runs were made at constant speed, the input used was a uniformly increasing voltage. This voltage was obtained by integrating a constant voltage by means of an electronic integrator. The value of the integrator input voltage was proportional to the desired vehicle speed. Where two input functions were required, as in the case of the four degree-of-freedom system in symmetric motion, two photoformers were operated utilizing the

same input, provision for the time lag from the front to rear being made by offset controls on the photoformers.

Non-linear suspension springs

The circuit shown in Figure 55 may be substituted for the condenser corresponding to the main suspension spring in the electrical analogies. Provision was made so that all of the quantities shown could be varied readily. Crystal diodes were used in all of the non-linear elements; and it was necessary in some cases to correct for their finite back and forward resistances, which ideally would be infinite and zero, respectively.

Non-linear damping

The non-linear damping characteristics were obtained by using the circuit shown in Figure 56. This circuit is substituted in the analogies for the resistor which corresponds to the main suspension damper. It was found necessary to use a transformer to couple the circuit shown to the analogy in order to obtain usable values of voltages, currents, and resistors.

Tire leaving the ground

Since the coordinates of the mechanical systems were measured from static equilibrium of the system, the effect of the tire leaving the ground was that the maximum downward force the tire can exert on the wheel was equal to the static load on the tire. The circuit used to give this effect is shown in Figure 57. This circuit incorporates the input function and the condenser corresponding to the tire spring; its output corresponds to the force of the tire on the wheel.

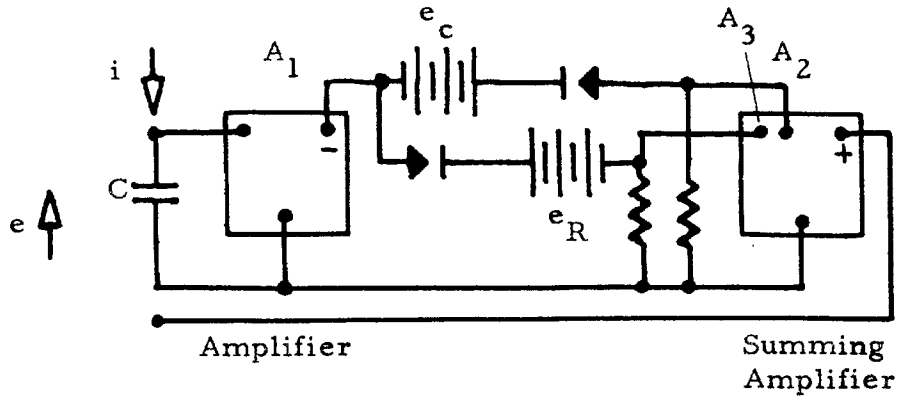

C = $1/f^2$ (main suspension spring rate).

A_1 = gain of amplifier, arbitrary.

A_2 = $(1/A_1)$ (Compression bump-stop to suspension spring stiffness ratio).

A_3 = $(1/A_1)$ (Rebound bump-stop to suspension spring stiffness ratio).

$e_c = \frac{f}{kA_1}$ [(Force at compression bump-stop contact) - (Static load)].

$e_R = \frac{f}{kA_1}$ [(Static load) - (Force at rebound bump-stop contact)].

Figure 55. Electrical circuit used to simulate non-linear suspension springs.

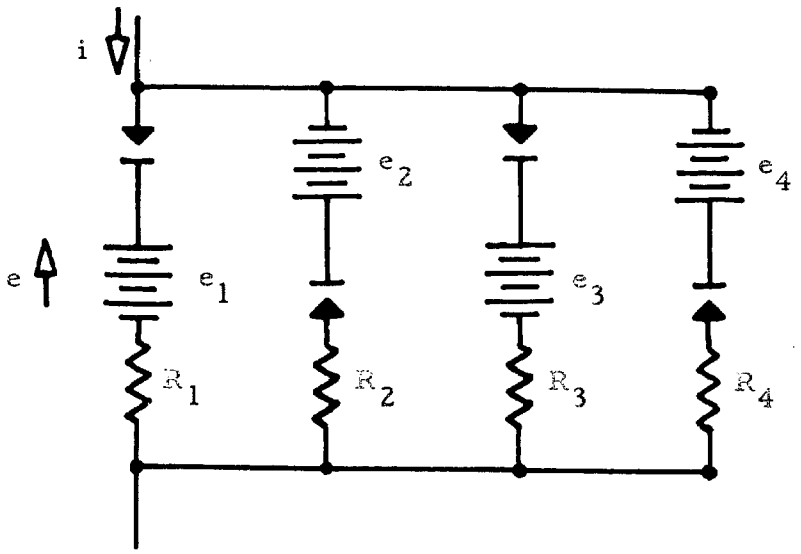

$e_1 = e_2 =$ (f/k) (Static friction force).

$e_3 =$ (f/k) (Damping force at shock absorber compression cutoff).

$e_4 =$ (f/k) (Damping force at shock absorber rebound cutoff).

$R_1 = (f^2/N)$ (Shock absorber compression damping constant before cutoff).

$R_2 = (f^2/N)$ (Shock absorber rebound damping constant before cutoff).

$\frac{R_1 R_3}{R_1 + R_3} = (f^2/N)$ (Shock absorber compression damping constant after cutoff).

$\frac{R_2 R_4}{R_2 + R_4} = (f^2/N)$ (Shock absorber rebound damping constant after cutoff).

Figure 56. Circuit used to simulate non-linear damping.

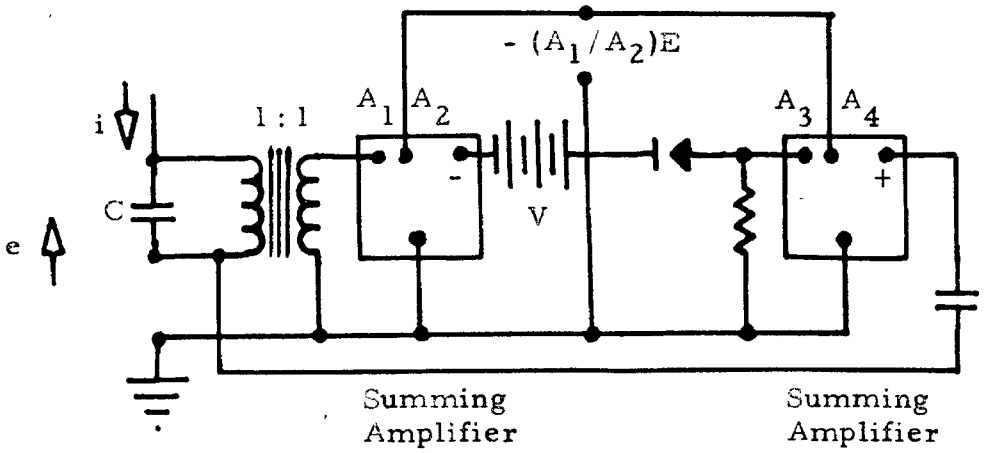

$C = 1/f^2$ (Tire spring rate).

$E = (f/k)$ (Tire spring rate) y.

$V = (f/k)$ (Static tire load).

A_1, A_2 = arbitrary amplifier gains.

$A_3 = 1/A_1$.

$A_4 = A_2/A_1$.

Figure 57. Circuit used to simulate the effect of the tire leaving the ground.

APPENDIX IV

Analytical Solution for the Response of a Linear Two Degree-of-Freedom System to a Half-Sine Pulse

The equations of motion of the system shown in Figure 15 are

$$m_1 \ddot{x}_1 + G_1(\dot{x}_1 - \dot{x}_2) + K_1(x_1 - x_2) = 0 \text{ , and} \qquad (13)$$

$$m_2 \ddot{x}_2 - G_1(\dot{x}_1 - \dot{x}_2) - K_1(x_1 - x_2) + K_2 x_2 = K_2 y \qquad (14)$$

The half-sine pulse excitation function may be written,

$$y = A \sin \frac{\pi V t}{L}, \quad \text{for } 0 \leq t \leq \frac{L}{V} ;$$

$$y = 0, \quad \text{for } t > \frac{L}{V} ; \qquad (15)$$

where

A = the height of the half-sine bump,

L = the length of the bump, and

V = the speed of the car over the bump.

The initial conditions are

$$x_1(0) = \dot{x}_1(0) = x_2(0) = \dot{x}_2(0) = 0 . \qquad (16)$$

Taking the Laplace transforms* of equations (13) and (14), using the initial conditions, equation (16), one obtains

$$(m_1 s^2 + G_1 s + K_1)X_1 - (G_1 s + K_1)X_2 = 0 , \text{ and} \qquad (17)$$

$$-(G_1 s + K_1)X_1 + (m_2 s^2 + G_1 s + K_1 + K_2)X_2 = K_2 Y, \qquad (18)$$

---

* Refer to Churchill, R. V., Modern Operational Mathematics in Engineering. McGraw-Hill (1944).

where the transformed functions are indicated by capitals, i.e., $X_1 = L\{X_1\}$, etc. Equations (17) and (18) can be solved simultaneously for X_1 and X_2, yielding,

$$X_1 = \frac{K_2 (G_1 s + K_1) Y}{(m_1 s^2 + G_1 s + K_1)(m_2 s^2 + G_1 s + K_1 + K_2) - (G_1 s + K_1)^2} ; \quad (19)$$

$$X_2 = \frac{K_2 (m_1 s^2 + G_1 s + K_1) Y}{(m_1 s^2 + G_1 s + K_1)(m_2 s^2 + G_1 s + K_1 + K_2) - (G_1 s + K_1)^2} . \quad (20)$$

The denominators of equations (19) and (20) may be factored,

$$(m_1 s^2 + G_1 s + K_1)(m_2 s^2 + G_1 s + K_1 + K_2) - (G_1 s + K_1)^2$$
$$= m_1 m_2 (s - \lambda_1)(s - \lambda_2)(s - \lambda_3)(s - \lambda_4) , \quad (21)$$

where λ_1, λ_2, λ_3, and λ_4 are the singular points of equations (19) and (20). These singular points are the roots of the characteristic equation;

$$(m_1 \lambda^2 + G_1 \lambda + K_1)(m_2 \lambda^2 + G_1 \lambda + K_1 + K_2) - (G_1 \lambda + K_1)^2 = 0 \quad (22)$$

The roots of this equation were obtained by using the test-function method described in Ref. (6). The values of the physical properties were as follows:

$m_1 = M_{11} = 48.7$ slugs ;

$m_2 = 6.55$ slugs ;

$K_1 = 2550$ lb/ft ;

$K_2 = 23300$ lb/ft ;

$G_1 = 87.9$ slug/sec.

Complex roots were obtained:

$$\lambda_1 = a_1 + b_1 i;\ \lambda_2 = a_1 - b_1 i;\ \lambda_3 = a_2 + b_2 i;\ \lambda_4 = a_2 - b_2 i,$$

where $a_1 = -.7336$, $b_1^2 = 46.84$, $a_2 = -6.8764$, $b_2^2 = 3883$. Using these values, the right side of equation (21) can be written,

$$m_1 m_2 \left[(s + .7336)^2 + 46.84\right]\left[(s + 6.8764)^2 + 3883\right]. \quad (23)$$

The method of partial fractions was applied to the right hand sides of equations (19) and (20) after substituting (23) for the denominator, and the following expressions for X_1 and X_2 were obtained,

$$X_1 = \frac{K_2 Y}{m_1 m_2}\left[\frac{.02065\,(s + .7336) + .6447}{(s + .7336)^2 + 46.84} - \frac{.02065\,(s + 6.8764) + .7715}{(s + 6.8764)^2 + 3883}\right]; \quad (24)$$

$$X_2 = \frac{K_2 Y}{m_1 m_2}\left[\frac{.004055\,(s + .7336) + .06014}{(s + .7336)^2 + 46.84} + \frac{-.004055\,(s + 6.8764) + 48.62}{(s + 6.8764)^2 + 3883}\right]. \quad (25)$$

These expressions are valid for $0 \le t \le \frac{L}{V}$.

The inverse transforms of equations (24) and (25) may be found in tables. The convolution theorem was applied, and integrals of the following form were obtained:

$$I_1^i = \int_o^t e^{-a_i(t - \tau)} \cos b_i(t - \tau) \sin \frac{\pi V}{L}\tau \, d\tau; \quad (26)$$

$$I_2^i = \frac{1}{b_i}\int_o^t e^{-a_i(t - \tau)} \sin b_i(t - \tau) \sin \frac{\pi V}{L}\tau \, d\tau, \quad (27)$$

where $i = 1, 2$.

Thus, the solution for $0 \leq t \leq \frac{L}{V}$ may be written

$$x_1 = \frac{K_2 A}{m_1 m_2} (.02065\ I_1^{\,1} + .6447\ I_2^{\,1} - .02065 I_1^{\,2} - .7715 I_2^{\,2}); \quad (28)$$

$$x_2 = \frac{K_2 A}{m_1 m_2} (.004055 I_1^{\,1} + .06014 I_2^{\,1} - .004055 I_1^{\,2} + 48.62 I_2^{\,2}). \quad (29)$$

For $t > \frac{L}{V}$, the problem is one of damped free vibrations since $y = 0$. The initial conditions may be evaluated from equations (28) and (29). These conditions are the values of x_1, $\dot{x}_1$, x_2 and $\dot{x}_2$ at $t = \frac{L}{V}$. Here $L = 2$ ft., $V = 22$ ft/sec., $A = 2$ in., and the initial conditions for the free vibrations were: $x_1 = 0.035199$ ft., $\dot{x}_1 = 0.6360$ ft/sec., $x_2 = 0.092475$ ft., $\dot{x}_2 = -9.985$ ft/sec. Taking the Laplace transforms of equations (13) and (14) with $y = 0$, using the above for initial conditions, yields the following:

$$X_1 = \frac{1}{m_1 m_2} \left[\frac{10.395 (s + .7336) + 122.61}{(s + .7336)^2 + 46.84} + \frac{.83350 (s + 6.8764) + 93.669}{(s + 6.8764)^2 + 3883} \right]; \quad (30)$$

$$X_2 = \frac{1}{m_1 m_2} \left[\frac{1.4045 (s + .7336) + 122.61}{(s + .7336)^2 + 46.84} + \frac{28.093 (s + 6.8764) - 3001.2}{(s + 6.8764)^2 + 3883} \right]. \quad (31)$$

The method of partial fractions has been applied.

The inverse transforms of equations (30) and (31) are the solutions for the free vibrations,

$$x_1 = e^{-.7336\,t'}(.032588\cos 6.844\,t' + .056162\sin 6.844\,t') + e^{-6.8764\,t'}(.0026130\cos 62.31\,t' + .0047127\sin 62.31\,t'); \quad (32)$$

$$x_2 = e^{-.7336\,t'}(.0044030\cos 6.844\,t' + .0048018\sin 6.844\,t') + e^{-6.8764\,t'}(.088070\cos 62.31\,t' - .150996\sin 62.31\,t'); \quad (33)$$

where $t' = t - \frac{L}{V} > 0.$

APPENDIX V.

Equations Describing the Systems Used in Part 2

Mechanical System

The mechanical system shown in Figure 45 is reproduced in Figure 58 in which the coordinates and system components are labeled. The equations of motion for this system are written below.

Equations of Motion

$$M_1 p \dot{x}_o + (G_1 + \frac{K_1}{p})(\dot{x}_1 - \dot{x}_4) + (G_2 + \frac{K_2}{p})(\dot{x}_2 - \dot{x}_5) + (G_3 + \frac{K_3}{p})(\dot{x}_6 - \dot{x}_3) = 0 ;$$

$$\frac{I_1}{d^2} p (\dot{x}_1 - \dot{x}_2) + \frac{c}{d}(G_1 + \frac{K_1}{p})(\dot{x}_1 - \dot{x}_4) - \frac{d-c}{d}(G_2 + \frac{K_2}{p})(\dot{x}_2 - \dot{x}_5) + \frac{c-a}{d}(G_3 + \frac{K_3}{p})(\dot{x}_6 - \dot{x}_3) = 0$$

$$M_2 p \dot{x}_3 - (G_3 + \frac{K_3}{p})(\dot{x}_6 - \dot{x}_3) = 0 ;$$

$$M_3 p \dot{x}_4 - (G_1 + \frac{K_1}{p})(\dot{x}_1 - \dot{x}_4) + \frac{K_4}{p}(\dot{x}_4 - \dot{x}_7) = 0 ;$$

$$M_4 p \dot{x}_5 - (G_2 + \frac{K_2}{p})(\dot{x}_2 - \dot{x}_5) + \frac{K_5}{p}(\dot{x}_5 - \dot{x}_8) = 0.$$

Operator, $p = \frac{d}{dt}$.

Electrical Analogy

Equations for the Circuit Shown in Figure 45

$$c_1 \bar{p} e_o + (\frac{1}{R_1} + \frac{1}{L_1 \bar{p}})(e_1 - e_4) + (\frac{1}{R_2} + \frac{1}{L_2 \bar{p}})(e_2 - e_5) + (\frac{1}{R_3} + \frac{1}{L_3 \bar{p}})(e_6 - e_3) = 0 ;$$

$$c_2 \bar{p} (e_1 - e_2) + \frac{N_3}{N}(\frac{1}{R_1} + \frac{1}{L_1 \bar{p}})(e_1 - e_4) - \frac{N - N_3}{N}(\frac{1}{R_2} + \frac{1}{L_2 \bar{p}})(e_2 - e_5)$$

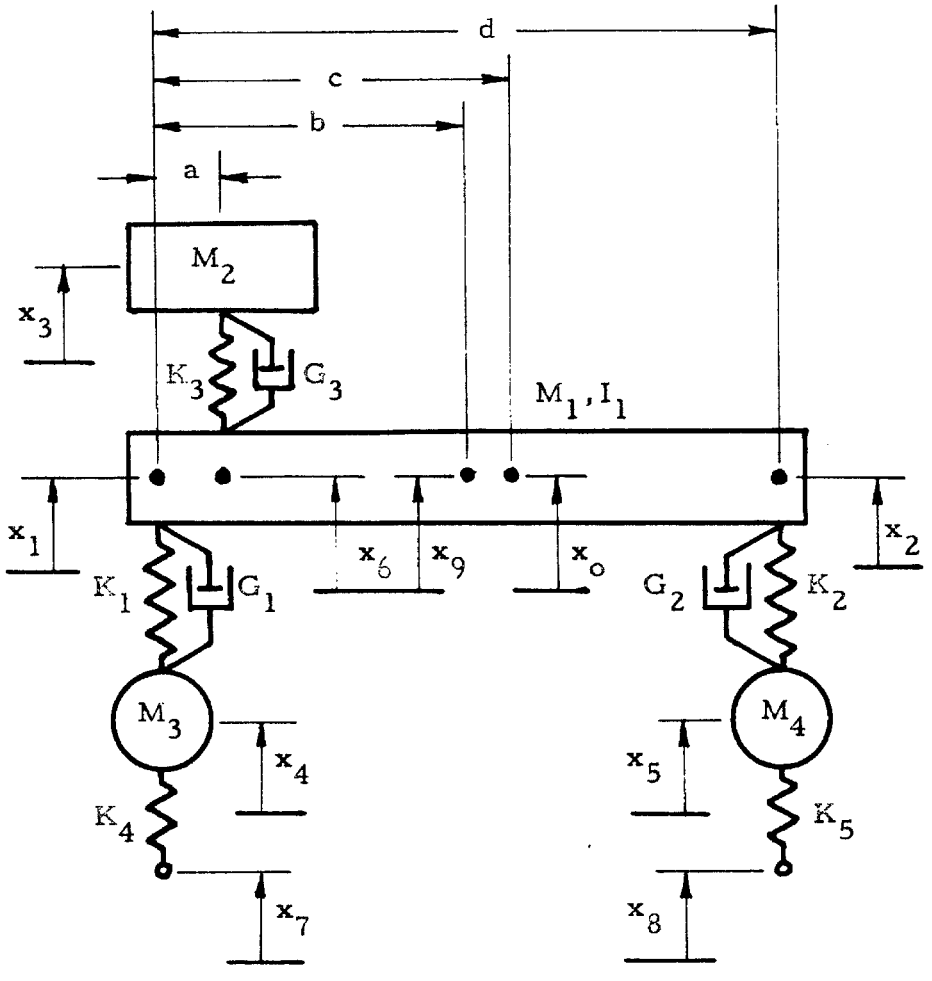

Figure 58. Mechanical system used to represent an automobile in studying the effect of varying engine mount stiffness.

$$+\frac{N_3 - N_1}{N}\left(\frac{1}{R_3} + \frac{1}{L_3\bar{p}}\right)(e_6 - e_3) = 0;$$

$$c_3\bar{p}e_3 - \left(\frac{1}{R_3} + \frac{1}{L_3\bar{p}}\right)(e_6 - e_3) = 0\ ;$$

$$c_4\bar{p}e_4 - \left(\frac{1}{R_1} + \frac{1}{L_1\bar{p}}\right)(e_1 - e_4) + \frac{1}{L_4\bar{p}}(e_4 - e_7) = 0\ ;$$

$$c_5\bar{p}e_5 - \left(\frac{1}{R_2} + \frac{1}{L_2\bar{p}}\right)(e_2 - e_5) + \frac{1}{L_5\bar{p}}(e_5 - e_8) = 0\ .$$

Operator, $\bar{p} = \frac{d}{d\bar{t}}$

N = total number of turns on transformer primary.

N_1 = number of turns, e_1 to e_6.

N_2 = number of turns, e_1 to e_9.

N_3 = number of turns, e_1 to e_o.

Conversion equations

$$n = \frac{\text{Actual time}}{\text{Computer time}} = \frac{t}{\bar{t}}$$

f = conversion constant.

k = power level constant.

$\bar{p} = n\,p$.

$$C = \frac{f^2}{n^2}M\ ;\ \frac{1}{R} = \frac{f^2}{n}G\ ;\ \frac{1}{L} = f^2K\ ;$$

$$C_2 = \frac{f^2}{n^2}\ \frac{I_1}{d^2}\ .\qquad e = \frac{n}{kf}\dot{x}\ .$$

$$\frac{N_1}{N} = \frac{a}{d}\ ;\ \frac{N_2}{N} = \frac{1}{2}\ ;\ \frac{N_3}{N} = \frac{c}{d}\ .$$

APPENDIX VI.

Symbols and Units

a	dimension of vehicle (feet)
b	dimension of vehicle (feet)
C	capacitance (farads)
c	dimension of vehicle (feet)
d	dimension of vehicle (feet)
e	dimension of vehicle (feet)
G	damping constant (slug/sec)
I	moment of inertia (slug-ft^2)
i	current (amperes)
K	spring constant (lb/ft)
L	inductance (henries)
M, m	mass (slugs)
p	operator d/dt
$\bar{p}$	operator d/d$\bar{t}$
R	resistance (ohms)
t	actual time (seconds)
$\bar{t}$	computer time (seconds)
x	linear displacement from static equilibrium (feet)
y	vertical displacement of ground (feet)
ϑ	angular displacement of sprung mass in roll (radians)
φ	angular displacement of sprung mass in pitch (radians)
ψ	angular displacement of the rear axle in roll (radians)

Glossary

brake hop: self-excited vertical oscillations of the unsprung masses occurring when brakes are applied.

bump stops: stops which limit the relative displacements between the sprung and unsprung masses.

compression: upward motion of the wheels relative to the frame.

fifth wheel: a wheel attached to the vehicle for the purpose of measuring the speed (Figure 8).

pitch: rotation about a horizontal axis perpendicular to the longitudinal axis of the vehicle.

power hop: self-excited vertical oscillations of the powered wheels.

primary motion: motion with a frequency approximately equal to the natural frequency of the sprung mass on the suspension springs.

rebound: downward motion of the wheels relative to the frame.

roll: rotation about an axis parallel to the longitudinal axis of the vehicle.

roll stabilizer: device used to cut down roll of the sprung mass.

secondary motion: motion with a frequency approximately equal to the natural frequency of the sprung mass on the tires.

sprung mass: the mass supported by the suspension springs.

suspension: mechanical system including springs, shock absorbers, and linkages, which connects the sprung and unsprung masses.

tread width: distance between left and right wheels.

unsprung mass: the mass not supported by the suspension springs.

wheel bounce: large vertical oscillations of the wheels in secondary motion.

wheelbase: distance between the front and rear wheel centers.